NASA CONTRACTOR REPORT

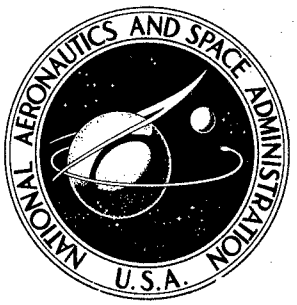

NASA CR-1197

NASA CR-1197

AMPTIAC

FATIGUE CRACK PROPAGATION IN CYLINDRICAL SHELLS

by W. M. Catanach, Jr., and F. Erdogan

Prepared by
LEHIGH UNIVERSITY
Bethlehem, Pa.
for

NATIONAL AERONAUTICS AND SPACE ADMINISTRATION • WASHINGTON, D. C. • OCTOBER 1968

NASA CR-1197

FATIGUE CRACK PROPAGATION IN CYLINDRICAL SHELLS

By W. M. Catanach, Jr., and F. Erdogan

Prepared under Grant No. NGR 39-007-011 by
LEHIGH UNIVERSITY
Bethlehem, Pa.

for

NATIONAL AERONAUTICS AND SPACE ADMINISTRATION

For sale by the Clearinghouse for Federal Scientific and Technical Information
Springfield, Virginia 22151 – CFSTI price $3.00

ABSTRACT

This report presents some of the results of the experimental and theoretical studies on the fatigue crack propagation in cylindrical shells of 6063-T6 aluminum subjected to fluctuating internal pressure. Most of the fatigue tests are performed on 6063-T6 aluminum alloys. Some 2024-T3 aluminum and mild steel specimens are also tested. Plexiglas specimens are used for static experiments.

In the analysis of the experimental results, the stress intensity factor is used as the correlation parameter. A modified crack propagation model is developed to take into account the effect of bending stresses, which are superimposed on membrane loads around the crack in shells. To evaluate the stress intensity factor, the integral equations obtained by Folias are solved numerically after separating the singularities. Partly to verify the theoretical results, strain measurements were made around the crack tip on the outside of the aluminum and inside and outside of the plexiglas cylinders. The results indicate that over the range of crack propagation data covering 10^{-7} to 10^{-3} in/cycle, the model adopted in this study seems to be highly satisfactory.

NOMENCLATURE

a	Half crack length
A, A', B	Materials constants
A_p, B_p	Complex constants
D	$Eh/[12](1-\nu^2)]$ = Flexural rigidity
E	Young's modulus
$F(X,Y)$	Stress function
g_i	Functions of h and ν
h	Shell thickness
K_n	Modified Bessel function of the third kind of order n
K	Stress intensity factor
K_e	Stress intensity factor in extension
K_{max}	Maximum stress intensity factor
K_r	Stress intensity factor range
K_{rb}	Stress intensity factor range in bending
K_{re}	Stress intensity factor range in extension
K_s	Stress intensity factor of a cylinder
L_i	Kernels as defined in text
M_x, M_y, M_{xy}	Bending moment components
m_o, n_o	Constants
N_x, N_y, N_{xy}	Membrane forces
n	Number of cycles
Δn	Difference in number of cycles

P	$P_b + P_e$
P_b	Stress intensity factor ratio in bending
P'_b	$- P_b \sqrt{1/3(1-\nu^2)}$
P_e	Stress intensity factor ratio in extension
P	Plastic zone size
Q_x, Q_y	Transverse shear forces
q	Pressure
R	Radius of shell
ΔR	Outer surface displacement
r_1	Correlation coefficient
r, θ	Polar coordinates
S_{yx}	Standard estimate of error
t_o, v_o	Constants
V_y	Effective transverse shear
$W(X,Y)$	Displacement function
X, Y, Z	Rectangular cartesian coordinates
x, y	Dimensionless coordinates
da/dn	Crack growth rate
α_1, α_2	Crack growth constants
α	$\sqrt{i}$
β	$\sqrt{-i}$
Ω	$(\sigma^{\infty}_{max} + \sigma^{\infty}_{min})/(\sigma^{\infty}_{max} - \sigma^{\infty}_{min})$
λ	$[12(1-\nu^2)]^{1/4} a/(Rh)^{1/2}$
γ	A crack growth parameter
ζ	$x - \xi$

ν	Poisson's ratio
ν_o	$1-\nu$
σ^{∞}_{max}, σ^{∞}_{min}, σ^{∞}_{y}	Applied stresses
σ_x, σ_y, τ_{xy}, σ_r, σ_θ, $\tau_{r\theta}$	Stress components
σ_{xc}, σ_{yc}	Stress components due to crack
σ_{xb}, σ_{yb}, τ_{xyb}	Bending stress components
σ_{xe}, σ_{ye}, τ_{xye}	Extensional stress components
ε_x, ε_y	Strain components in rectangular coordinates
ε^{∞}_{x}, ε^{∞}_{y}	Applied strain components
ε_{xc}, ε_{yc}	Strain components due to crack
μ in	Microinches

INTRODUCTION

The problem of fatigue crack propagation in thin plate and shell structures is of considerable technological importance, as it relates directly to the fail-safe design of aerospace vehicles and some ship structures. In such structures, because of the unavoidable existence of stress raisers,(e.g., holes, various forms of joining, material imperfections), generally the fatigue crack nucleates after relatively small number of load cycles compared to the total useful life of the structure. Hence, fatigue crack propagation studies become necessary for rational design as well as maintenance procedures.

The main objective of the present study is to investigate the effect of shell curvature, and to a lesser extent, that of bending stresses superimposed on the membrane loads on the crack propagation rate in thin-walled structures. In published literature there is a great wealth of data as well as the results of studies on the crack propagation in a large variety of structural materials subjected to repeated uniaxial tension. Thus, it becomes desirable to develop a method by which the fatigue crack growth characteristics of thin-walled structures may be predicted from the fatigue information on flat plates of the same material subjected to uniaxial extension.

Experience with the fatigue crack propagation in flat plates indicate that from an engineering view point the stress intensity factor for the propagating crack is a very simple and effective parameter in analyzing and correlating the results of the fatigue tests. This will also be the view point which will be adopted in this study, particularly in the modification of the crack propagation model to take into account the effect of the combined loads. It appears then that there are two main problems which should be considered. One is the evaluation of the stress intensity factor through the elastostatic analysis of an internally pressurized cylindrical shell containing a longitudinal crack, and the other is the experimental verification of the crack growth model by using the results of the elastic analysis and the fatigue tests.

For the stress intensity factor an assymptotic solution is given by Folias [1,2,3]. However this solution is reliable only for very small crack lengths and a more refined solution is needed for the crack dimensions or, more precisely for the shell parameters which may be encountered in practice. To obtain such a solution the integral equations governing the problem is solved numerically after separating the singularities.

Most of the fatigue crack propagation data in this study

are obtained by using 6063-T6 aluminum tubes. In the subsequent series of tests 6061-T3 tubes and plates of the same thickness are being used.

FATIGUE CRACK PROPAGATION MODEL

Almost all of the existing quantitative fatigue crack propagation models deal with the thin plates with straight, through cracks, which are subjected to uniaxial repeated extensional loads [4-16]. A summary of various models as well as the description of a crack propagation model based on plastic deformations around the propagating crack were given in an earlier report [17]. In this model the crack propagation rate is expressed as

$$\frac{da}{dn} = A\, p_{max}^{\alpha_1}\, p_r^{\alpha_2} \qquad (1)$$

where a is the half crack length, n is the number of cycles A, α_1, α_2 are positive constants, p_{max} and p_r are, respectively, the maximum and range values of the plastic zone size around the crack tip.

In flat plates, a reliable estimate of the plastic zone size may be obtained by using Dugdale's technique [18], which gives

$$p = a\left[\sec\left(\frac{\pi\sigma^{\infty}}{2\sigma_{ys}}\right) - 1\right] \qquad (2)$$

where σ^{∞} is the uniaxial stress perpendicular to the plane of and away from the crack and σ_{ys} is the yield stress.

For the so-called small scale yielding, that is, for small values of p/a, (2) may be approximated by

$$p \simeq \frac{1}{2}\left(\frac{\pi}{2\sigma_{ys}}\right)^2 K^2 \tag{3}$$

where $K = \sigma^{\infty} a^{1/2}$ is the stress intensity factor. By substituting from (3) into (1) and defining

$$K_r = a^{1/2}(\sigma^{\infty}_{max} - \sigma^{\infty}_{min})/2$$
$$\Omega = (\sigma^{\infty}_{max} + \sigma^{\infty}_{min})/(\sigma^{\infty}_{max} - \sigma^{\infty}_{min}) \tag{4}$$

we obtain

$$\frac{da}{dn} = B(1 + \Omega)^{2\alpha_1} K_r^{2(\alpha_1+\alpha_2)} \tag{5}$$

Similarly, in the case of cylindrical bending the fatigue crack propagation rate may be expressed as [15,16,17]

$$\left(\frac{da}{dn}\right)_b = B(1+\Omega)^{2\alpha_1} (\gamma K_{rb})^{2(\alpha_1+\alpha_2)} \tag{6}$$

where Ω and K_{rb} are given by (4) with σ^{∞} as the bending stress on the surface of the plate and γ has a theoretical value of 0.5.

Another model, which accounts for the effect of mean

stress as well as stress range, is that given by Forman and others [19]

$$da/dn = C(K_r)^m/[(1 - \frac{\sigma^{\infty}_{max}}{\sigma^{\infty}_{min}})K_c - 2K_r] \qquad (7)$$

where C and m are material constants and K_c is the critical stress intensity factor. The crack growth models used in this report to express the crack growth rate in cylindrical shells will be of the same form as (5) and (6), subject to the limitation that small scale yielding exists at the crack tip.

In the neighborhood of the fatigue crack if the plate is subjected to a combination extension and bending, because of linearity, the resulting stress field would be the direct addition of the two separate fields. This means that the range component of the resultant stress intensity factor would be $K_r = K_{re} + K_{rb}$. It is obvious that using this value in the crack propagation models expressed in terms of K, e.g., (5) or (7), would give erroneous results, since it would not reduce to (6) as K_r, the extensional component of the stress intensity factor goes to zero. Thus, one way of superimposing the effects of extension and bending in fatigue crack propagation is suggested by (5) and (6), namely, replacing K_r in crack growth models by $K_{re} + \gamma K_{rb}$, giving

$$\frac{da}{dn} = B(1 + \Omega)^{2\alpha_1} (K_{re} + \gamma K_{rb})^{2(\alpha_1+\alpha_2)} \qquad (8)$$

In (8) it is assumed that mean-to-range stress ratios, i.e., the values of Ω in bending and extension are the same. This is the case in shells. If Ω values in bending and extension are not equal, (8) would have to be modified accordingly.

Note that (8) may be obtained by assuming that for small scale yielding, the plastic zone size in the neighborhood of a crack in a plate subjected to combined plane extension and cylindrical bending loads may be estimated as

$$p \simeq \frac{1}{2} \left(\frac{\pi}{2\sigma_{ys}}\right)^2 (K_e + \gamma K_b)^2 \qquad (9)$$

Due to the nonlinear nature of the phenomenon, methods of superposition of the effects of combined loads based on the addition of plastic zone sizes or crack growth rates are not justifiable.

ELASTIC SOLUTION FOR CRACKED CYLINDRICAL SHELLS

The details of the elastic solution for a cylindrical shell containing a longitudinal crack are given in Appendix I. This is an extension of the solution given by Folias [2]. It is restricted to shallow shell theory of isotropic, homogeneous, elastic circular cylinders of constant thickness.

In this case, the system of differential equations derived by Marguerre [20] takes the form

$$\frac{Eh}{R}\frac{\partial^2 W}{\partial X^2} + \nabla^4 F = 0$$

$$\nabla^4 W - \frac{1}{RD}\frac{\partial^2 F}{\partial X^2} = \frac{q(X,Y)}{D} \qquad (10)$$

where W is the displacement along the Z axis, F is the stress function, X, Y, Z are the rectangular coordinates shown in Figure 1, E is the modulus of elasticity, h is the shell wall thickness, R is the shell radius, q is the internal pressure, and D is the flexural rigidity defined by

$$D = Eh^3/[12(1-\nu^2)]$$

The bending moment components M_x, M_y, and M_{xy} are given by

$$M_x = -D\left[\frac{\partial^2 W}{\partial X^2} + \nu\frac{\partial^2 W}{\partial Y^2}\right]$$

$$M_y = -D\left[\frac{\partial^2 W}{\partial Y^2} + \nu\frac{\partial^2 W}{\partial X^2}\right] \qquad (11)$$

$$M_{xy} = -D(1-\nu)\frac{\partial^2 W}{\partial X \partial Y}$$

where ν is Poisson's ratio. The membrane forces N_x, N_y, and N_{xy} are given as

$$N_x = \frac{\partial^2 F}{\partial Y^2}$$

$$N_y = \frac{\partial^2 F}{\partial X^2} \tag{12}$$

$$N_{xy} = - \frac{\partial^2 F}{\partial X \partial Y}$$

and the transverse shear forces Q_x and Q_y are given as

$$Q_x = - D \frac{\partial}{\partial X} (\nabla^2 W)$$

(13)

$$Q_y = - D \frac{\partial}{\partial Y} (\nabla^2 W)$$

In view of equations (11), the bending stress components become

$$\sigma_{xb} = - \frac{EZ}{(1-\nu^2)} \left[\frac{\partial^2 W}{\partial X^2} + \nu \frac{\partial^2 W}{\partial Y^2}\right]$$

$$\sigma_{yb} = - \frac{EZ}{(1-\nu^2)} \left[\frac{\partial^2 W}{\partial Y^2} + \nu \frac{\partial^2 W}{\partial X^2}\right] \tag{14}$$

$$\tau_{xyb} = - 2GZ \frac{\partial^2 W}{\partial X \partial Y}$$

and from equations (12) the extensional stress components are obtained as

$$\sigma_{xe} = \frac{1}{h} \frac{\partial^2 F}{\partial Y^2}$$

$$\sigma_{ye} = \frac{1}{h} \frac{\partial^2 F}{\partial X^2} \tag{15}$$

$$\tau_{xye} = - \frac{1}{h} \frac{\partial^2 F}{\partial X \partial Y}$$

Introducing the dimensionless coordinates

$$x = \frac{X}{a}, \; y = \frac{Y}{a} \tag{16}$$

where a is the half crack length, the homogeneous parts of (10) become

$$\frac{Eha^2}{R} \frac{\partial^2 W}{\partial x^2} + \nabla^4 F = 0$$

$$\nabla^4 W - \frac{a^2}{RD} \frac{\partial^2 F}{\partial x^2} = 0 \tag{17}$$

The solution for the internally pressurized cracked cylinder is obtained by first evaluating the stresses in a cylinder without a crack, obtaining the bending moments, membrane forces and transverse shear loads at the location of the crack, and then applying equal and opposite of these moments and loads on the sur-

face of the crack in a cylinder with no other external loads. Superposition of these two results gives the desired solution. Since the first problem has no contribution to the singularity at the crack tip, and since we are interested in evaluating the stress intensity factor only, the main problem is the solution of the homogeneous system (17) with nonvanishing loads at the crack surfaces.

In solving (17), additional requirements to be met are that the displacement function W and stress function F with their first derivatives must be finite far away from the crack and the stresses and displacement for $y = 0$ and $|x|>1$ must be continuous i.e., F and W and all their partial derivatives must be continuous for all x and y except for points on the crack surface,

$$\lim_{|y|\to 0} \left[\frac{\partial^n}{\partial y^n}(W^+) - \frac{\partial^n}{\partial y^n}(W^-)\right] = 0$$

$$\lim_{|y|\to 0} \left[\frac{\partial^n}{\partial y^n}(F^+) - \frac{\partial^n}{\partial y^n}(F^-)\right] = 0 \qquad , (n = 0,1,2,3) \qquad (18)$$

For the symmetric case, N_{xy} and the effective transverse shear resultant, $V_y = Q_y + \frac{\partial M_{xy}}{\partial x}$, are zero at $y=0$ and the functions W and F may be represented in terms of Fourier cosine integrals. Then the boundary conditions and the continuity requirements lead to a system of dual integral equations. These dual inte-

gral equations can be reduced to singular integral equations with kernels L_1, L_2, L_3 and L_4. These singular integral equations have the form

$$\int_{-1}^{1} \frac{2\pi N_y a^2}{i\sqrt{EhD}}\, dx = \int_{-1}^{1} [u_1(\xi)\, L_1(\xi,x) + u_2(\xi)\, L_2(\xi,x)]\, d\xi$$

$$\int_{-1}^{1} a^2 \pi M_y \frac{2}{D}\, dx = \int_{-1}^{1} [u_1(\xi)\, L_3(\xi,x) + u_2(\xi)\, L_4(\xi,x)]\, d\xi \qquad (19)$$

where $N_y = \frac{n_o}{a^2}$ and $M_y = \frac{Dm_o}{a^2}$ (n_o and m_o are chosen as constants). The solutions $u_1(\xi)$ and $u_2(\xi)$ may then be expressed as

$$u_1(\xi) = \sqrt{1 - \xi^2}\, [A_o + \lambda^2 A_1(1\ \xi^2) + \ldots]; \quad |\xi|<1$$

$$u_2(\xi) = \sqrt{1 - \xi^2}\, [B_o + \lambda^2 B_1(1-\xi^2) + \ldots]; \quad |\xi|<1 \qquad (20)$$

where A_p and B_p are complex constants and

$$\lambda = [12(1-\nu^2)]^{1/4} a/(Rh)^{1/2}$$

A_p and B_p are generally functions of λ. Substituting (20) into (19) and writing the kernels in series form, good for the range $0<\lambda<2$, the resulting integrals can be solved in closed form. The resulting values of the integrals are polynomials in odd powers of x of the following form

$$\frac{2\pi n_o x}{i\sqrt{EhD}} = \sum_{o}^{m} C_k x^{2k+1}$$

$$-2\pi m_o x = \sum_{o}^{m} D_k x^{2k+1} \qquad (21)$$

where C_k and D_k are functions of λ, A_p and B_p. By comparing coefficients of x_n, a system of simultaneous equations can be obtained and solved for A_p and B_p.

The strength of the singularities at the crack tips depend on the constants A_o and B_o only, and the stresses in a small neighborhood of the crack tip may be expressed as

$$\sigma_{xb} \simeq \frac{\pm P'_b}{\sqrt{1/3(1-\nu^2)}} \frac{K_e}{\sqrt{2r}} \left(\frac{3-3\nu}{4} \cos\frac{\theta}{2} - \frac{1-\nu}{4} \cos\frac{5\theta}{2}\right)$$

$$\sigma_{yb} \simeq \frac{\pm P'_b}{\sqrt{1/3(1-\nu^2)}} \frac{K_e}{\sqrt{2r}} \left(\frac{11+5\nu}{4} \cos\frac{\theta}{2} + \frac{1-\nu}{4} \cos\frac{5\theta}{2}\right)$$

$$\tau_{xyb} \simeq \frac{\pm P_b'}{\sqrt{1/3(1-\nu^2)}} \frac{K_e}{\sqrt{2r}} \left(\frac{7+\nu}{4} \sin\frac{\theta}{2} + \frac{1-\nu}{4} \sin\frac{5\theta}{2}\right) \tag{22}$$

$$\sigma_{xe} \simeq P_e \frac{K_e}{\sqrt{2r}} \left(\frac{3}{4} \cos\frac{\theta}{2} + \frac{1}{4} \cos\frac{5\theta}{2}\right)$$

$$\sigma_{ye} \simeq P_e \frac{K_e}{\sqrt{2r}} \left(\frac{5}{4} \cos\frac{\theta}{2} - \frac{1}{4} \cos\frac{5\theta}{2}\right) \tag{23}$$

$$\tau_{xye} \simeq - P_e \frac{K_e}{\sqrt{2r}} \left(\frac{1}{4} \sin\frac{\theta}{2} - \frac{1}{4} \sin\frac{5\theta}{2}\right)$$

where P_b' and P_e are functions of A_o and B_o, K_e is the stress intensity factor for a plate under extensional loads ($K_e = \sigma_\infty\sqrt{a}$), and r is the distance from the crack tip. The values $+P_b'$ and $-P_b'$ are used for stresses on the inner and outer surfaces of the shell, respectively. As $\lambda\to 0$ (i.e., $R\to\infty$), $P_b'\to 0$ and $P_e\to 1$ and the stresses of a flat plate in extension and bending are recovered. Thus the stresses in the crack tip region of the shell are expressed in terms of stresses in a flat sheet. The stress intensity factors for a shell with a meridional crack due to bending and extension become, respectively

$$K_{bs} = \left[-P_b'/\sqrt{(1-\nu^2)/3}\right] K_e \tag{24}$$

$$K_{es} = P_e K_e \tag{25}$$

Note that because of the Kirchhoff boundary conditions, the bending shear stress does not vanish at the free edge of the crack.

Since K_e is the stress intensity factor of a plate under extensional loading, the combined stress intensity factor, K_s, for a cylinder containing a meridional crack can be written as

$$K_s = (P_e + P_b)K_e \qquad \text{for the outer surface} \qquad (26)$$

$$K_s = (P_e - P_b)K_e \qquad \text{for the inner surface} \qquad (27)$$

where $P_b = - P_b'/\sqrt{(1-\nu^2)/3}$

Therefore, the values P_e and P_b combine to form the stress intensity ratio of a shell under internal pressure to a plate under extension, for a particular material.

Computed values of P_b' and P_e are given in Table I for values of λ from 0.2 to 2.2 in increments of 0.2 and for number of terms of A_p and B_p in the series expansion (20). As could be expected, the convergence becomes slower as λ is increased. For $\lambda>2$, the convergence is not expected to be good because of the limits imposed on λ in this particular series form of the kernels. A minimum accuracy of three digits was achieved for all P_e for $.2 \leq \lambda \leq 2.2$. This was not the case for

P_b'. But, since $P_e >> |P_b'|$, the accuracy achieved for P_b' was considered sufficient. Figures 3 and 4 are plots of P_e and P_b'; and P_b for $\nu = 1/3$ obtained from the asymptotic solution [2], a two term and an eight term expansion in (20). In the asymptotic solution, orders of λ^4 and greater were neglected in the kernels and the solution for A_o and B_o. Four simultaneous equations were used in solving for A_o and B_o. Figures 3 and 4 compare this result with the two and eight term solutions, which consisted of the solution of four and sixteen simultaneous equations. In the latter, the highest degree term in λ which is neglected is λ^{28}. The eight term solution shows that the sign change in the bending stress intensity ratio P_b' (Figure 4) does not take place in the interval under consideration. This means that for this λ range, the maximum stress in the crack region is on the outside of the shell.

A least squares curve fitting program was used to express P_b' and P_e as polynomials in λ which are given below.

$$P_b' = -5.6207 \times 10^{-5} + .0016268\lambda - .14611\lambda^2 + .25010\lambda^3 - .21721\lambda^4 + .097711\lambda^5 - .017632\lambda^6 \qquad (28)$$

$$P_e = 1.0004 - .062432\lambda + .67419\lambda^2 - 1.0367\lambda^3$$
$$+ 1.0184\lambda^4 - .49949\lambda^5 + .094455\lambda^6 \qquad (29)$$

A comment is in order concerning the use of the Kirchhoff theory in the above solution, according to which only the effective transverse shear rather than Q_y and M_{xy} is required to vanish along the crack. While the stress distribution outside the local region should be accurate, it might be expected that near the crack boundary the same type of difference exists as that found by Feridun [21], Knowles and Wang [22] and Hartranft [23] in comparing the stress distributions due to bending using Kirchhoff's and Reissner's theories. In this case, the order of the stress singularity was the same for both theories but the stress distribution in the crack region was different, Reissner's theory, which accounts for all the physical boundary conditions, giving the same angular dependence as the plane stress solution.

The important fact is that the ratio of the stress intensity of a cylinder to that of a plate, $P_e + P_b$, is the desired result for use in the crack growth model and that the ratio will be the same no matter which one of the two theories is used to establish the ratio in bending. In addition, the ef-

fect of bending is small for $0 \leq \lambda \leq 2.2$ where P_b varies from 0 to 10% that of P_e.

EXPERIMENTAL PROCEDURE

The experiments were conducted to determine the crack propagation rates and the stresses caused by the crack in thin-walled, cylindrical shells under different loading conditions. The loading employed in all tests produced various applied mean and range stresses from one-eighth to one-quarter of the yield stress.

Description of Test Specimens. - Three materials were tested with varying degrees of success - 2024-T3 aluminum, 6063-T6 aluminum, and mild steel. The best results were obtained from the tests of the 6063-T6 aluminum. Thin-walled 2024-T3 bare aluminum tubing could not be purchased commercially. So, these specimens were rolled into a cylinder from a flat sheet. The rolled cylinder was 8 5/8 inches in diameter, 27 inches in length and 0.050 of an inch in wall thickness. The mating edges as well as the ends of the shell were clamped to a mount to form the pressure chamber. The only thin-walled tubing that was commerically available was 6063-T6 extruded aluminum cylinders. Eight test specimens were cut from one 20 foot long tube. The mechanical properties and dimensions of the 6063-T6 aluminum specimens are given in Tables II and III. The steel shells were rolled from a 0.050 inch thick flat plate into an 8 inch diameter cylinder and then seam welded. Hence, only the ends of the 6063-T6 aluminum and the steel

shells needed to be clamped to a mount to form the pressure chamber.

Experimental equipment. - The experimental set-up and a schematic diagram of the hydraulic system are shown in Figures 5 and 6, respectively.

The pressurization control system basically consisted of the control panel, control manifold, and hydraulic power supply. It maintained any desired pressure loading characteristics in the specimen by means of a simple proportional feed back control system. The function generator, located in the control panel, determined the shape of the pressure variation curve and the rate and character of the pressure loading. The mean and range pressures were established by the control panel's set point and span controls.

A 50 power microscope, mounted on a 4 inch micrometer stage, was used for crack readings. It had a smallest division reading of 5×10^{-5} inches, which was actually more accurate than needed since the crack tip was not definable to more than 10^{-4} inches.

The strain indicator, used for static strain measurements, was accurate to 0.1% of the reading or 5 microinches/inch, whichever was greater. The oscilloscope, used for dynamic strain measurements had a smallest division reading of 4 microinches/inch.

Specimen preparation. - A crack was initiated in the shell by first drilling a 0.020 inch diameter hole at the point representing the center of the crack, and then making a cut that was symmetrical about the hole with a 0.011 inch wide jewelers saw. A notch was then formed at each end of the saw cut by "sawing" with a razor blade. The minimum total length of the manufactured crack was 0.200 inches. Next, the specimen was sanded and polished in the crack region to remove the surface flaws and make the crack tip visible.

Since the shells were pressurized with oil, the crack had to be sealed with a seal that had little or no effect on the stress distribution of the shell in the crack region. This was accomplished with a steel shim and vinyl patch. The shim was .003 inch thick and about 2 inches by 3 inches in size, was placed behind the crack on the inner portion of the shell, and was coated with a thin layer of graphite to eliminate any possible effect of friction. The vinyl patch was .008 inch thick and about 6 inches square, and was cemented to the shell and to the center of the shim. Thus the shim was prevented from shifting from behind the crack while still free to slide on the shell and to conform to the shell contour in the crack region.

Specimen mounting. - The shell was mounted on a machined steel pipe. Figure 7 is a cross-sectional drawing of the

shell and mount for the 6063-T6 aluminum and the steel shells. The mount for the 2024-T3 aluminum was basically the same except for additional holes for clamping the edges of the shell. A layer of cement was applied to the oil pressure side of all contact surfaces of the shell, mount, and spacer to keep oil leakage to a workable minimum. The rest of the contact surfaces were bare so that when pressure was applied, the surfaces would not slip and the strain in the x direction would be zero.

The end clamps were 1/2 inch wider than the inside contact surface. This 1/2 inch overhang had a two degree chamber so that, when the shell expanded under pressure, there would be no high stress concentration in the shell at its ends. A soft aluminum (1100-0) split ring was used between the outer surface of the shell and end clamps to uniformly distribute the clamping force. After the shell was clamped to the mount, strain gages were cemented to the shell's outer surface. The gages were BLH type A-5 with nominal resistance of 120 ohms and gage factor of 2.

Experimental procedure. - The test results of the 2024-T3 aluminum did not give reproducible crack growth results, either due to the necessity of clamping down the edges as well as the ends of the cylinder, or due to a large geometrical deviation from a true cylinder. However, reproductible crack growth results were obtained for the 6063-T6 aluminum. No conclusions could be reached on the steel because of the small amount of

data collected. Therefore, this report will use only the results from the 6063-T6 aluminum unless stated otherwise.

The pressure was calibrated with a dead weight tester to insure the proper prediction of the internal pressure of the shell from the control settings. The output was found to be linear with the control settings. Maximum variation from linearity was found to be 10 microinches/inch. Since the readings were greater or less than a linear relationship, it was felt that most of this was caused by small deviations in manually setting the controls and that this error would be self-compensating.

The pressurization unit was found to give a null or zero shift in the pressure curve. Therefore, constant monitoring of the unit to maintain the zero position was required during the crack growth tests.

The mean stress and stress range varied from shell to shell but were held constant for a given shell. The stress varied sinusoidally with a cyclic speed of 8/9 cps and a variation in peak to peak stress of less than 1%. No tests were conducted with a maximum hoop stress, σ_y^∞ (applied stress), greater than one-half the yield stress. The hoop stress is found from the relation

$$\sigma_y^\infty = \frac{qR}{h} \tag{30}$$

where q is pressure, R is internal radius, and h is wall thickness.

For a cylinder with fixed ends, i.e., $\varepsilon_x^\infty = 0$, we have the following additional relations

$$\sigma_x^\infty = \frac{\nu q R}{h} \tag{31}$$

$$\varepsilon_y^\infty = \frac{(1-\nu^2)}{E} \frac{qR}{h} \tag{32}$$

where ν is Poisson's ratio.

Strain gages were added to the outer surface of the shell to measure the hoop strains. The gages were placed along the prolongation of the crack where they would be unaffected by the perturbed strains due to the end clamps or the crack. Strain measurements were then calibrated with the internal pressure through equation (32) and the calibration curve is shown in Figure 8. The maximum static pressure used in calibration was not greater than the maximum test pressure for that shell. This prevented any unwarranted strain hardening in the crack tip area.

The measured strain gage readings gave differences from the theoretical of as much as 11% for the 6063-T6 aluminum, and 25% for the 2024-T3 aluminum. To find an explanation for this, an investigation of the change in geometry of the outer

surface of the shell due to a change in internal pressure was conducted.

The outer surface displacement, ΔR, for a perfect cylinder with uniform wall thickness should be

$$\Delta R = \varepsilon_y^{\infty} R \tag{33}$$

Substituting from (32) into (33), we find

$$\Delta R = \frac{1-\nu^2}{E} \frac{R^2}{h} q \tag{34}$$

The outer surface displacement of the test cylinders, taken with a dial indicator, did not agree with the results predicted by (34). The readings were taken at a position away from the influence of the crack and end clamps. The readings were very erratic as the pressure was increased. In some places the displacement would decrease while at other places it would increase more than predicted by (34). This was due to the fact that initially the cylinder was not perfectly round and straight.

Even though the strain gage readings were different from the theoretical, they were useful in insuring constant range and mean stress. A minimum of two gages at different locations on the shell surface were used to measure the hoop strains

throughout the tests in case one gage failed. None of the gages failed during the tests and the readings were found to be very reproducible.

Foil strain gages with 1/16 inch square grids were used to determine the strains ahead of the crack tip in plexiglas G and in shells #12, #14 and #18 of 6063-T6 aluminum. Each gage gave the average strain of the surface covered by the grid. This average strain was assumed to be the strain at the midpoint of the grid. The distance of the midpoint from the crack tip varied from 0.041 to 0.294 inches at half crack lengths ranging from 0.151 to 0.795 inches for the aluminum and from 0.195 and 1.00 inches for the plexiglas.

EXPERIMENTAL RESULTS

Physical observations of the crack. - There was an objectionable amount of surface roughening ahead of the crack tip for the longer crack lengths in the 6063-T6 aluminum shells. This roughening made it difficult to find the exact location of the crack tip. The surface roughening was worse in the 6063-T6 aluminum than in the 2024-T3 aluminum. There was a negligible amount of branching of the crack that took place during its growth. What branching did occur quickly disappeared.

Bulging. - Bulging here is defined as large outward normal displacements of the shell in the crack region. Since the elastic stress analysis used to correlate the crack propagation results is based on the small deflection theory, excessive bulging may reduce the reliability of the final results. Hence, measurements of the shell surface ahead of the crack in shells #9, #10 and #11 were taken with a dial indicator to see how much, if any, bulging was present. Figures 9 and 10 are plots of the radial displacement of the surface of the shell due to the presence of the crack only. The displacements ahead of the crack, caused by an increase in applied stress of 6,900 psi, are given in Figure 9 for four different crack lengths. The curves of the points can be thought of as profiles of the shell surface ahead of the cracks, Figure 10 compares the radial displacement at the crack tip of shells #9 and #10 with that of

shell #11 due to pressure changes of 13,500 psi and 6,900 psi, respectively. Since the maximum operating stresses involved in the fatigue tests were in the range of 7,000 to 14,000 psi, these curves were considered as the extremes of the radial displacements for all specimens. For $\lambda<2.2$, the radial displacements of the shell surface can be seen to be less than 0.005 inches. For an 8 inch diameter shell, this may be considered as "small deflection" and hence for the stress range under consideration, bulging does not appear to be a problem.

Analysis of crack growth data. - The proposed crack growth model for combined loading is

$$da/dn = B(1+\Omega)^{2\alpha_1} [K_{re} + \gamma K_{rb}]^{2(\alpha_1+\alpha_2)} \qquad (35)$$

Substituting from (24) and (25) into (35), we obtain

$$da/dn = B(1+\Omega)^{2\alpha_1} [(P_e + \gamma P_b)K_{re}]^{2(\alpha_1+\alpha_2)} \qquad (36)$$

In the experimental data given in Appendix II, σ^∞, 2a and Δn are known. da/dn is obtained by differentiating the data by means of a three point central difference technique (except at the ends, where a forward or backward difference scheme is used). Using (24), (25), (30) and (31), the stress intensity factors may be evaluated. In the computer program, least squares fit of log da/dn vs. log K_{re} was used to establish the

values of B, $2\alpha_1$ and $2(\alpha_1+\alpha_2)$ for $\gamma = 1$ and $\gamma = 0.5$. The results are tabulated in Table V for $K_{re} + 0.5\ K_{rb}$ and $K_{re} + K_{rb}$ for the range of convergence of the theoretical solution ($\lambda \leq 2.2$). The range of λ for the experimental work exceeded the range for the theoretical solution. However, this was no great handicap since the growth rate for $\lambda > 2.2$ was very rapid and only a small percentage of the total life of the shell was left. The term r_1 in Table V is the coefficient of correlation and is essentially equal for $K_e + 0.5\ K_b$ and $K_e + K_b$ for each shell. When r_1 is close to 1.0, as it is for the shells tested, the assumption of a linear relationship for the data is valid. The term S_{yx} is the standard estimate of error and establishes the scatter band that cover 95% of the population.

As can be seen in the table, the differences in A', B, $2\alpha_1$ and $2(\alpha_1+\alpha_2)$, for twice the effect of bending, are too small to be significant, meaning that the effect of bending has very little influence on the crack growth for the geometry and loading conditions considered. For the remainder of the analysis of experimental results, $\gamma = 0.5$ is used.

On the basis of combined experimental data, which is given in Figure 19, the crack propagation rate for 6063-T6 aluminum may be expressed as

$$da/dn = 1.068 \times 10^{-19}(1+\Omega)^{0.753} K_r^{3.85} \qquad (32)$$

Figures 11 through 18 show da/dn vs. $K_r = K_{re} + 0.5\ K_{rb}$ for individual shells with their respective scatter bands. In Figure (19), showing the combined data, the three basic levels of Ω are designated separately. For increasing Ω, the shift of the data to the left is characteristic of flat plate fatigue experiments.

Figure 20 shows the comparison of the crack growth rates for $\Omega = 1.07$ in 6063-T6, 2024-T3 and 7075-T6 aluminums. The crack growth rates for 2024-T3 and 7075-T6 aluminums used for the figure were taken from [16]:

$$da/dn = 2.68 \times 10^{-19}(1+\Omega)^{1.54}(K_r)^{3.62} \text{ for 2024-T3}$$

$$da/dn = 6.22 \times 10^{-20}(1+\Omega)^{2.22}(K_r)^{3.90} \text{ for 7075-T6}$$

The line for 6063-T6 aluminum falls between those of 2024-T3 and 7075-T6 aluminums for growth rates greater than 10^{-7} inches/cycle. The slope of the line is almost the same for 6063-T6 and 7075-T6 aluminums.

Transition zone. - The transition zone of flat to shear fracture gives another means of comparing the various types of aluminums. According to Wilhem [24], the zone of transition from flat to shear fracture is dependent on the stress intensity factor. It is stated in [24] that for 2024-T3 and

7075-T6 clad aluminums, the transition takes place within the range of K_r of 3540 ± 1770 #/inch$^{3/2}$. To see if this range also applies to 6063-T6 aluminum, the range stress intensity factors at the beginning and end of transition of the fatigue cracks of five specimens were determined from the crack lengths at these extremes. For the purpose of calculating the range stress intensity factor, it was assumed that the shear fracture was a function of the outer surface stress, hence $K_r = (P_b+P_e)K_{re}$. The transition initiation and termination are given in Table IV. The results for the 6063-T6 aluminum fall within a range of K_r of 3440 ± 1220 #/inch$^{3/2}$ which is within the acceptable range of 2024-T3 and 7075-T6 aluminums.

Strain measurements ahead of the crack. - For a partial verification of theoretical results, static strain measurements were made ahead of the fatigue crack for various crack lengths and load levels. The measured strains are the circumferential strains in an internally pressurized cylinder with fixed ends, which contains a longitudinal crack free of edge loadings. Thus away from the crack, the principal strains are

$$\varepsilon_x^\infty = 0, \quad \varepsilon_y^\infty = \frac{1-\nu^2}{E}\sigma^\infty \tag{38}$$

In the shell loaded at the crack surface only, at y = 0 and

and for small values of $r = x - a$, we have*

$$\sigma_x \simeq \sigma_y, \quad \varepsilon_y \simeq \frac{1-\nu}{E} P\sigma^{\infty} \sqrt{\frac{a}{2r}} \tag{39}$$

where $P = P_b + P_e$. Adding circumferential strains ε_y given by (38) and (39), we obtain an approximate expression for the strain ahead of the crack in terms of stress intensity ratio P as follows:

$$\varepsilon_{ys} \simeq \varepsilon_y^{\infty} \left(1 + \frac{P}{1+\nu} \sqrt{\frac{a}{2r}}\right) \tag{40}$$

The measured strains for three cylinders (#12, #14, and #18) as well as that obtained from equation (40) for $\nu = 1/3$ are shown in Figures 21, 22, and 23. Even though the approximate strains given by (40) have the same trend as the measured strains, the agreement is obviously unsatisfactory. The difference is due to finite gage length**, partial plastic deformations, and, perhaps most importantly, the fact that the stress intensity factor (i.e., the singular term alone) does not correctly predict the perturbed strains caused by the crack in a

---

* Here, for σ_{yb} the results of a higher order bending theory (e.g., [22]) rather than equation (22) are used. In the higher order theory, which satisfies all the physical boundary conditions, ahead of the crack $\sigma_{yb} = \sigma_{xb}$ and the angular distribution of stresses is the same as that in plane extension.

** In these measurements, 1/16 inch square foil gages were used.

homogeneous strain field. In the shell, the details of the evaluation of stresses away from the crack are very cumbersome and difficult. However, a reasonable estimate of this far field effect may be given by using an analogy with the flat plate solution.

In the case of flat plate containing a crack of length 2a and subjected to uniform compressive tractions σ^{∞} on the crack surfaces, the strain at y = 0 and a distance r from the crack tip may be expressed as,

$$\varepsilon_{yp} = \frac{1-\nu}{E}\,\sigma^{\infty} T \sqrt{\frac{a}{2r}} \qquad (41)$$

$$T = \sqrt{\frac{2r}{a}}\left(\frac{a+r}{\sqrt{r(2a+r)}} - 1\right)$$

For small values of r, T ≃ 1 and (41) gives the plate equivalent of (39). Thus, if we assume that the perturbed stress fields in plate and shell are similar up to distances r under consideration, an approximate value of ε_y for the shell may be obtained by multiplying (39) by factor T which is given in (41). With this, (40) may be modified as

$$\varepsilon_{ys} \simeq \varepsilon_y^{\infty}\left(1 + \frac{P \cdot T}{1+\nu}\sqrt{\frac{a}{2r}}\right) \qquad (42)$$

Again, for $\nu = 1/3$, the comparison of measured strains with those obtained from (42) is seen in Figures 24, 25 and 26. Since T is always less than unity, (40) gives a higher (theoretical) estimate for the strains - partly explaining the discrepancy in Figures 21 to 23. However, differences also exist in Figures 24 to 26. This, of course, is due partly to the assumption concerning the similarity of stress fields in flat plate and shell which leads to (42), and partly to inelastic deformations around the crack tip. The fact that the differences are more noticeable at higher load levels (i.e., ε_y^∞) and larger a/r ratios substantiates the validity of the latter contention.

The effects of a finite gage width can be estimated by examining the error involved in assuming the mean strain to be at the center of the gage. As seen from Figure 27, the actual mean strain is closer to the crack tip than the center of the gage. The mean strain point is established when the shaded areas are equal. This means that the data will be plotted closer to the ordinate than it should be. This puts the data above the prediction curve for the higher applied strain or smaller distances r. For small applied strains or large distances r where the elastic strain curve is relatively flat, the measured strain and the mean strain are essentially equal, and the effect of the finite gage length is negligible (see Figure 24).

To obtain further knowledge of the stresses in the crack tip area, static tests were conducted on Plexiglas G of a plate under tension and a cylinder under pressure. Strains were measured ahead of the crack at room temperature. Plexiglas was chosen so that the distance of a strain gage ahead of the crack tip could be measured when the gage was mounted on the inner surface of the cylinder. The nominal dimensions were 12" x 24" x 1/8" for the plate and 9 1/2" diameter, 20" length and 1/8" thickness for the cylinder.

The pressure in the cylinder was measured with a dead weight tester since the test pressures were too low to be accurately controlled with the test set up described in this report. Higher test pressures were not possible without risking catastrophic failure.

The stress intensities on the inner and outer surfaces of the shell were computed from the strain readings ahead of the crack. They were then compared with the stress intensity computed from the strain reading ahead of an equal length crack and applied stress in a plate. The comparison was made for three different crack lengths. The ratio of the stress intensities in the cylinder to that of the plate should equal $P_e + P_b$ and $P_e - P_b$ on the outer and inner surface of the cylinder, respectively.

Figure 28 is a plot of the ratio of the stress intensity factors vs. crack length for the test on the plexiglas and for the eight terms and Folias' [2] solutions. These experimental results are largely qualitative. They were not pursued further because of the steady drift in the gage readings caused by creep and the fact that the creep compliance for the two materials were not quite the same.

CONCLUSIONS

The results obtained in this study indicate that within the practical range of fatigue crack propagation rates, i.e., 10^{-7} to 10^{-3} in/in/cycle, the stress intensity factor is an effective correlation parameter in analyzing the fatigue data, and provides a powerful means of predicting fatigue crack growth characteristics of shells from that of flat plates. With the exception of problems involving "low cycle fatigue", from the design engineer's view point, essentially the problem may be reduced to one of evaluating the stress intensity factor. After this, one may use the flat plate results correlated against the stress intensity factor to predict the proper growth rates.

For the "low cycle fatigue", it is suggested that a crack propagation model based on the plastic deformations around the crack tip mentioned in this report may prove to be more effective.

REFERENCES

1. Folias, E. S., Int. J. Fracture Mechanics, 1, p. 20, (1965).

2. Folias, E. S., ibid, p. 104.

3. Folias, E. S., J. Math. Phys., 44, p. 164, (1965).

4. Head, A. K., Phil. Mag., 44, p. 925, (1953).

5. Frost, N. E., and Dugdale, D. S., J. Mech. Phys. Solids, 6, p. 92, (1958).

6. Liu, H. W., J. Basic Engng., Trans. ASME, 83, p. 23, (1961).

7. Liu, H. W., J. Basic Engng., Trans. ASME, 85, p. 116, (1963).

8. McEvily, A. J., and Illg, W., NACA Tech. Note 4394, (1958).

9. Hardrath, H. F., and McEvily, A. J., Proc. Crack Propagation Symposium, Cranfield, England, (1961).

10. Paris, P. C., ASME Paper No. 62 - Met. - 3.

11. Paris, P. C., and Erdogan, F., J. Basic Engng., Trans. ASME, 85, p. 528, (1963).

12. Paris, P. C., Ph.D. Dissertation, Lehigh University, (1962).

13. Donaldson, D. R., and Anderson, W. E., Proc. Crack Propagation Symposium, Cranfield, England, (1961).

14. Schijve, J., N.L.R., TR M. 2122, Amsterdam, (1964).

15. Erdogan, F., and Roberts, R., Proc. 1st Int. Conf. on Fracture, Sendai, Japan, (1965).

16. Roberts, R., and Erdogan, F., J. Basic Engng., Trans. ASME, 89, p. 885, (1967).

17. Erdogan, F., "Crack Propagation Theories", NASA CR-901, (1967).

18. Dugdale, D. S., J. Mech. Phys. Solids, 8, p. 100, (1960).

19. Forman, R. G., Kearney, V. E., Engle, R. M., J. Basic Engng., Trans. ASME, 89, p. 459, (1967).

20. Marguerre, K., Proc. 5th Cong. Appl. Mech., p. 93, (1938).

21. Feridun, K. K., Ph.D. Dissertation, Lehigh University, (1964).

22. Knowles, J. K., and Wang, N. M., J. Math. Phys., 39, p. 223, (1960).

23. Hartranft, R. J., Ph.D. Dissertation, Lehigh University, (1966).

24. Wilhem, D. P., Paper No. 38 presented at the Annual ASTM Meeting, (1966).

APPENDIX I

Details Of Elastic Solution

The coupled differential equations to be solved are

$$\frac{Eha^2}{R}\frac{\partial^2 W}{\partial x^2} + \nabla^4 F = 0 \tag{I.1}$$

$$\nabla^4 W - \frac{a^2}{RD}\frac{\partial^2 F}{\partial x^2} = 0 \tag{I.2}$$

subject to the following boundary conditions on the crack surface

$$M_y(x,0) = -\frac{D}{a^2}\left[\frac{\partial^2 W}{\partial y^2} + \nu\frac{\partial^2 W}{\partial x^2}\right] = \frac{Dm_o}{a^2} \tag{I.3}$$

$$V_y(x,0) = -\frac{D}{a^3}\left[\frac{\partial^3 W}{\partial y^3} + (2-\nu)\frac{\partial^3 W}{\partial x^2 \partial y}\right] = \frac{Dv_o}{a^3} \tag{I.4}$$

$$N_y(x,0) = \frac{1}{a^2}\frac{\partial^2 F}{\partial x^2} = \frac{n_o}{a^2} \tag{I.5}$$

$$N_{xy}(x,0) = -\frac{1}{a^2}\frac{\partial^2 F}{\partial x \partial y} = \frac{t_o}{a^2} \tag{I.6}$$

and the continuity requirements

$$\lim_{|y|\to o}\left(\frac{\partial^n}{\partial y^n}W^+ - \frac{\partial^n}{\partial y^n}W^-\right) = 0,\ n = 0,1,2,3 \tag{I.7}$$

$$\lim_{|y|\to o}\left(\frac{\partial^n}{\partial y^n}F^+ - \frac{\partial^n}{\partial y^n}F^-\right) = 0,\ n = 0,1,2,3 \tag{I.8}$$

along the prolongation of the crack. Also W and F and their first derivatives must be finite far away from the crack.

For the symmetric case, i.e., $v_o = 0$ and $t_o = 0$, W and F can be represented as

$$W(x,y) = \int_0^\infty w(s,y) \cos xs \, ds \tag{I.9}$$

$$F(x,y) = \int_0^\infty f(s,y) \cos xs \, ds \tag{I.10}$$

If uniform convergence is assumed, then the order of integration and differentiation can be interchanged. Therefore

$$\nabla^4 F = \int_0^\infty [s^4 f - 2s^2 \frac{d^2 f}{dy^2} + \frac{d^4 f}{dy^4}] \cos xs \, ds$$

$$\nabla^4 W = \int_0^\infty [s^4 w - 2s^2 \frac{d^2 w}{dy^2} + \frac{d^4 w}{dy^4}] \cos xs \, ds$$

$$\frac{\partial^2 F}{\partial x^2} = \int_0^\infty - s^2 f \cos xs \, ds$$

$$\frac{\partial^2 W}{\partial x^2} = \int_0^\infty - s^2 w \cos xs \, ds$$

Equations (I.1) and (I.2) can now be written as

$$\int_0^\infty [- \frac{Eha^2}{R} s^2 w + s^4 f - 2s^2 \frac{d^2 f}{dy^2} + \frac{d^4 f}{dy^2}] \cos xs \, ds = 0 \tag{I.11}$$

$$\int_0^\infty [s^4 w - 2s^2 \frac{d^2 w}{dy^2} + \frac{d^4 w}{dy^4} + \frac{a^2 s^2}{RD} f] \cos xs \, ds = 0 \tag{I.12}$$

For the integrals to be zero, the integrands must vanish. Therefore, we have

$$-\frac{Eha^2s^2}{R}w + s^4f - 2s^2\frac{d^2f}{dy^2} + \frac{d^4f}{dy^4} = 0 \qquad (I.13)$$

$$\frac{d^4w}{dy^4} - 2s^2\frac{d^2w}{dy^2} + s^4w + \frac{a^2s^2}{RD}f = 0 \qquad (I.14)$$

the solution of which may be written as

$$w = \sum_1^8 Q_j e^{\Gamma_j y}$$

$$f = \sum_1^8 R'_j e^{\Gamma_j y} \qquad (I.15)$$

where Q_j and R'_j are arbitrary constants and Γ_j are

$$\Gamma_1 = +\sqrt{s(s - \alpha\lambda)}$$

$$\Gamma_2 = -\sqrt{s(s - \alpha\lambda)}$$

$$\Gamma_3 = +\sqrt{s(s + \alpha\lambda)}$$

$$\Gamma_4 = -\sqrt{s(s + \alpha\lambda)}$$

$$\Gamma_5 = + \sqrt{s(s - \beta\lambda)}$$

$$\Gamma_6 = - \sqrt{s(s - \beta\lambda)} \qquad \text{(I.16)}$$

$$\Gamma_7 = + \sqrt{s(s + \beta\lambda)}$$

$$\Gamma_8 = - \sqrt{s(s + \beta\lambda)}$$

$$\alpha = \sqrt{i}, \quad \beta = \sqrt{-i}, \quad \lambda^4 = \frac{12(1-\nu^2)a^4}{R^2h^2}$$

For $|y| \to \infty$, w and f must vanish; therefore, $Q_j = R'_j = 0$ for odd j. The remaining constants are not linearly independent. Thus, substituting equations (I.15) into, say (I.13), we obtain

$$R'_j = \frac{Eha^2s^2}{R} \left[\frac{1}{(s^2 - r_j^2)^2}\right] Q_j \qquad \text{(I.17)}$$

Now substituting the values for Γ_j from equations (I.16) into (I.17), we find

$$R'_{2,4} = - i \sqrt{EhD}\, Q_{2,4}$$

$$\text{(I.18)}$$

$$R'_{6,8} = i \sqrt{EhD}\, Q_{6,8}$$

Letting $Q_{2,4,6,8}$ become $P_{1,2,3,4}$ from equations (I.9), (I.10),

(I.15) and (I.18), we obtain

$$W(x,y^{\pm}) = \int_0^{\infty} (P_1 e^{-\sqrt{s(s - \alpha\lambda)}\,|y|} + P_2 e^{-\sqrt{s(s + \alpha\lambda)}\,|y|}$$

$$+ P_3 e^{-\sqrt{s(s - \beta\lambda)}\,|y|}$$

$$+ P_4 e^{-\sqrt{s(s + \beta\lambda)}\,|y|}) \cos xs\, ds \qquad (I.19)$$

and

$$F(x,y^{\pm}) = - i \sqrt{EhD} \int_0^{\infty} (P_1 e^{-\sqrt{s(s - \alpha\lambda)}\,|y|}$$

$$+ P_2 e^{-\sqrt{s(s + \alpha\lambda)}\,|y|} - P_3 e^{-\sqrt{s(s - \beta\lambda)}\,|y|}$$

$$- P_4 e^{-\sqrt{s(s + \beta\lambda)}\,|y|}) \cos xs\, ds \qquad (I.20)$$

where ± sign refers to $y>0$ and $y<0$, respectively. Equations (I.19) and (I.20) are the same as those obtained by Folias [2]. The procedure to be followed to arrive at the corresponding singular integral equations is then given in [2]. Thus defining

$$u_1(x) = \int_0^{\infty} [\sqrt{s(s - \alpha\lambda)}\, P_1 + \sqrt{s(s + \alpha\lambda)}\, P_2$$

$$+ \frac{\alpha\lambda}{s} \left(\sqrt{s(s - \alpha\lambda)}\, P_1 - \sqrt{s(s + \alpha\lambda)}\, P_2\right)] \cos xs\, ds \tag{I.21}$$

$$u_2(x) = \int_0^\infty [\sqrt{s(s - \alpha\lambda)}\, P_1 + \sqrt{s(s + \alpha\lambda)}\, P_2$$

$$- \frac{\alpha\lambda}{s} \left(\sqrt{s(s - \alpha\lambda)}\, P_1 - \sqrt{s(s + \alpha\lambda)}\, P_2\right)] \cos xs\, ds$$

$$(|x|<1,\ y = 0) \tag{I.22}$$

we obtain

$$\int_{-1}^{1} [u_1(\xi)L_1 + u_2(\xi)L_2]\, d\xi = \frac{2\pi n_o}{i\sqrt{EhD}}\, x;\ |x|<1,\ |\xi|<1 \tag{I.23}$$

$$\int_{-1}^{1} [u_1(\xi)L_3 + u_2(\xi)L_4]\, d\xi = -2\pi m_o x;\ |x|<1,\ |\xi|<1 \tag{I.24}$$

where the kernels L_1, L_2, L_3, and L_4 are ($\zeta = x - \xi$)

$$L_1 = \alpha\lambda \sin\left(\frac{\alpha\lambda\zeta}{2}\right)K_o\left(\frac{\beta\lambda|\zeta|}{2}\right) + \frac{\beta\lambda\zeta}{|\zeta|} \cos\left(\frac{\alpha\lambda\zeta}{2}\right)K_1\left(\frac{\beta\lambda|\zeta|}{2}\right)$$

$$+ \nu_o\beta\lambda \sin\left(\frac{\beta\lambda\zeta}{2}\right)K_o\left(\frac{\alpha\lambda|\zeta|}{2}\right) + \frac{\nu_o\alpha\lambda\zeta}{|\zeta|} \cos\left(\frac{\beta\lambda\zeta}{2}\right)K_1\left(\frac{\alpha\lambda|\zeta|}{2}\right)$$

$$- \frac{\beta}{2\alpha|\zeta|} \sin\left(\frac{\alpha\lambda\zeta}{2}\right)K_1\left(\frac{\beta\lambda|\zeta|}{2}\right)$$

$$- \frac{(2\nu_o+1)\alpha}{2\beta|\zeta|} \sin\left(\frac{\beta\lambda\zeta}{2}\right)K_1\left(\frac{\alpha\lambda|\zeta|}{2}\right) \tag{I.25}$$

$$L_2 = (\nu_o - 1)\ \beta\lambda\ \sin\left(\frac{\beta\lambda\zeta}{2}\right)K_o\left(\frac{\alpha\lambda|\zeta|}{2}\right)$$

$$+ (\nu_o - 1)\ \frac{\alpha\lambda\zeta}{|\zeta|}\ \cos\left(\frac{\beta\lambda\zeta}{2}\right)K_1\left(\frac{\alpha\lambda|\zeta|}{2}\right)$$

$$+ \frac{\beta}{2\alpha|\zeta|}\ \sin\left(\frac{\alpha\lambda\zeta}{2}\right)K_1\left(\frac{\beta\lambda|\zeta|}{2}\right)$$

$$- \propto \frac{(2\nu_o - 1)}{2\beta|\zeta|}\ \sin\left(\frac{\beta\lambda\zeta}{2}\right)K_1\left(\frac{\alpha\lambda|\zeta|}{2}\right) \qquad \text{(I.26)}$$

$$L_3 = (\nu_o - \tfrac{3}{2})\ \alpha\lambda\ \left[\sin\left(\frac{\alpha\lambda\zeta}{2}\right)K_o\left(\frac{\beta\lambda|\zeta|}{2}\right)\right]$$

$$+ (\nu_o - \tfrac{1}{2})\ \frac{\beta\lambda\zeta}{|\zeta|}\ \left[\cos\left(\frac{\alpha\lambda\zeta}{2}\right)K_1\left(\frac{\beta\lambda|\zeta|}{2}\right)\right]$$

$$+ \beta\lambda\ (-\nu_o^2 + \nu_o - \tfrac{1}{2})\ \left[\sin\left(\frac{\beta\lambda\zeta}{2}\right)K_o\left(\frac{\alpha\lambda|\zeta|}{2}\right)\right]$$

$$+ \frac{\alpha\lambda\zeta}{|\zeta|}\ (-\nu_o^2 + \nu_o + \tfrac{1}{2})\ \left[\cos\left(\frac{\beta\lambda\zeta}{2}\right)K_1\left(\frac{\alpha\lambda|\zeta|}{2}\right)\right]$$

$$- \nu_o\ \frac{\beta}{2\alpha|\zeta|}\ \left[\sin\left(\frac{\alpha\lambda\zeta}{2}\right)K_1\left(\frac{\beta\lambda|\zeta|}{2}\right)\right]$$

$$+ (2\nu_o^2 + \nu_o)\ \frac{\alpha}{2\beta|\zeta|}\ \left[\sin\left(\frac{\beta\lambda\zeta}{2}\right)K_1\left(\frac{\alpha\lambda|\zeta|}{2}\right)\right] \qquad \text{(I.27)}$$

$$L_4 = \frac{\beta\lambda\zeta}{2|\zeta|}\ \left[\cos\left(\frac{\alpha\lambda\zeta}{2}\right)K_1\left(\frac{\beta\lambda|\zeta|}{2}\right)\right]$$

$$+ \frac{\beta\lambda}{2}\ (4\nu_o - 3 - 2\nu_o^2)\ \left[\sin\left(\frac{\beta\lambda\zeta}{2}\right)K_o\left(\frac{\alpha\lambda|\zeta|}{2}\right)\right]$$

$$+ \frac{\alpha\lambda\zeta}{2|\zeta|}(4\nu_o - 2\nu_o^2 - 1)\left[\cos\left(\frac{\beta\lambda\zeta}{2}\right)K_1\left(\frac{\alpha\lambda|\zeta|}{2}\right)\right]$$

$$+ \frac{\alpha}{2\beta|\zeta|}(2\nu_o^2 - \nu_o)\left[\sin\left(\frac{\beta\lambda\zeta}{2}\right)K_1\left(\frac{\alpha\lambda|\zeta|}{2}\right)\right]$$

$$+ \frac{\beta\nu_o}{2\alpha|\zeta|}\left[\sin\left(\frac{\alpha\lambda\zeta}{2}\right)K_1\left(\frac{\beta\lambda|\zeta|}{2}\right)\right]$$

$$- \frac{\alpha\lambda}{2}\left[\sin\left(\frac{\alpha\lambda\zeta}{2}\right)K_o\left(\frac{\beta\lambda|\zeta|}{2}\right)\right] \qquad (I.28)$$

In the foregoing equations, $\nu_o = 1 - \nu$ and K_n is a Bessel function of the third kind of order n.

The solutions $u_1(x)$ and $u_2(x)$ must be Hölder continuous for some positive Hölder indices μ_1, and μ_2 for all x in the closed interval (-1,1), and $u_1(x)$ and $u_2(x)$ are bounded near the ends of the crack. These details are discussed in [1].

The kernels can now be written in series form. Folias eliminates all terms of order λ^4 and greater in his series expansions which puts a severe limitation on the useful range of λ. In this report, polynomial approximations of the Bessel functions are used which contain terms up to λ^{24}, and are good for $\lambda<2$. The sine and cosine series are expanded up to terms of λ^{26} with corresponding errors of 2.5×10^{-8} and 3.2×10^{-9} respectively, for $\lambda<2$. This is in the range of error for the Bessel functions. The Bessel functions are regular throughout the $(x-\xi)$ plane, cut along the negative real axis. Multiplying

all series together that are now present in the kernel and collecting terms, the integral equations can now be written in the form

$$-\frac{i2\pi n_o x}{(EhD)^{1/2}} = \int_{-1}^{1} \frac{(1+\nu_o)u_1(\xi) + (\nu_o-1)u_2(\xi)}{(x-\xi)}\, d\xi$$

$$+ \lambda \int_{-1}^{1} \{[(1+\nu_o)u_1(\xi)$$

$$+ (\nu_o-1)u_2(\xi)] \left[\sum_{0}^{13} D_m \lambda^{2m+1}(x-\xi)^{2m+1}\right.$$

$$\left. + \sum_{0}^{6} H_b \lambda^{4b+3}(x-\xi)^{4b+3} \log \frac{\lambda|x-\xi|}{4}\right]$$

$$+ i[u_1(\xi) + u_2(\xi)] \left[(1-\nu_o)\left[\sum_{0}^{13} E_m \lambda^{2m+1}(x-\xi)^{2m+1}\right.\right.$$

$$\left. + \sum_{0}^{6} L_n \lambda^{4b+1}(x-\xi)^{4b+1} \log \frac{\lambda|x-\xi|}{4}\right]$$

$$+ \nu_o \left[\sum_{0}^{13} G_m \lambda^{2m+1}(x-\xi)^{2m+1}\right.$$

$$\left.\left. + \sum_{0}^{6} M_b \lambda^{4b+1}(x-\xi)^{4b+1} \log \frac{\lambda|x-\xi|}{4}\right]\right\}\, d\xi \qquad (I.29)$$

and

$$
\begin{aligned}
-2\pi m_o x = & \int_{-1}^{1} \frac{(4\nu_o-\nu_o^2)[u_1(\xi) + u_2(\xi)]}{x-\xi}\, d\xi \\
& + \lambda \int_{-1}^{1} \{[u_1(\xi) + u_2(\xi)] \Big[\sum_{0}^{13} [(2\nu_o-\nu_o^2-2)N_m \\
& + (2\nu_o-\nu_o^2)Q_m + \nu_o^2 R_m] \lambda^{2m+1}(x-\xi)^{2m+1} \\
& + \sum_{0}^{6} [(2\nu_o-\nu_o^2-2)V_b + (2\nu_o-\nu_o^2)W_b \\
& + \nu_o^2 Y_b] \lambda^{4b+3}(x-\xi)^{4b+3} \log \frac{\lambda|x-\xi|}{4}] \\
& + i\{[(\nu_o^2-1)u_1(\xi) + (1-2\nu_o+\nu_o^2)u_2(\xi)]\cdot \\
& \cdot [\sum_{0}^{13} E_m \lambda^{2m+1}(x-\xi)^{2m+1} \\
& + \sum_{0}^{6} L_b \lambda^{4b+1}(x-\xi)^{4b+1} \log \frac{\lambda|x-\xi|}{4}] \\
& + [(-\nu_o^2-\nu_o)u_1(\xi) + (\nu_o-\nu_o^2)u_2(\xi)]\cdot \\
& \cdot [\sum_{0}^{13} G_m \lambda^{2m+1}(x-\xi)^{2m+1}
\end{aligned}
$$

$$+ \sum_{0}^{6} M_b \lambda^{4b+1} (x-\xi)^{4b+1} \log \frac{\lambda|x-\xi|}{4}]\}\} \, d\xi \qquad (I.30)$$

where the constants D_m, H_b, etc., are listed in Appendix III. These constants are independent of the shell parameters and materials constants.

The unique solution of (I.29) and (I.30) are of the form

$$u_1(\xi) = \sqrt{1 - \xi^2} \sum_{p=o}^{\infty} A_p \lambda^{2p} (1-\xi^2)^p; \quad |\xi|<1 \qquad (I.31)$$

$$u_2(\xi) = \sqrt{1 - \xi^2} \sum_{p=o}^{\infty} B_p \lambda^{2p} (1-\xi^2)^p; \quad |\xi|<1 \qquad (I.32)$$

where A_p and B_p are, generally, complex functions of λ.

Substitution of (I.31) and (I.32) into (I.29) and (I.30) leads to the following integrals which have to be evaluated:

$$I_p(x) = C.P.V. \int_{-1}^{1} \frac{(1-\xi^2)^{p+1/2} d\xi}{x-\xi}$$

$$I_{pn}(x) = \int_{-1}^{1} (1-\xi^2)^{p+1/2} (x-\xi)^n d\xi \qquad (I.33)$$

$$J_{pn}(x) = \int_{-1}^{1} (1-\xi^2)^{p+1/2} (x-\xi)^n \log |x-\xi| \, d\xi$$

where n is an odd integer.

Through contour integration and using a table of integrals, we obtain

$$I_p(x) = \frac{\pi}{2p+3} \sum_{s=o}^{p} \frac{(-1)^s}{2!2^s} \prod_{b=o}^{s} (2p+3-2b)x^{2p+1-2s} \qquad (I.34)$$

$$I_{pn}(x) = \pi \prod_{s=o}^{p} \frac{(2p+1-2s)}{(2p+2-2s)} [x^n$$

$$+ \sum_{r=1}^{q} \frac{n!}{(n-2r)!(2r)!} \prod_{b=1}^{r} \frac{(2b-1)}{(2p+2+2b)} x^{n-2r}] \qquad (I.35)$$

where $q = (n-1)/2$ for odd n and $q = n/2$ for even n. $J_{pn}(x)$ can be determined by first considering, for $n = 0$,

$$J_{po}(x) = \int_{-1}^{1} (1-\xi^2)^{p+1/2} \log |x-\xi| \, d\xi$$

Differentiating with respect to x, we have

$$J'_{po}(x) = \text{C.P.V.} \int_{-1}^{1} (1-\xi^2)^{p+1/2} \frac{d\xi}{x-\xi} = I_p(x)$$

where $I_p(x)$ is known. Integrating $I_p(x)$ in x gives $J_{po}(x)$ plus a constant of integration, or

$$J_{po}(x) = \frac{\pi}{2p+3} \sum_{s=o}^{p} \frac{(-1)^s}{s!2^s} \prod_{b=o}^{s} \frac{(2p+3-2b)}{(2p+2-2s)} x^{2p+2-2s} + J_{po}(0)$$

(I.36)

$$J_{pn}(0) = \int_{-1}^{1} (1-\xi^2)^{p+1/2} \xi^n \log |\xi| \, d\xi$$

$$= -\pi \sum_{r=o}^{p} \frac{p!(-1)^r(2r+n-1)!}{r!(p-r)!2^{4+n/2+1}(r+n/2+1)!} \left[\frac{1}{2r+n+2}\right.$$

$$\left. + \log 2 + \sum_{k=1}^{2r+n} \frac{(-1)^k}{k}\right] \quad \text{for n even} \qquad (I.37)$$

$J_{pn}(0) = 0$, for n odd.

Letting now n = 1 in $J_{pn}(x)$ and differentiating with respect to x, we find

$$J'_{p1}(x) = \int_{-1}^{1} (1-\xi^2)^{p+1/2} d\xi + \int_{-1}^{1} (1-\xi^2)^{p+1/2} \log |x-\xi| \, d\xi$$

But from (I.35)

$$\int_{-1}^{1} (1-\xi^2)^{p+1/2} d\xi = I_{po}(x) = \pi \prod_{s=o}^{p} \frac{(2p+1-2s)}{(2p+2-2s)}$$

Hence,

$$J'_{p1}(x) = I_{po}(x) + J_{po}(x)$$

$$J_{p1}(x) = \int I_{po}(x)dx + \int J_{po}(x)dx + J_{p1}(0)$$

Or, in general, we obtain

$$J_{pn}(x) = \int I_{p(n-1)}(x)dx + n\int J_{p(n-1)}(x)dx$$

$$+ J_{pn}(0) \qquad (I.38)$$

Therefore, $J_{pn}(x)$ can be reduced to a combination of $I_p(x)$, $I_{pn}(x)$ and $J_{pn}(0)$.

With the integrals given by (I.33) known, (I.29) and (I.30) can be written in series form in odd powers of x. The contributions of $I_p(x)$, $I_{pn}(x)$ and $J_{pn}(x)$ to each coefficient of x^{2m+1}, where m = 0,1,..., 13, are given below.

For $I_p(x)$

$$x \to \pi \frac{(-1)^p}{p!2^p} \prod_{s=o}^{p} \frac{(2p+3-2s)}{2p+3}$$

$$x^3 \to \pi \frac{(-1)^{p-1}}{(p-1)!2^{p-1}} \prod_{s=o}^{p-1} \frac{(2p+3-2s)}{2p+3}$$

.

.

.

$$x^{2m+1} \to \pi \frac{(-1)^{p-m}}{(p-m)!2^{p-m}} \prod_{s=o}^{p-m} \frac{(2p+3-2s)}{2p+3}$$

For $I_{pn}(x)$

$$x \to \pi \prod_{s=o}^{p} \frac{(2p+1-2s)}{(2p+2-2s)} \left[C_o + \sum_{n=1}^{13} C_n(2n+1) \prod_{b=1}^{n} \frac{(2n+1-2b)}{(2p+2+2b)}\right]$$

$$x^3 \to \pi \prod_{s=o}^{p} \frac{(2p+1-2s)}{(2p+2-2s)} \left[C_1 + \sum_{n=2}^{13} C_n \frac{(2n+1)(2n)(2n-1)}{3!} \prod_{b=2}^{n} \frac{(2n+1-2b)}{(2p+2b)}\right]$$

$$x^5 \to \pi \prod_{s=o}^{p} \frac{(2p+1-2s)}{(2p+2-2s)} \left[C_2 + \sum_{n=3}^{13} C_n \frac{(2n+1)\cdots(2n-3)}{5!} \prod_{b=3}^{n} \frac{(2n+1-2b)}{(2p-2+2b)}\right]$$

.

.

.

$$x^{2m+1} \to \pi \prod_{s=o}^{p} \frac{(2p+1-2s)}{(2p+2-2s)} \left[C_m + \sum_{n=m=1}^{13} C_n \frac{\prod_{r=1}^{2m+1}(2n+r-2m)}{(2m+1)!} \prod_{b=m+1}^{n} \frac{(2n+1-2b)}{(2p+2+2b-2m)}\right]$$

where C_n are appropriate constants D_m, E_m, etc.

For $J_{pn}(x)$

$$x \to -\sum_{s=0}^{p} \pi \sum_{n=0}^{13} C_n \frac{p!(-1)^s}{s!(p-s)!} \frac{(2s+2n-1)!!(2n+1)}{2^{s+n+1}(s+n+1)!} \left\{\frac{1}{2s+2n+2}\right.$$

$$\left. + \log 2 + \sum_{k=1}^{2s+2n} \frac{(-1)^k}{k}\right\} + \pi \prod_{s=0}^{p} \frac{2p+1-2s}{2p+2-2s} \left[C_o\right.$$

$$\left. + \sum_{n=1}^{13} \prod_{b=1}^{n} C_n \left[\frac{2n+1-2b}{2p+2+2b}\right]\right] = \sum_{n=0}^{13} C_n A_{np}$$

letting $\sum_{n=1}^{13} C_n A_{(n-1)p} = B_{1p}$

$$x^3 \to B_{1p} + \pi \frac{(-1)^p}{p!2^p} \prod_{s=0}^{p} C_o \frac{(2p+3-2s)}{(2p+3)2.3} + \frac{\pi}{2.3} \prod_{s=0}^{p} \frac{(2p+1-2s)}{(2p+2-2s)} \left[3C_1\right.$$

$$\left. + \sum_{n=2}^{13} C_n(2n+1) \prod_{b=2}^{n} \frac{(2n-1)(2n+1-2b)}{2p+2b}\right]$$

$$+ \frac{\pi}{3} \prod_{s=0}^{p} \frac{(2p+1-2s)}{(2p+2-2s)} \left[C_1 + \sum_{n=2}^{13} C_n \frac{(2n)(2n-1)}{1.2} \prod_{b=2}^{n} \frac{(2n+1-2b)}{(2p+2b)}\right]$$

$$= \sum_{n=1}^{13} C_n D_{np} + C_o E_{np}$$

letting $\sum_{n=2}^{13} C_n D_{(n-1)p} = B_{2p}$

$$x^5 \to B_{2p} + C_o \frac{\pi(-1)^{p-1}}{(p-1)!2^{p-1}} \prod_{s=o}^{p-1} \frac{(2p+3-2s)}{(2p+3)4.5} + C_1 \pi \frac{(-1)^p}{p!2^p} \prod_{s=o}^{p} \frac{(2p+3-2s)2.3}{(2p+3)5!}$$

$$+ \frac{\pi}{4.5} \prod_{s=o}^{p} \frac{(2p+1-2s)}{(2p+2-2s)} [5C_2$$

$$+ \sum_{n=3}^{13} C_n(2n+1) \frac{(2n-1)(2n-2)(2n-3)}{1.2.3}$$

$$\cdot \prod_{b=3}^{n} \frac{(2n+1-2b)}{(2p+2b-2)}] + \frac{\pi}{5} \prod_{s=o}^{p} \frac{(2p+1-2s)}{(2p+2-2s)} [C_2$$

$$+ \sum_{n=3}^{13} C_n \frac{(2n)(2n-1)(2n-2)(2n-3)}{4!} \prod_{b=3}^{n} \frac{(2n+1-2b)}{(2p+2b-2)}]$$

$$= \sum_{n=2}^{13} C_n F_{np} + \sum_{n=o}^{1} C_n G_{np}$$

letting $\sum_{n=3}^{13} C_n F_{(n-1)p} = B_{3p}$

$$x^7 \to B_{3p} + \sum_{r=o}^{2} \pi \frac{(-1)^{p-r}}{(p-r)!2^{p-r}} C_{(2-r)} \prod_{s=o}^{p-r} \frac{(2p+3-2s)(5-2r)!}{(2p+3)7!} (2r+1)!$$

$$+ \frac{\pi}{6.7} \prod_{s=o}^{p} \frac{(2p+1-2s)}{(2p+2-2s)} [7C_3$$

$$+ \sum_{n=4}^{13} C_n(2n+1) \frac{(2n-1)\cdots\cdot(2n-5)}{5!} \prod_{b=4}^{n} \frac{(2n+1-2b)}{(2p-4+2b)}]$$

$$+ \frac{\pi}{7} \prod_{s=o}^{p} \frac{(2p+1-2s)}{(2p+2-2s)} [C_3 + \sum_{n=4}^{13} C_n \frac{(2n)\cdots\cdot(2n-5)}{6!} \prod_{b=4}^{n} \frac{(2n+1-2b)}{(2p-4+2b)}]$$

etc., where C_n are appropriate constants H_b, L_b, etc.

By comparing coefficients of x in the resultant series form of (I.29) and (I.30), a system of 2p + 2 simultaneous equations can be formed to solve for A_p and B_p. As the number of simultaneous equations increases, the value for a particular A_p or B_p converges to its exact value. Since the stresses at the crack tip are desired, it is necessary only to compute the coefficients A_o and B_o.

The computer programs for comparing coefficients are given in Appendix IV. For the first program (coefficients of x^n) the

range and increment of λ must be established along with the maximum number of simultaneous equations desired. The card output of the first program becomes the input of the second program. For the second program (solution for P_e and P_b') the values of ν and m_o must first be established. This way, the output of the first program can be used for various values of ν. The output of the second program gives the values of A_o, B_o, P_b' and P_e. P_b' and P_e are designated as P10A and RP20A, respectively, in the program.

From (21-24) and

$$\int_0^\infty s^{-\mu} J_\mu(gs)\cos xs\, ds =$$

$$\begin{cases} \sqrt{\pi}(2g)^{-\mu}[\Gamma(\mu+1/2)]^{-1}(g^2-x^2)^{\mu-1/2}; & 0<x<g \\ & ; \ \mathrm{Re}\,\mu > -1/2 \\ 0 & ; \ g<x<\infty \end{cases}$$

we obtain

$$4P_1(s) = \frac{J_1(s)}{\sqrt{s(s-\alpha\lambda)}}\left[\frac{A_o+B_o}{s} + \frac{A_o-B_o}{\alpha\lambda}\right] + \ldots \qquad (I.39)$$

$$4P_2(s) = \frac{J_1(s)}{\sqrt{s(s+\alpha\lambda)}}\left[\frac{A_o+B_o}{s} - \frac{A_o-B_o}{\alpha\lambda}\right] + \ldots \qquad (I.40)$$

$$\sqrt{s(s-\lambda\beta)}\, P_3(s) = -\left(\frac{\nu_o s}{\beta\lambda} - \frac{1}{2}\right) \frac{A_o+B_o}{2} \frac{J_1(s)}{s}$$

$$- \frac{\alpha}{2\beta} \left(\frac{A_o-B_o}{2}\right) \frac{J_1(s)}{\alpha\lambda} + \ldots \qquad \text{(I.41)}$$

$$\sqrt{s(s+\lambda\beta)}\, P_4(s) = \left(\frac{\nu_o s}{\beta\lambda} + \frac{1}{2}\right) \left(\frac{A_o+B_o}{2}\right) \frac{J_1(s)}{s}$$

$$- \frac{\alpha}{2\beta} \left(\frac{A_o-B_o}{2}\right) \frac{J_1(s)}{\alpha\lambda} + \ldots \qquad \text{(I.42)}$$

The stresses may then be obtained by a) substituting equations (139) through (142) into equations (19) and (20); b) substituting the result into the boundary conditions, equations (3) through (6); and c) changing the order of integration and differentiation.

APPENDIX II

Crack Growth Data

Shell #9 - 6063-T6

Mean stress = 6850 psi
Stress range = 6300 psi

2a	Δn
0.28620	0,000
0.30610	3,000
0.32310	2,000
0.33470	2,000
0.35820	2,000
0.38300	2,000
0.40640	1,500
0.42420	1,000
0.43060	1,000
0.44905	1,000
0.46365	1,000
0.47835	1,000
0.49540	1,000
0.51085	1,000
0.53320	1,000
0.55655	1,000
0.58300	1,000
0.62025	1,000
0.64550	600
0.67170	600
0.69660	600
0.74250	600
0.76110	300
0.79300	300
0.83430	300
0.87125	300
0.91830	300
0.96850	300
1.00325	200
1.05730	200
1.08470	100
1.12240	100
1.15820	100
1.20280	100
1.26430	100
1.32980	75
1.38800	45
1.42360	30
1.46950	30
1.49250	30
1.56720	30
1.64260	30

Shell #10 - 6063-T6

Mean stress = 7220 psi
Stress range = 6770 psi

2a	Δn
0.31280	0,000
0.34320	3,000
0.36270	2,000
0.38400	2,000
0.41310	2,000
0.44970	2,000
0.49010	1,000
0.52250	1,000
0.55050	1,000
0.60010	1,000
0.63720	600
0.69000	600
0.75670	600
0.82720	600
0.89240	300
0.94890	200
1.03220	200
1.11260	100
1.17960	100
1.21130	100

Shell #11 - 6063-T6

Mean stress = 3590 psi
Stress range = 3370 psi

2a	Δn
0.28900	0,000
0.29320	6,000
0.29850	6,000
0.29960	6,000
0.30280	6,000
0.30560	6,000
0.30800	6,000
0.31280	6,000
0.31620	6,000
0.32330	6,000
0.32530	6,000
0.32610	6,000
0.33040	6,000
0.33700	6,000
0.34010	6,000
0.34440	6,000
0.34630	12,000
0.34910	6,000
0.35320	6,000
0.35370	12,000
0.36630	6,000
0.36980	6,000
0.37010	6,000
0.37450	6,000
0.37600	6,000
0.38270	6,000
0.38400	6,000
0.38810	6,000
0.39470	6,000
0.40090	6,000
0.40440	6,000
0.40860	6,000
0.41380	6,000
0.42080	6,000
0.42720	6,000
0.43770	6,000
0.45300	12,000
0.46310	6,000
0.47300	6,000
0.47910	6,000
0.48430	6,000
0.49510	6,000
0.50460	6,000

Shell #11 cont.

2a	Δn
0.51730	6,000
0.52220	6,000
0.54410	6,000
0.55770	6,000
0.56610	6,000
0.57430	6,000
0.58610	6,000
0.59560	6,000
0.60880	6,000
0.62840	6,000
0.64720	6,000
0.66160	6,000
0.68450	6,000
0.70430	6,000
0.72880	6,000
0.75840	6,000
0.83490	6,000
0.87040	6,000
0.92110	6,000
0.94750	3,000
0.97910	3,000
1.02800	3,000
1.05350	3,000
1.10690	3,000
1.15780	3,000
1.22710	3,000
1.25570	1,000
1.28530	1,000
1.32240	1,000
1.35580	1,000
1.39430	1,000
1.44950	1,000
1.53580	1,000
1.58210	600
1.65430	600
1.75300	600
1.88270	600
2.00240	312

Shell #12 - 6063-T6

Mean stress = 5370 psi
Stress range = 5040 psi

2a	Δn
0.33450	0,000
0.34220	1,500
0.34420	1,500
0.35240	1,500
0.35480	1,500
0.36340	1,500
0.37090	1,500
0.37800	1,500
0.38740	1,500
0.39510	1,500
0.40070	1,500
0.41290	3,000
0.41620	1,500
0.41750	1,500
0.42060	1,500
0.42300	1,500
0.42520	1,500
0.42560	1,500
0.42850	1,500
0.42930	1,500
0.42980	1,500
0.43320	3,000
0.43690	1,500
0.44070	1,500
0.44270	1,500
0.44640	1,500
0.44710	1,500
0.44860	1,500
0.45370	1,500
0.45730	1,500
0.45940	1,500
0.46560	1,500
0.46940	1,500
0.47580	1,500
0.47880	1,500
0.48920	1,500
0.49790	1,500
0.50750	1,500
0.51480	1,500
0.52130	1,500
0.53130	1,500
0.53970	1,500
0.55170	1,500

Shell #12 cont.

2a	Δn
0.56040	1,500
0.56770	1,500
0.57930	1,500
0.59360	1,500
0.60710	1,500
0.62290	1,500
0.65300	1,500
0.65980	1,000
0.66890	1,000
0.68900	1,000
0.69620	1,000
0.70560	1,000
0.72300	1,000
0.78370	1,000
0.79750	1,000
0.81930	1,000
0.85630	1,000
0.88090	1,000
0.91360	1,000
0.94950	1,000
1.00120	1,000
1.09680	1,000
1.18510	600
1.21030	150
1.24630	150
1.30530	150
1.38350	150
1.44970	100
1.48700	100
1.55740	100
1.67910	100

Shell #13 - 6063-T6

Mean stress = 11080 psi
Stress range = 3400 psi

2a	Δn
0.51790	0,000
0.52680	2,000
0.53760	2,000
0.54700	2,000
0.55740	2,000
0.58920	2,000
0.59870	2,000
0.60770	2,000
0.61640	2,000
0.62810	2,000
0.64240	2,000
0.65850	2,000
0.67170	2,000
0.68820	2,000
0.70370	2,000
0.72050	2,000
0.73160	2,000
0.74890	2,000
0.76630	2,000
0.78440	2,000
0.81170	2,000
0.83320	2,000
0.85840	2,000
0.88040	1,500
0.90100	1,500
0.92500	1,500
0.95730	1,500
0.98810	1,500
1.02400	1,500
1.05530	1,000
1.08860	1,000
1.13280	1,000
1.17450	1,000
1.24830	1,000
1.30170	600
1.40980	300
1.44390	300
1.48710	300
1.53030	300
1.56740	200
1.60530	200
1.62170	100
1.64340	100
1.67250	100
1.69460	100

Shell #14 - 6063-T6

Mean stress = 5460 psi
Stress range = 5070 psi

2a	Δn
0.28800	0,000
0.30380	3,000
0.31530	3,000
0.32990	3,000
0.34250	3,000
0.35640	3,000
0.37490	3,000
0.39010	3,000
0.43630	3,000
0.46130	3,000
0.48830	3,000
0.51920	3,000
0.55080	3,000
0.59870	3,000
0.66260	3,000
0.74190	1,500
0.80430	1,500
0.84530	1,000
0.89250	1,000
0.95310	1,000
1.02590	900
1.11490	600
1.21180	600
1.39390	600
1.43850	100
1.51110	100
1.61260	60

Shell #15 - 6063-T6

Mean stress = 8420 psi
Stress range = 5120 psi

2a	Δ n
0.28130	0,000
0.29500	3,000
0.30880	3,000
0.32070	3,000
0.33390	3,000
0.35100	3,000
0.36650	3,000
0.39070	3,000
0.41720	3,000

Shell #15 cont.

2a	Δn
0.44460	3,000
0.47680	3,000
0.51440	3,000
0.55910	3,000
0.61560	3,000
0.64430	1,500
0.68910	1,500
0.72360	1,500
0.79160	1,500
0.85290	1,500
0.91370	1,000
0.97620	1,000
1.08060	1,000
1.15850	600
1.24910	600
1.33480	300
1.42010	200
1.45870	100
1.48930	60
1.50910	60

Shell #18 - 6063-T6

Mean stress = 5350 psi
Stress range = 5070 psi

2a	Δn
0.28820	0,000
0.30200	3,000
0.30970	3,000
0.32320	3,000
0.33930	3,000
0.35550	3,000
0.37220	3,000
0.38340	3,000
0.39370	3,000
0.40900	3,000
0.42080	3,000
0.43850	3,000
0.45520	3,000
0.47400	3,000
0.49440	3,000
0.51450	3,000
0.53510	3,000

Shell #18 cont.

2a	Δn
0.56170	3,000
0.58920	3,000
0.62890	3,000
0.67040	3,000
0.72020	3,000
0.75680	1,500
0.80430	1,500
0.85100	1,500
0.93120	1,500
1.02170	1,000
1.17970	1,000
1.37290	600
1.59050	150

Shell #19 - SAE 1018 Steel

Mean stress = 7000 psi
Stress range = 7000 psi

2a	Δn
0.32575	0,000
0.32635	6,000
0.32645	6,000
0.32720	6,000
0.32755	12,000
0.32800	6,000
0.32830	6,000
0.33080	6,000
0.33455	12,000
0.33655	6,000
0.33925	4,000

Mean stress= 7500 psi
Stress range= 7500 psi

2a	Δn
0.33925	00,000
0.34070	12,000
0.34395	12,000
0.34425	12,000
0.34660	12,000
0.34915	6,000
0.35880	6,000

APPENDIX III

$D_m = N_m + Q_m - R_m$

$H_n = V_n + W_n - Y_n$

m	E_m	G_m	N_m
0	$-5.5791176 \times 10^{-1}$	$-5.1318632 \times 10^{-2}$	$-3.9269908 \times 10^{-1}$
1	7.1585753×10^{-2}	7.1585759×10^{-3}	1.1866800×10^{-3}
2	$-1.5027655 \times 10^{-3}$	$-1.4570399 \times 10^{-4}$	1.6106839×10^{-3}
3	$-6.1278490 \times 10^{-5}$	$-3.4002697 \times 10^{-6}$	$-2.9019260 \times 10^{-5}$
4	8.8787107×10^{-7}	4.4362985×10^{-8}	$-4.0143251 \times 10^{-7}$
5	6.3429898×10^{-9}	$2.4395960 \times 10^{-10}$	$-1.8654274 \times 10^{-10}$
6	$-6.0045804 \times 10^{-11}$	$-2.1138323 \times 10^{-12}$	$1.9537601 \times 10^{-11}$
7	$-1.6814260 \times 10^{-13}$	$-4.9414796 \times 10^{-15}$	$-1.5540472 \times 10^{-13}$
8	$1.1431171 \times 10^{-15}$	$2.8896248 \times 10^{-17}$	$-3.0005865 \times 10^{-16}$
9	$1.5924912 \times 10^{-18}$	$3.6827901 \times 10^{-20}$	$1.8927971 \times 10^{-18}$
10	$-7.4005562 \times 10^{-21}$	$-1.0961288 \times 10^{-22}$	$1.6359083 \times 10^{-21}$
11	$-5.2590588 \times 10^{-24}$	$-9.0371123 \times 10^{-26}$	$-7.4051638 \times 10^{-24}$
12	$1.2557491 \times 10^{-26}$	0.0	$-2.2267587 \times 10^{-27}$
13	$2.8131237 \times 10^{-30}$	0.0	0.0

m	Q_m	R_m
0	1.9634954×10^{-1}	$-9.8174770 \times 10^{-2}$
1	$-2.3651856 \times 10^{-3}$	$-1.7050709 \times 10^{-3}$
2	1.3422335×10^{-3}	2.1092260×10^{-4}
3	$-2.4743023 \times 10^{-5}$	$-3.4679912 \times 10^{-6}$
4	$-3.6127755 \times 10^{-7}$	$-3.4668622 \times 10^{-8}$
5	4.2211942×10^{-9}	$3.6464548 \times 10^{-10}$
6	$1.8149490 \times 10^{-11}$	$1.2562638 \times 10^{-12}$
7	$-1.4354576 \times 10^{-13}$	$-9.0591396 \times 10^{-15}$
8	$-2.8357870 \times 10^{-16}$	$-1.5243436 \times 10^{-17}$
9	$1.4685126 \times 10^{-18}$	$6.7308017 \times 10^{-20}$
10	$1.7197282 \times 10^{-21}$	$6.7792208 \times 10^{-23}$
11	$-4.3214861 \times 10^{-24}$	$-1.0959706 \times 10^{-25}$
12	$-3.5201050 \times 10^{-27}$	$-7.8767464 \times 10^{-29}$
13	0.0	0.0

n	L_n	M_n	V_n
0	-7.5000000×10^{-1}	-1.2500000×10^{-1}	-5.2083315×10^{-2}
1	3.7597711×10^{-3}	2.6855499×10^{-4}	4.1561584×10^{-5}
2	-9.7111261×10^{-7}	-4.4141460×10^{-8}	-4.2136356×10^{-9}
3	4.7984694×10^{-11}	1.5995248×10^{-12}	1.1054316×10^{-13}
4	-7.4311015×10^{-16}	-1.9408545×10^{-17}	-1.0269010×10^{-18}
5	4.2725291×10^{-21}	8.6315720×10^{-23}	3.0250342×10^{-24}
6	-7.3171341×10^{-27}	-1.0028985×10^{-28}	0.0

n	W_n	Y_n
0	-3.9062497×10^{-2}	-9.1145820×10^{-3}
1	-3.8625199×10^{-9}	4.3293579×10^{-6}
2	-3.8571553×10^{-9}	-3.1061901×10^{-10}
3	1.0354265×10^{-13}	6.2916872×10^{-15}
4	-1.0007218×10^{-18}	-4.6890740×10^{-20}
5	3.6710074×10^{-25}	1.1506409×10^{-25}
6	-3.5817803×10^{-30}	0.0

APPENDIX IV

```
005 2021   CATANACH   COEFFICIENTS OF X
AUG 29 67      14 47.3
```



```
#     SEQ  LABL TYP                STATEMENT                                  C ZERO   NOT 0   PLUS   MINUS   FLSE
001.             FIXP,M,S,N,B,U,V,A,R,SIZE,MR                                 [  ]    [  ]    [  ]   [  ]    [  ]
002.             FIXC,D,F,FMAX                                                [  ]    [  ]    [  ]   [  ]    [  ]
003.                $ FMAX IS THE NUMBER OF INCREMENTS OF LA                   [  ]    [  ]    [  ]   [  ]    [  ]
004.                FMAX=7                                                    [  ]    [  ]    [  ]   [  ]    [  ]
005.                $ THERE ARE SIZE+1 SUBSCRIPTS OF A AND B                  [  ]    [  ]    [  ]   [  ]    [  ]
006.                SIZE=7                                                    [  ]    [  ]    [  ]   [  ]    [  ]
007.                LAMBDA=.2  $ INITIAL VALUE OF LAMBDA                      [  ]    [  ]    [  ]   [  ]    [  ]
008.                DEL LA = .2   $ INCREMENT OF LAMBDA                       [  ]    [  ]    [  ]   [  ]    [  ]
009.             D  LAM[196]                                                  [  ]    [  ]    [  ]   [  ]    [  ]
010.             D  X1[90],X2E[75],X2G[75],X2L[75]                            [  ]    [  ]    [  ]   [  ]    [  ]
011.             D  X2M[75],X2N[75],X2Q[75],X2R[75],X2V[75]                   [  ]    [  ]    [  ]   [  ]    [  ]
012.             D  X2W[75],X2Y[75],X3L[75],X3M[75],X3V[75]                   [  ]    [  ]    [  ]   [  ]    [  ]
013.             D  X3W[75],X3Y[75],PROD[135],NEXP[13],LNLA[15]               [  ]    [  ]    [  ]   [  ]    [  ]
014.             D  LE[12],ME[12],E[13],G[13],NN[13],Q[13],RR[13]             [  ]    [  ]    [  ]   [  ]    [  ]
015.             D  VO[13],WO[13],YO[13]                                      [  ]    [  ]    [  ]   [  ]    [  ]
016.             PL                                                           [  ]    [  ]    [  ]   [  ]    [  ]
017.             PL          C          I          M          C
    .                        R          X       LAMBDA        C
    .                        P          M
                                                                             [  ]    [  ]    [  ]   [  ]    [  ]
018.             PL                                                          [  ]    [  ]    [  ]   [  ]    [  ]
019.             PL                                                          [  ]    [  ]    [  ]   [  ]    [  ]
020.                LA=LAMBDA                                                [  ]    [  ]    [  ]   [  ]    [  ]
021.                M=0,N=-1                                                 [  ]    [  ]    [  ]   [  ]    [  ]
022.          3  ORDE[M],G[M],LE[M],ME[M],NN[M],Q[M],RR[M]                   [  ]    [  ]    [  ]   [  ]    [  ]
023.                N=N*[-1]                                                 [  ]    [  ]    [  ]   [  ]    [  ]
024.                NEXP[M]=N                                                [  ]    [  ]    [  ]   [  ]    [  ]
025.                M=M+1                                                    [  ]    [  ]    [  ]   [  ]    [  ]
026.             ORDE[M],G[M],NN[M],Q[M],RR[M],VO[M],WO[M],YO[M]             [  ]    [  ]    [  ]   [  ]    [  ]
027.                N=N*[-1]                                                 [  ]    [  ]    [  ]   [  ]    [  ]
028.                NEXP[M]=N                                                [  ]    [  ]    [  ]   [  ]    [  ]
029.                [M=M+1]-13                                               [3  ]    [  ]    [  ]   [3  ]    [  ]
030.                LOG2=LN.[2.]                                             [  ]    [  ]    [  ]   [  ]    [  ]
031.                F=0                                                      [  ]    [  ]    [  ]   [  ]    [  ]
032.          A2    LA2=LA*LA                                                [  ]    [  ]    [  ]   [  ]    [  ]
033.                LAM[14*F]=LA2                                            [  ]    [  ]    [  ]   [  ]    [  ]
034.                M=1                                                      [  ]    [  ]    [  ]   [  ]    [  ]
035.          8     C=F*14+M                                                 [  ]    [  ]    [  ]   [  ]    [  ]
036.                LAM[C]=LAM[C-1]*LA2                                      [  ]    [  ]    [  ]   [  ]    [  ]
037.                [M=M+1]-13                                               [8  ]    [  ]    [  ]   [8  ]    [  ]
038.                LNLA[F]=LN.[LA/4.]                                       [  ]    [  ]    [  ]   [  ]    [  ]
039.                LA=LA+DEL LA                                             [  ]    [  ]    [  ]   [  ]    [  ]
040.                [F=F+1]-FMAX                                             [A2 ]    [  ]    [  ]   [A2 ]    [  ]
041.                M=0                                                      [  ]    [  ]    [  ]   [  ]    [  ]
042.                P=0                                                      [  ]    [  ]    [  ]   [  ]    [  ]
043.          5     A=P*P                                                    [  ]    [  ]    [  ]   [  ]    [  ]
044.                V=P*14                                                   [  ]    [  ]    [  ]   [  ]    [  ]
045.          4     S=0                                                      [  ]    [  ]    [  ]   [  ]    [  ]
046.                CPS=1                                                    [  ]    [  ]    [  ]   [  ]    [1  ]
047.          2     CPS=CPS*[2*P+3-2*S]/[-2*S]                               [  ]    [  ]    [  ]   [  ]    [  ]
048.          1     X1[A+S]=CPS                                              [  ]    [  ]    [  ]   [  ]    [  ]
049.                [S=S+1]-P                                                [2  ]    [  ]    [  ]   [2  ]    [  ]
050.                S=0                                                      [  ]    [  ]    [  ]   [  ]    [  ]
051.                EPNSK=0                                                  [  ]    [  ]    [  ]   [  ]    [  ]
052.                ESP=1                                                    [  ]    [  ]    [  ]   [  ]    [  ]
053.                M=0                                                      [  ]    [  ]    [  ]   [  ]    [  ]
```

```
#      SEQ  LABL TYP   STATEMENT                                  C ZERO   NOT 0   PLUS   MINUS   ELSE
054.                  SPL=1                                      [     ]  [     ]  [     ]  [     ]  [     ]
055.                  SMI=-1                                     [     ]  [     ]  [     ]  [     ]  [     ]
056.                  ENSS=.5                                    [     ]  [     ]  [     ]  [     ]  [     ]
057.                  SUMKS=0                                    [     ]  [     ]  [     ]  [     ]  [30   ]
058.           51     ESP=ESP*[P-S+1]/[+S]                       [     ]  [     ]  [     ]  [     ]  [     ]
059.                  SMI=2*S-1                                  [     ]  [     ]  [     ]  [     ]  [     ]
060.                  SPL=S+1                                    [     ]  [     ]  [     ]  [     ]  [     ]
061.                  ENSS=ENSS*SMI/[2*SPL]                      [     ]  [     ]  [     ]  [     ]  [     ]
062.                  SUMKS=SUMKS-1/[2*S*[2*S-1]]                [     ]  [     ]  [     ]  [     ]  [     ]
063.           30     ENS=ENSS                                   [     ]  [     ]  [     ]  [     ]  [     ]
064.                  SUMK=SUMKS                                 [     ]  [     ]  [     ]  [     ]  [     ]
065.                  SPLN=2*SPL                                 [     ]  [     ]  [     ]  [     ]  [32   ]
066.                  N=0                                        [     ]  [     ]  [     ]  [     ]  [     ]
067.           34     SPLN=2*[SPL+N]                             [     ]  [     ]  [     ]  [     ]  [     ]
068.                  ENS=ENS*[SMI+2*N]/SPLN                     [     ]  [     ]  [     ]  [     ]  [     ]
069.                  SUMK=SUMK+1/[2*[N+S]*[2*[N+S]-1]]          [     ]  [     ]  [     ]  [     ]  [     ]
070.           32     ERNSK=ESP*ENS*[2*N+1]*[1/SPLN+LOG2+SUMK]   [     ]  [     ]  [     ]  [     ]  [     ]
071.                  S                                          [     ]  [36   ]  [     ]  [     ]  [     ]
072.                  PROD[N+V]=0                                [     ]  [     ]  [     ]  [     ]  [     ]
073.           36     PROD[N+V]=PROD[N+V]-ERNSK                  [     ]  [     ]  [     ]  [     ]  [     ]
074.                  [Y=N+1]-13                                 [34   ]  [     ]  [     ]  [34   ]  [     ]
075.                  [S=S+1]-P                                  [31   ]  [     ]  [     ]  [31   ]  [     ]
076.                  [P=P+1]-SIZE                               [5    ]  [     ]  [     ]  [5    ]  [     ]
077.           45     P=0                                        [     ]  [     ]  [     ]  [     ]  [     ]
078.           60     F=0                                        [     ]  [     ]  [     ]  [     ]  [     ]
079.           A8     C=F*[SIZE+1]+M                             [     ]  [     ]  [     ]  [     ]  [     ]
080.                  X2E[C]=X2G[C]=X2L[C]=X2M[C]=X2N[C]      C
                      =X2Q[C]=X2R[C]=X2V[C]=X2W[C]=X2Y[C]=0      [     ]  [     ]  [     ]  [     ]  [     ]
081.                  X3L[C]=X3M[C]=X3V[C]=X3W[C]=X3Y[C]=0       [     ]  [     ]  [     ]  [     ]  [     ]
082.                  [F=F+1]-FMAX                               [A8   ]  [     ]  [     ]  [A8   ]  [     ]
083.                  M                                          [44   ]  [     ]  [     ]  [     ]  [     ]
084.                  R=0                                        [     ]  [     ]  [     ]  [     ]  [     ]
085.                  A=P*P+P                                    [     ]  [     ]  [     ]  [     ]  [     ]
086.           40     EPS=1/[2*M*[2*M+1]]                        [     ]  [     ]  [     ]  [     ]  [     ]
087.                  R                                          [37   ]  [     ]  [     ]  [     ]  [     ]
088.                  EPS=EPS*[2*R+1]*2*R/[[2*M-2*R]*[2*M-2*R+1]]  [     ]  [     ]  [     ]  [     ]  [     ]
089.           57     M=M-1-R                                    [     ]  [     ]  [     ]  [     ]  [     ]
090.                  F=0                                        [     ]  [     ]  [     ]  [     ]  [     ]
091.                  NEXP[MR]                                   [     ]  [     ]  [     ]  [50   ]  [     ]
092.           A3     C=F*[SIZE+1]+M                             [     ]  [     ]  [     ]  [     ]  [     ]
093.                  D=F*14+MR                                  [     ]  [     ]  [     ]  [     ]  [     ]
094.                  X3L[C]=X3L[C]+EPS*LE[MR]*X1[A]*LAM[D]      [     ]  [     ]  [     ]  [     ]  [     ]
095.                  X3M[C]=X3M[C]+EPS*ME[MR]*X1[A]*LAM[D]      [     ]  [     ]  [     ]  [     ]  [     ]
096.                  [F=F+1]-FMAX                               [A3   ]  [     ]  [     ]  [A3   ]  [51   ]
097.           50     C=F*[SIZE+1]+M                             [     ]  [     ]  [     ]  [     ]  [     ]
098.                  D=F*14+MR                                  [     ]  [     ]  [     ]  [     ]  [     ]
099.                  X3V[C]=X3V[C]+EPS*VO[MR]*X1[A]*LAM[D]      [     ]  [     ]  [     ]  [     ]  [     ]
100.                  X3W[C]=X3W[C]+EPS*WO[MR]*X1[A]*LAM[D]      [     ]  [     ]  [     ]  [     ]  [     ]
101.                  X3Y[C]=X3Y[C]+EPS*YO[MR]*X1[A]*LAM[D]      [     ]  [     ]  [     ]  [     ]  [     ]
102.                  [F=F+1]-FMAX                               [50   ]  [     ]  [     ]  [50   ]  [     ]
103.           51     R=P                                        [44   ]  [     ]  [     ]  [     ]  [     ]
104.                  [R=R+1]-M+1                                [     ]  [     ]  [44   ]  [     ]  [     ]
105.                  A=A-1                                      [     ]  [     ]  [     ]  [     ]  [40   ]
106.           44     S=0                                        [     ]  [     ]  [     ]  [     ]  [     ]
107.                  V=P*14                                     [     ]  [     ]  [     ]  [     ]  [     ]
108.                  DPS=[2*P+1]/[2*P+2]                        [     ]  [     ]  [     ]  [     ]  [10   ]
```

#	SEQ	LABL	TYP	STATEMENT	C ZERO	NOT 0	PLUS	MINUS	ELSE
109.		11		DPS=DPS*(2*P+1-2*S)/(2*P+2-2*S)					
110.		10		(S=S+1)-P	(11			(11	
111.				N=M					
112.				DN=DPS					(20
113.		19		B=M+1					
114.				DPNB=1					
115.		14		DPNB=DPNB*(2*N+1-2*B)/(2*P+2+2*B-2*M)					
116.				(B=B+1)-N	(14			(14	
117.				U=0					
118.				N2=N*2+1					(16
119.		17		N2=N2*(2*N+2-2*U)*(2*N+1-2*U)/(2*U*(2*U+1))					
120.		16		(U=U+1)-M	(17			(17	
121.				DN=DPNB*DPS*N2					
122.		20		M		(22			
123.				X3=DN/(2*N+1)*PROD(N+V)					
124.				F=0					
125.				N=XP(N)				(38	
126.		A4		C=F*(SIZE+1)+M					
127.				D=F*14+N					
128.				X3L(C)=X3L(C)+X3*LE(N)*LAM(D)					
129.				X3M(C)=X3M(C)+X3*ME(N)*LAM(D)					
130.				(F=F+1)-FMAX	(A4			(A4	(42
131.		38		C=F*(SIZE+1)+M					
132.				D=F*14+N					
133.				X3V(C)=X3V(C)+X3*VO(N)*LAM(D)					
134.				X3W(C)=X3W(C)+X3*WO(N)*LAM(D)					
135.				X3Y(C)=X3Y(C)+X3*YO(N)*LAM(D)					
136.				(F=F+1)-FMAX	(38			(38	(42
137.		22		ENA=DN*(1/(2*N+1)+1/(2*N))					
138.				X3=ENA*PROD(N+V)					
139.				F=0					
140.				N=XP(N)				(43	
141.		A5		C=F*(SIZE+1)+M					
142.				D=F*14+N					
143.				X3L(C)=X3L(C)+X3*LE(N)*LAM(D)					
144.				X3M(C)=X3M(C)+X3*ME(N)*LAM(D)					
145.				(F=F+1)-FMAX	(A5			(45	(42
146.		43		C=F*(SIZE+1)+M					
147.				D=F*14+N					
148.				X3V(C)=X3V(C)+X3*VO(N)*LAM(D)					
149.				X3W(C)=X3W(C)+X3*WO(N)*LAM(D)					
150.				X3Y(C)=X3Y(C)+X3*YO(N)*LAM(D)					
151.				(F=F+1)-FMAX	(43			(43	
152.		42		PROD(N+V)=X3					
153.				F=0					
154.		A6		C=F*(SIZE+1)+M					
155.				D=F*14+N					
156.				X2F(C)=X2E(C)+F(N)*LAM(D)*DN					
157.				X2G(C)=X2G(C)+G(N)*DN*LAM(D)					
158.				X2N(C)=X2N(C)+HN(N)*DN*LAM(D)					
159.				X2Q(C)=X2Q(C)+G(N)*DN *LAM(D)					
160.				X2R(C)=X2R(C)+HR(N)*DN*LAM(D)					
161.				N=XP(N)				(12	
162.				X2L(C)=X2L(C)+LE(N)*DN*LAM(D)					
163.				X2M(C)=X2M(C)+ME(N)*DN*LAM(D)					(21
164.		12		X2V(C)=X2V(C)+VO(N)*DN*LAM(D)					

```
#     SEQ  LABL TYP   STATEMENT                                  C ZERO   NOT 0   PLUS   MINUS   ERSE
165.                    X2W[C]=X2W[C]+W0[N]*DN*LAM[D]
166.                    X2Y[C]=X2Y[C]+Y0[N]*DN*LAM[D]
167.               21   [F=F+1]-FMAX                              [46      [46
168.                    [N=N+1]-13                                [19      [19
169.                    F=0
170.                    LA=LAMBDA
171.               A7   C=F*(SIZE+1)+M
172.                    C4=X2E[C]+X3L[C]+X2L[C]*LNLA[F]
173.                    P=M                                       [70      [70
174.                    HA=0                                                       [71
175.               70   HA=-X1[P*P+P-M]
176.               71   IA=X2F[C]-X2N[C]-X2Q[C]+X3Y[C]-X3V[C]-X3W[C] C
                        +[X2Y[C]-X2V[C]-X2W[C]]*LNLA[F]+HA
177.                    MA=2.*[X3V[C]+X3W[C]+X2N[C]+X2Q[C]+       C
                        [X2V[C]+X2W[C]]*LNLA[F]] -4.*HA
178.                    RA=-2.*[X2N[C]+X3V[C]+X2V[C]*LNLA[F]]
179.                    XA=-X2G[C]+X3M[C]+X2M[C]*LNLA[F]
180.                PV  CA,IA,MA,RA,XA,LA,P,M
181.                    IA=LA+DEL LA
182.                    MODE.[1]
183.                PV  CA,IA,MA,RA,XA
184.                    MODE.[0]
185.                    [F=F+1]-FMAX                              [47      [47
186.                PL
187.                    [P=P+1]-SIZE                              [60      [60
188.                    [M=M+1]-SIZE                              [45      [45
189.                END
```

*****SYMBOL TABLE*****

A	A2	AM
A3	A4	A5
B	A6	A7
C	CPS	CA
D	DELLA	DPS
DN	DPNB	E
EPNSK	ESP	EPSS
ENS	FPS	F
FMAX	FNA	G
HA	IA	LAMBDA
LAM	LNLA	LF
LA	LOG2	M
MR	ME	LN
LA2	MA	N
NEXP	NN	N2
MODE	P	PROD
Q	M	RC
RA	S	SIZE

SP_	SMI	SUMKS
SUMK	SPLN	U
V	V0	W0
X1	X2F	X2G
X2_	X2M	X2N
X2Q	X2R	X2V
X2W	X2Y	X3L
X3M	X3V	X3W
X3Y	Y0	X3
XA		

UNUSED MEMORY FROM [OCTAL] 07536 TO [OCTAL] 10573.

```
005 2021   CATANACH    SOLUTION FOR P SUB H PRIME AND F SUB F
AUG 29 67      14 49.4                                                    PAGE 1.        AUG 29 67

#     SEQ  LABL TYP                  STATEMENT                      C ZERO    NOT 0     PLUS      MINUS     FLSE

001.             FIXMM,P,Q,V,T,N,R1,Z,SS,R,F,FMAX                    (    )    (    )    (    )    (    )    (    )
002.                7$6  $ HIGHEST SUBSCRIPT FOR A AND B             (    )    (    )    (    )    (    )    (    )
003.                FMAX=14   $  NUMBER OF LAMBDA INCREMENTS         (    )    (    )    (    )    (    )    (    )
004.                LA=.2  $ INITIAL VALUE OF LAMBDA                 (    )    (    )    (    )    (    )    (    )
005.                DEL LA=.2 $ INCREMENT OF LAMBDA                  (    )    (    )    (    )    (    )    (    )
006.             I  NU(.33333333)                                    (    )    (    )    (    )    (    )    (    )
007.             I  NUZERO(.666666667)                               (    )    (    )    (    )    (    )    (    )
008.                V=(Z+1)*(Z+1)                                    (    )    (    )    (    )    (    )    (    )
009.                SS=4*(Z+1)+1                                     (    )    (    )    (    )    (    )    (    )
010.             D  C(812),AR(28),F(812)                             (    )    (    )    (    )    (    )    (    )
011.             D  A(49),I(49),M(49),RR(49),X(49)                   (    )    (    )    (    )    (    )    (    )
012.             D  SCOAM(8),JCOAM(8),JCOBM(8)                       (    )    (    )    (    )    (    )    (    )
013.             D  SCOAN(8),JCOAN(8),SCOBN(8)                       (    )    (    )    (    )    (    )    (    )
014.       2        Q=1                                              (    )    (    )    (    )    (    )    (    )
015.       1     ORDA(Q),I(Q),M(Q),RR(Q),X(Q)                        (    )    (    )    (    )    (    )    (    )
016.                (Q=Q+1)-V                                        (1   )    (    )    (    )    (1   )    (    )
017.             PL NU=1/3                                           (    )    (    )    (    )    (    )    (    )
018.             PL                                                  (    )    (    )    (    )    (    )    (    )
019.             PL                                                  (    )    (    )    (    )    (    )    (    )
020.             PL      LAMBDA          LEFT SIDE              MM   C
                              P       RCOAN/RCOAM     ICOAN/ICOAM   C
                   RCOBN/RCOBM     ICOBN/ICOBM                      (    )    (    )    (    )    (    )    (    )
021.                MM=0,Q=1                                         (    )    (    )    (    )    (    )    (    )
022.                R=SS                                             (    )    (    )    (    )    (    )    (    )
023.                R1=R-1                                           (    )    (    )    (    )    (    )    (    )
024.                R1R=R1*R                                         (    )    (    )    (    )    (    )    (    )
025.                N=1                                              (    )    (    )    (    )    (    )    (    )
026.       3        LEFT=1,LA2P=1.                                   (    )    (    )    (    )    (    )    (    )
027.                MM                                               (9   )    (    )    (    )    (    )    (    )
028.             PV S(P,Q,MM                                         (    )    (    )    (    )    (    )    (1   )0
029.       9     PV LA,LEFT,MM                                       (    )    (    )    (    )    (    )    (    )
030.       10       P=0                                              (    )    (    )    (    )    (    )    (    )
031.       4        EF=NUZERO*(-X(Q)+A(Q))                           (    )    (    )    (    )    (    )    (    )
032.                CN=EF+A(Q)                                       (    )    (    )    (    )    (    )    (    )
033.                DNU=NUZERO*I(Q)                                  (    )    (    )    (    )    (    )    (    )
034.                LS=M(Q)*NUZERO+RR(Q)                             (    )    (    )    (    )    (    )    (    )
035.                ICOAN=LA2P*CN                                    (    )    (    )    (    )    (    )    (    )
036.                ICOAM=(NUZERO*(-EF+X(Q))-A(Q))*LA2P              (    )    (    )    (    )    (    )    (    )
037.                ICOBM=(NUZERO*(-EF-2.*A(Q)-X(Q))+A(Q))*LA2P      (    )    (    )    (    )    (    )    (    )
038.                RCOAM=LA2P*(NUZERO*DNU+LS)                       (    )    (    )    (    )    (    )    (    )
039.                RCOAN=LA2P*(-DNU-I(Q))                           (    )    (    )    (    )    (    )    (    )
040.                RCOBN=LA2P*(-DNU+I(Q))                           (    )    (    )    (    )    (    )    (    )
041.             PV S(P,SK(P,SK(P,P,RCOAN,ICOAN,RCOBN,ICOAN          (    )    (    )    (    )    (    )    (    )
042.             PV S(P,SK(P,SK(P,SK(P,RCOAM,ICOAM,RCOAM,ICOBM       (    )    (    )    (    )    (    )    (    )
043.                SCOAN(P)=RCOAN,JCOAN(P)=ICOAN,SCOBN(P)=RCOBN     (    )    (    )    (    )    (    )    (    )
044.                SCOAM(P)=RCOAM,JCOAM(P)=ICOAM,JCOBM(P)=ICOBM     (    )    (    )    (    )    (    )    (    )
045.                Q=Q+1                                            (    )    (    )    (    )    (    )    (    )
046.                (P=P+1)-Z                                        (    )    (    )    (6   )    (    )    (    )
047.                LA2P=LA2P*LA*LA                                  (    )    (    )    (    )    (    )    (4   )
048.       6        P=0                                              (    )    (    )    (    )    (    )    (    )
049.       5        C(N)=SCOAN(P),C(N+1)=JCOAN(P)                    (    )    (    )    (    )    (    )    (    )
050.                C(N+2)=SCOBN(P),C(N+3)=JCOAN(P)                  (    )    (    )    (    )    (    )    (    )
051.                C(N+R)=C(N+1),C(N+R+2)=C(N+3)                    (    )    (    )    (    )    (    )    (    )
052.                C(N+R+1)=C(N),C(N+R+3)=C(N+2)                    (    )    (    )    (    )    (    )    (    )
053.                C(N+1)=-C(N+1),C(N+3)=-C(N+3)                    (    )    (    )    (    )    (    )    (    )
```

```
#    SEQ  LABL TYP  STATEMENT                                          C ZERO  NOT 0  PLUS  MINUS  ELSE
054.                  C[N+2*R]=C[N+3*R+1]=C[N+2*R+2]=C[N+3*R+3]=       C
.                     SCOAM[P]                                         [  ]   [  ]   [  ]  [  ]   [  ]
055.                  C[N+2*R+1]=-JCOAM[P]                             [  ]   [  ]   [  ]  [  ]   [  ]
056.                  C[N+3*R]= JCOAM[P]                               [  ]   [  ]   [  ]  [  ]   [  ]
057.                  C[N+2*R+3]=-JCOBM[P]                             [  ]   [  ]   [  ]  [  ]   [  ]
058.                  C[N+3*R+2]= JCOBM[P]                             [  ]   [  ]   [  ]  [  ]   [  ]
059.                  N=N+4                                            [  ]   [  ]   [  ]  [  ]   [  ]
060.                  [P=P+1]-Z                                        [5 ]   [  ]   [  ]  [5 ]   [  ]
061.                  C[N]=C[N+2*R]=C[N+3*R]=0                         [  ]   [  ]   [  ]  [  ]   [  ]
062.                  MM                                               [  ]   [  ]   [12 ]  [  ]   [  ]
063.                  C[N+R]=LEFT                                      [  ]   [  ]   [  ]  [  ]   [11 ]
064.          12      C[N+R]=0                                         [  ]   [  ]   [  ]  [  ]   [  ]
065.          11      N=N+1+3*R                                        [  ]   [  ]   [  ]  [  ]   [  ]
066.                  [MM=MM+1]-Z                                      [3 ]   [  ]   [  ]  [3 ]   [  ]
067.                  R=5                                              [  ]   [  ]   [  ]  [  ]   [  ]
068.                SL                                                 [  ]   [  ]   [  ]  [  ]   [  ]
069.          60      N=1,Q=1,T=1,R1=[R=1]                             [  ]   [  ]   [  ]  [  ]   [  ]
070.                  R1R=R1*R                                         [  ]   [  ]   [  ]  [  ]   [  ]
071.                PL                                                 [  ]   [  ]   [  ]  [  ]   [  ]
072.                PVLR1                                              [  ]   [  ]   [  ]  [  ]   [  ]
073.          50      R[N]=C[Q]                                        [  ]   [  ]   [  ]  [  ]   [  ]
074.                  Q=Q+1                                            [  ]   [  ]   [  ]  [  ]   [  ]
075.                  [N=N+1]-R*T                                      [  ]   [  ]   [  ]  [50 ]   [  ]
076.                  Q=Q+SS-R                                         [  ]   [  ]   [  ]  [  ]   [  ]
077.                  B[N]=C[Q]                                        [  ]   [  ]   [  ]  [  ]   [  ]
078.                  N=N+1,T=T+1,Q=Q+1                                [  ]   [  ]   [  ]  [  ]   [  ]
079.                  N-R1R                                            [  ]   [  ]   [  ]  [50 ]   [  ]
080.                PL                                                 [  ]   [  ]   [  ]  [  ]   [  ]
081.                  SMEQS,[R1,%B%,%AB%]                              [  ]   [  ]   [  ]  [  ]   [  ]
082.                  Q=1                                              [  ]   [  ]   [  ]  [  ]   [  ]
083.          40    PVLQ,AB[Q],AB[Q+1],AB[Q+2],AB[Q+3]                 [  ]   [  ]   [  ]  [  ]   [  ]
084.                  P10A=2.*NU*[AB[Q]+AB[Q+2]]                       [  ]   [  ]   [  ]  [  ]   [  ]
085.                PVLP10A                                            [  ]   [  ]   [  ]  [  ]   [  ]
086.                  RP20A=2.*AB[Q+1]                                 [  ]   [  ]   [  ]  [  ]   [  ]
087.                PVLRP20A                                           [  ]   [  ]   [  ]  [  ]   [  ]
088.                PL                                                 [  ]   [  ]   [  ]  [  ]   [  ]
089.                  [R=R+4]-[SS-3]                                   [  ]   [  ]   [  ]  [60 ]   [  ]
090.                  R1=R-1                                           [  ]   [  ]   [  ]  [  ]   [  ]
091.                PVLR1                                              [  ]   [  ]   [  ]  [  ]   [  ]
092.                PL                                                 [  ]   [  ]   [  ]  [  ]   [  ]
093.                  SMEQS,[R1,%C%,%AB%]                              [  ]   [  ]   [  ]  [  ]   [  ]
094.                  Q=1                                              [  ]   [  ]   [  ]  [  ]   [  ]
095.          90    PVLQ,AB[Q],AB[Q+1],AB[Q+2],AB[Q+3]                 [  ]   [  ]   [  ]  [  ]   [  ]
096.                  P10A=2.*NU*[AB[Q]+AB[Q+2]]                       [  ]   [  ]   [  ]  [  ]   [  ]
097.                PVLP10A                                            [  ]   [  ]   [  ]  [  ]   [  ]
098.                  RP20A=2.*AB[Q+1]                                 [  ]   [  ]   [  ]  [  ]   [  ]
099.                PVLRP20A                                           [  ]   [  ]   [  ]  [  ]   [  ]
100.                  MODE,[1]                                         [  ]   [  ]   [  ]  [  ]   [  ]
101.                PV P10A                                            [  ]   [  ]   [  ]  [  ]   [  ]
102.                PV RP20A                                           [  ]   [  ]   [  ]  [  ]   [  ]
103.                  MODE,[0]                                         [  ]   [  ]   [  ]  [  ]   [  ]
104.                PL                                                 [  ]   [  ]   [  ]  [  ]   [  ]
105.                SL                                                 [  ]   [  ]   [  ]  [  ]   [  ]
106.                  LA=LA+DEL LA                                     [  ]   [  ]   [  ]  [  ]   [  ]
107.                  [F=F+1]-FMAX                                     [2 ]   [  ]   [  ]  [2 ]   [  ]
108.                END                                                [  ]   [  ]   [  ]  [  ]   [  ]
```

*****SYMBOL TABLE*****

AR	A	B
C	CN	DELTA
DNJ	FF	F
FMAX	I	ICOAN
ICOAM	ICOBM	JCCAM
JCORM	JCOAN	LA
LEFT	LA2P	LS
MM	M	MODE
N	NU	NUZERO
P	P10A	Q
R1	R	RR
R1R	RCOAM	RCOAN
RCORN	RP20A	SS
SCOAM	SCOAN	SCORN
SKIP	SMEQS	T
V	X	Z

UNUSED MEMORY FROM (OCTAL) 06102 TO (OCTAL) 07323.

FIGURE 1

SHELL COORDINATES

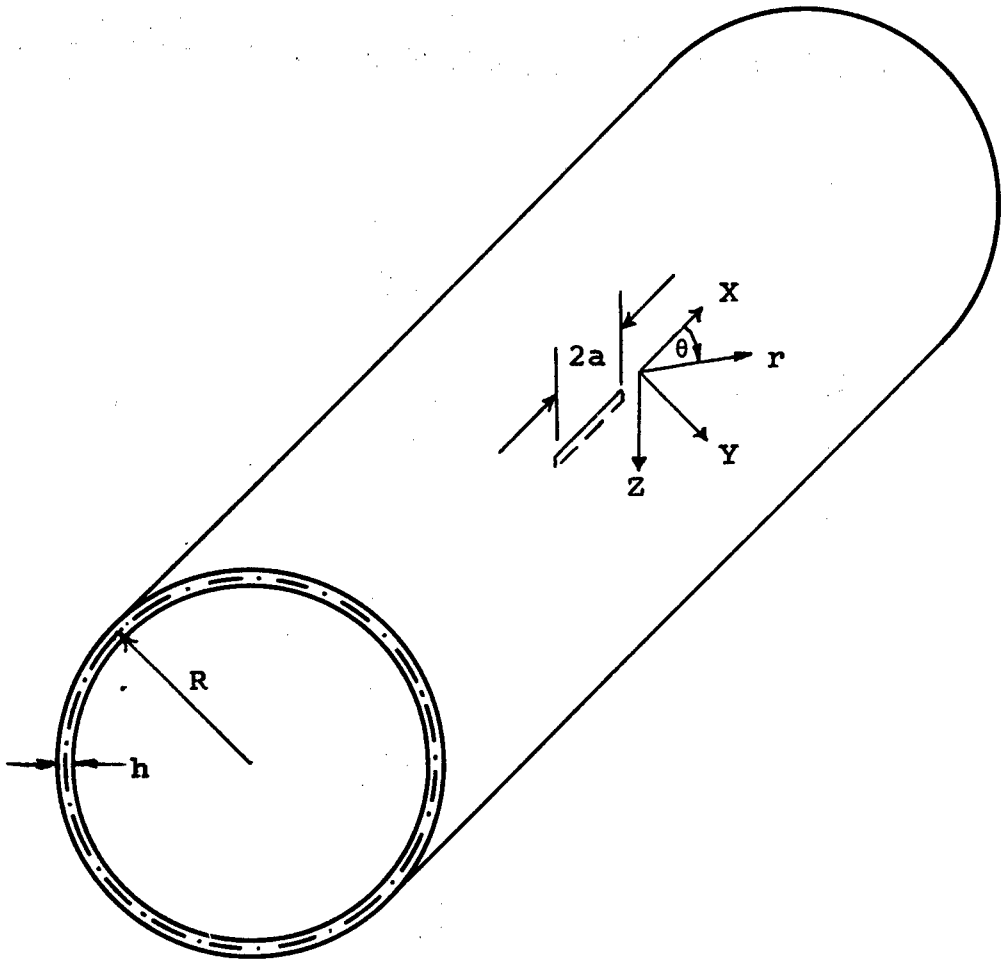

FIGURE 2

Superposition Principle

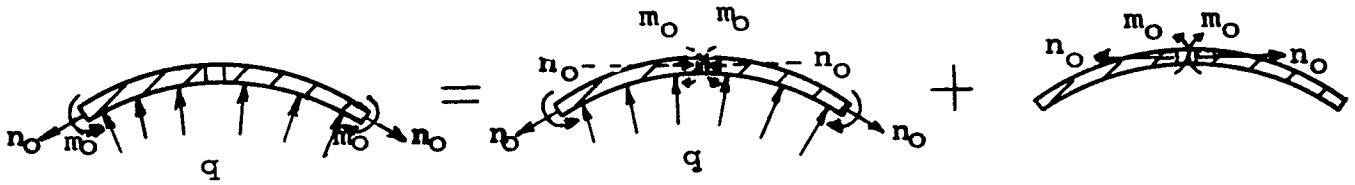

FIGURE 3

Stress Intensity Ratio in Tension vs. λ

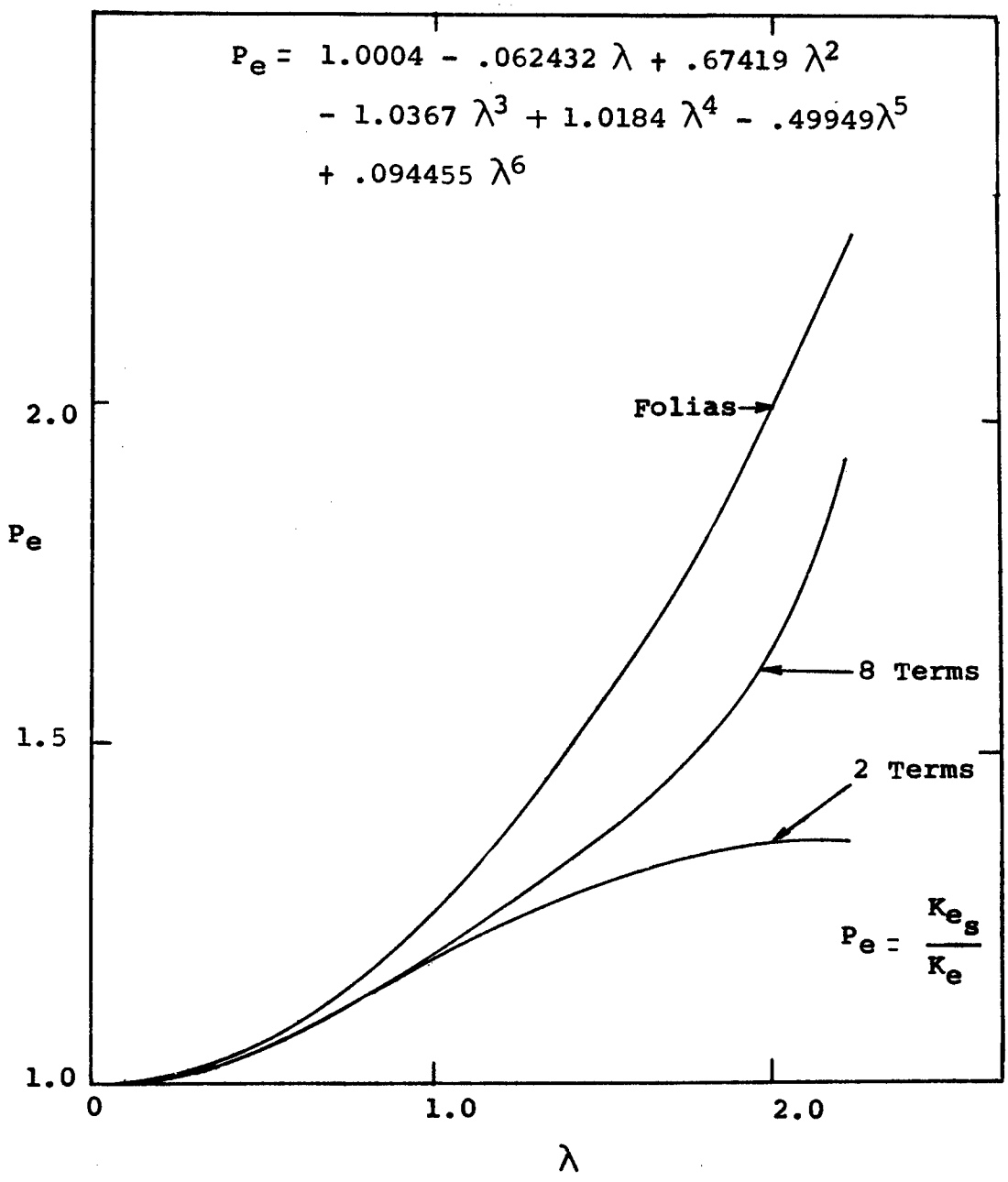

FIGURE 4

Stress Intensity Ratio in Bending vs. λ

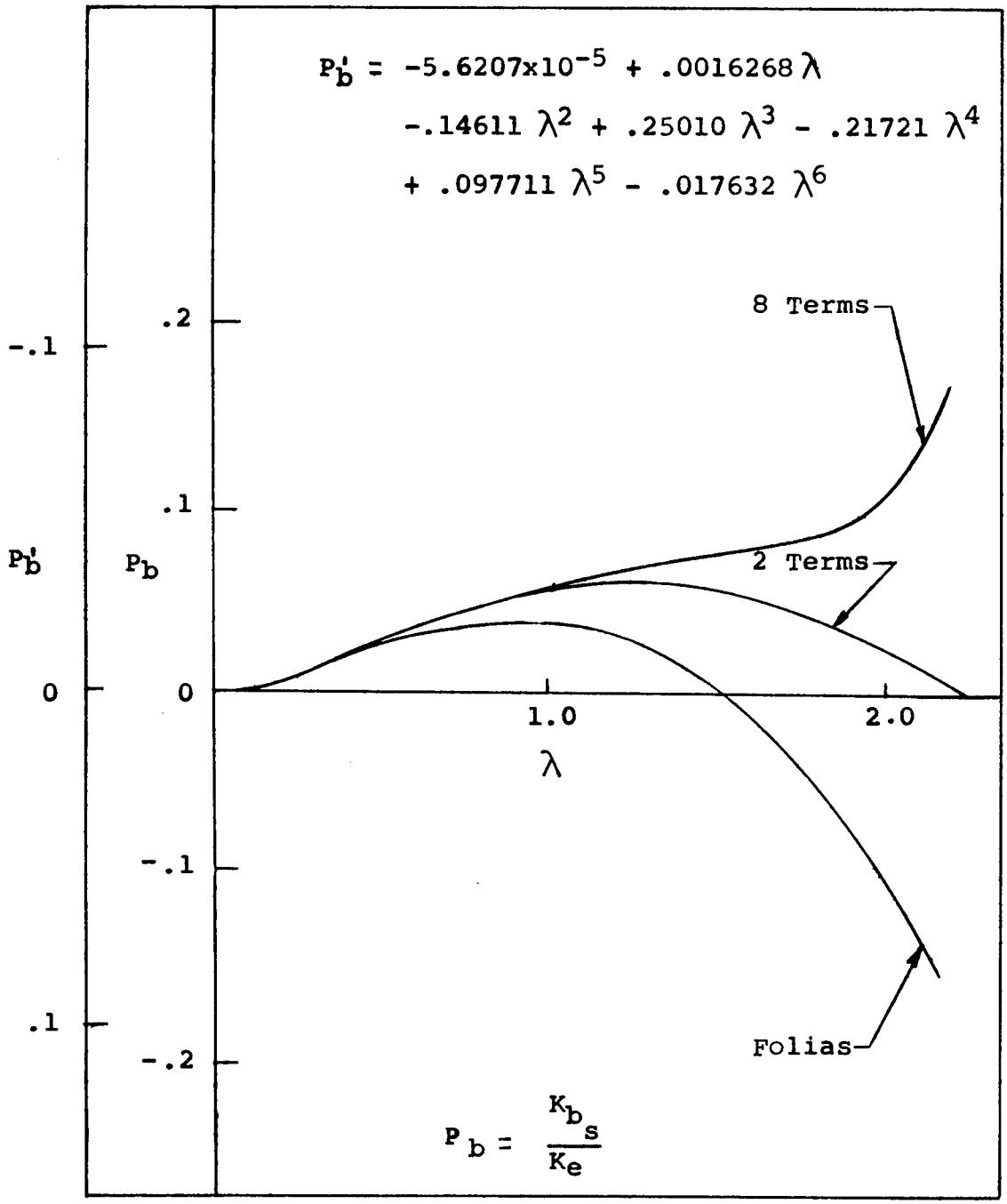

FIGURE 5

Experimental Test Set Up

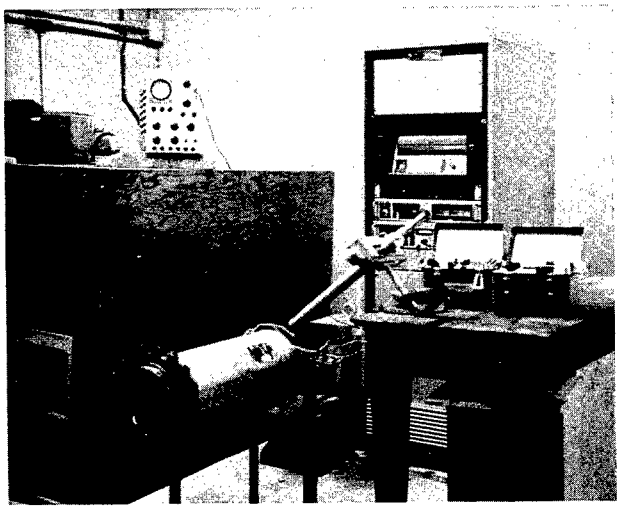

FIGURE 6

Schematic Diagram of Pressurization System

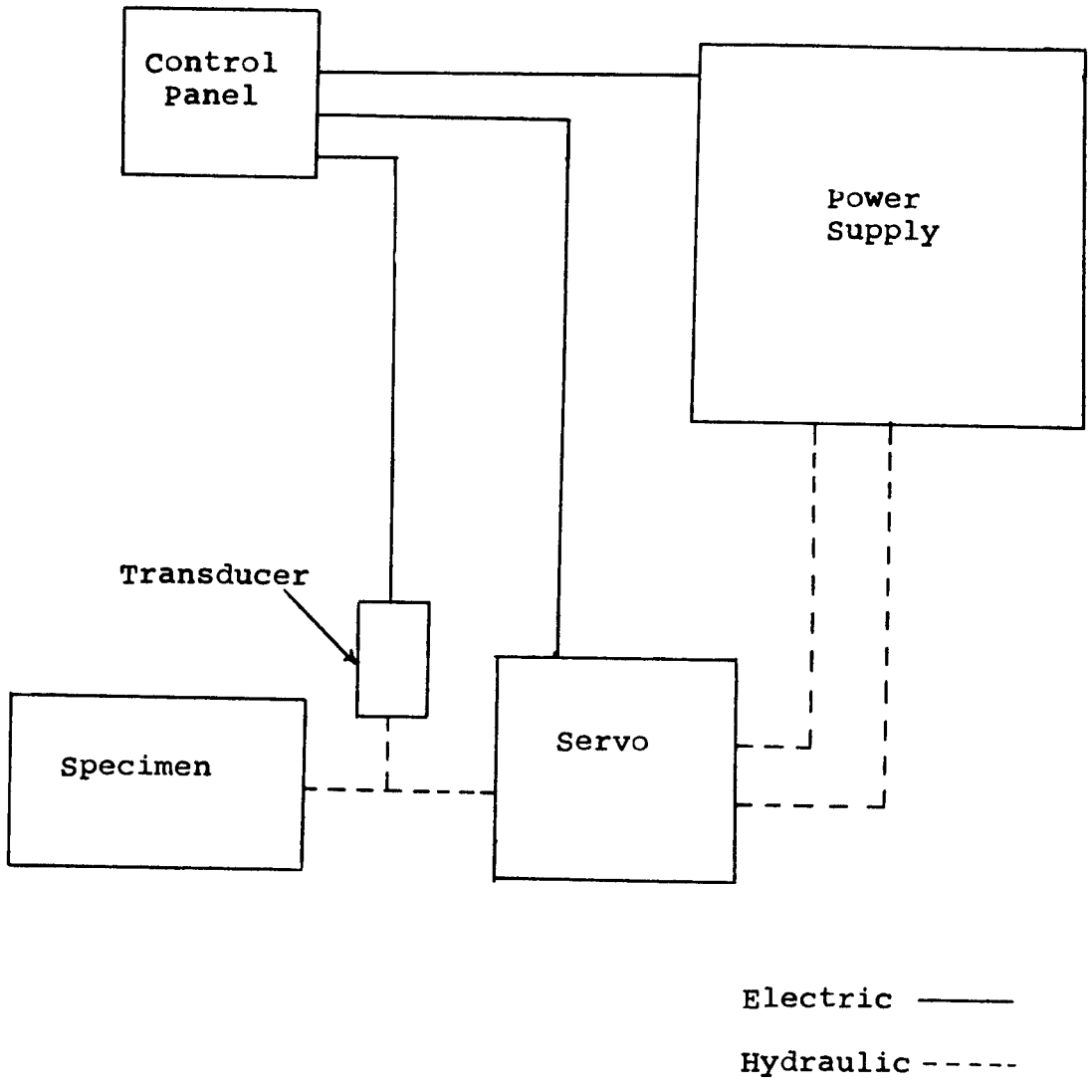

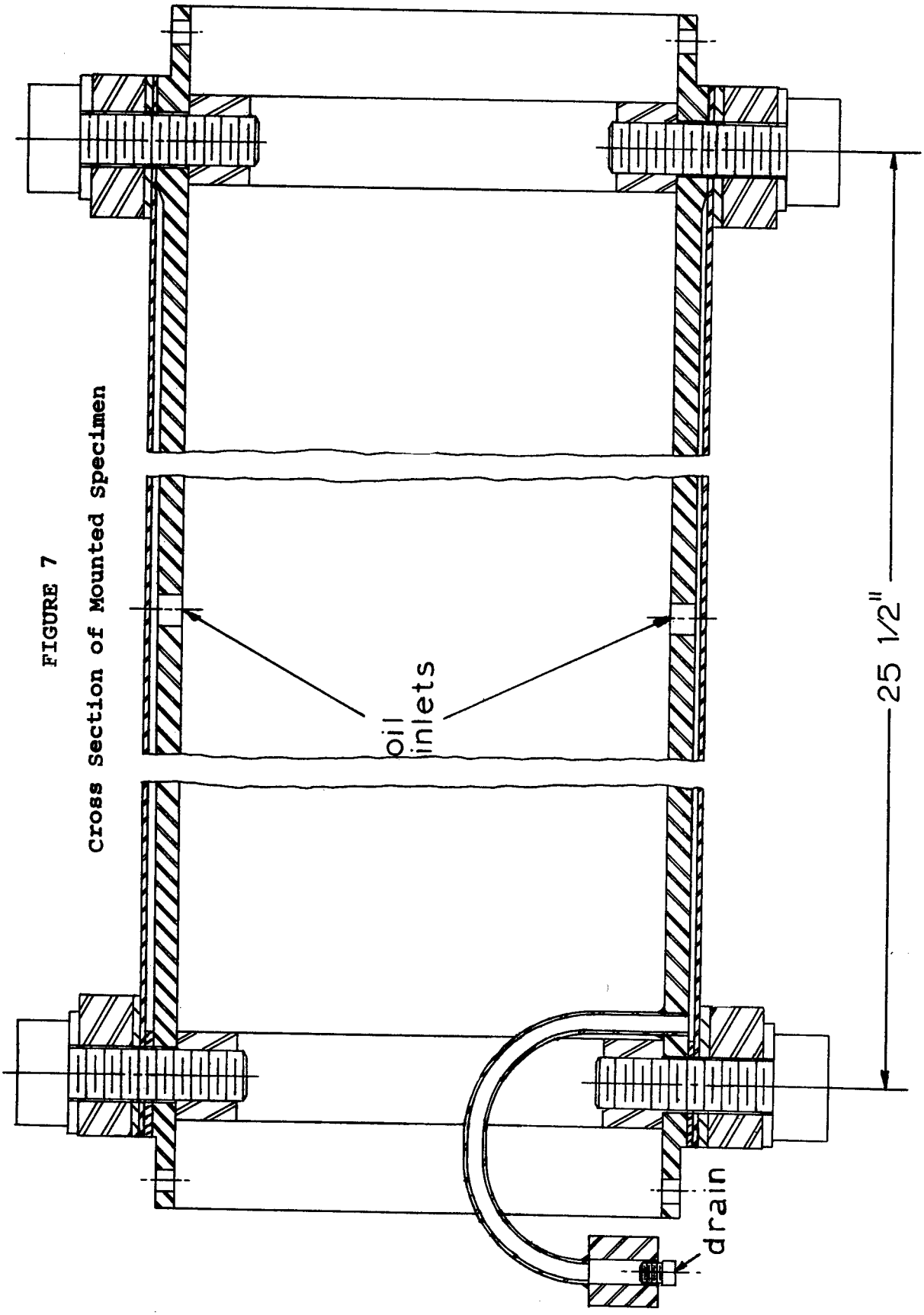

FIGURE 7
Cross Section of Mounted Specimen

FIGURE 8
Measured Hoop Strain vs. Pressure

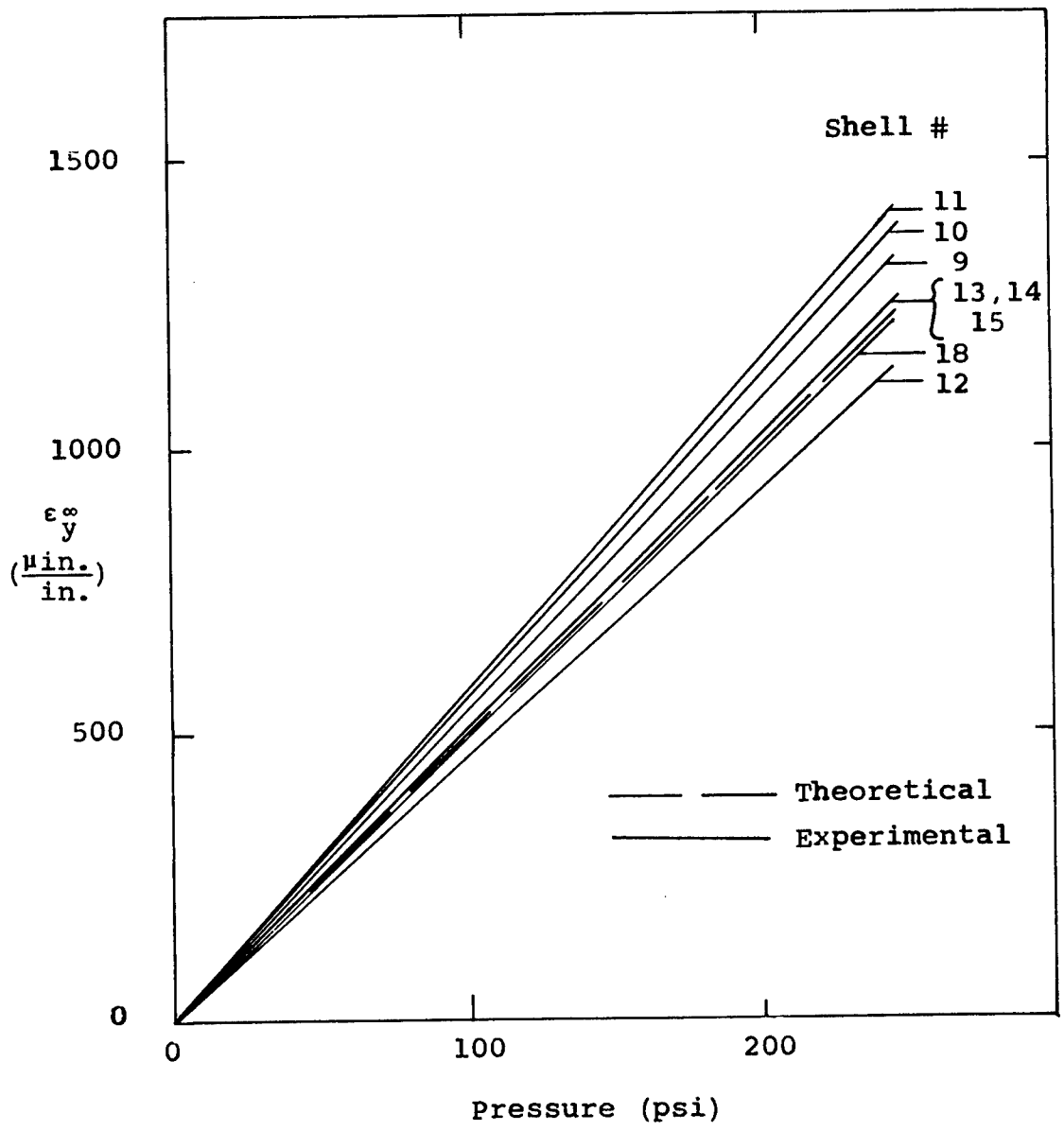

FIGURE 9

Surface Displacements Ahead of Crack

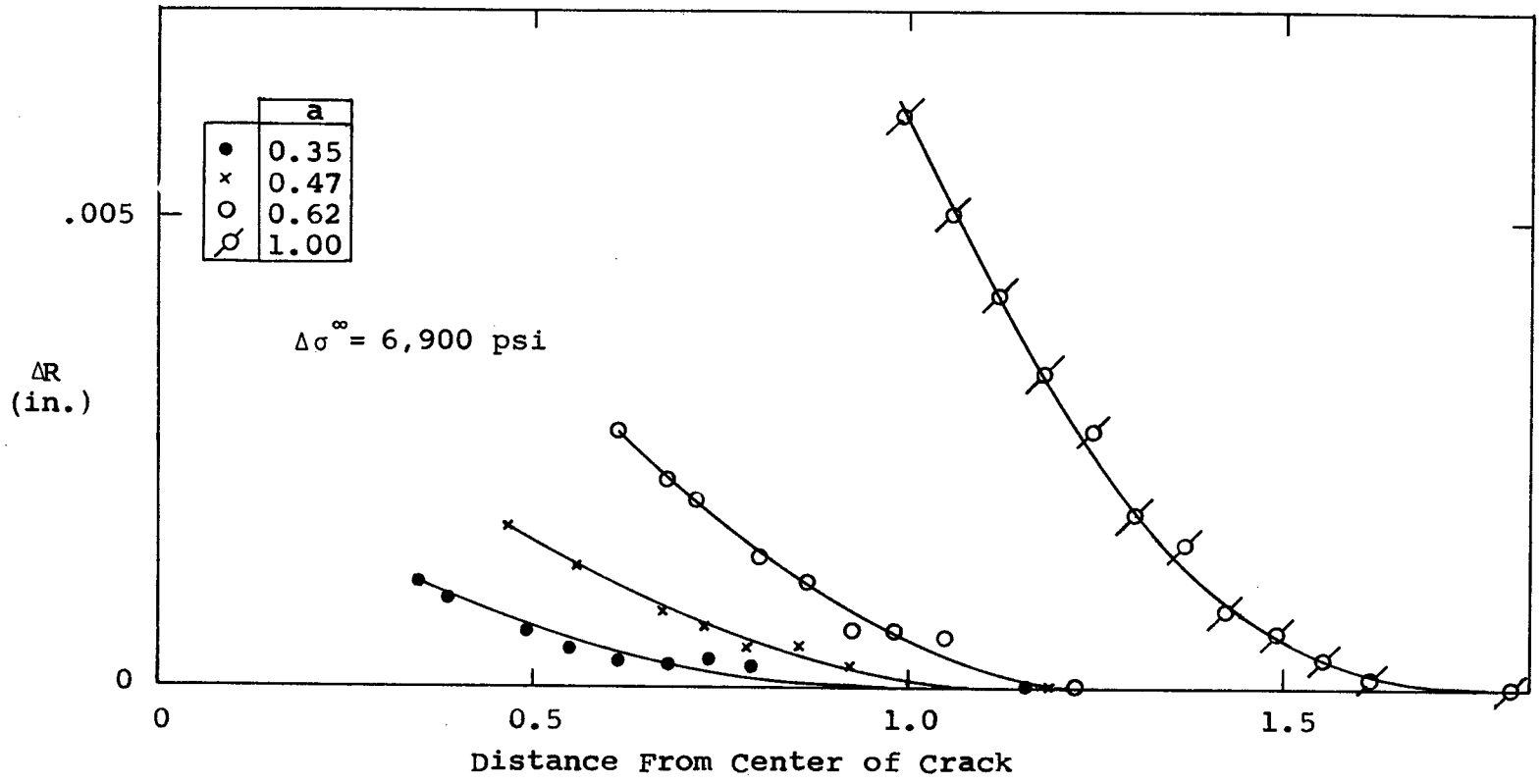

FIGURE 10

Radial Displacements at Crack Tip

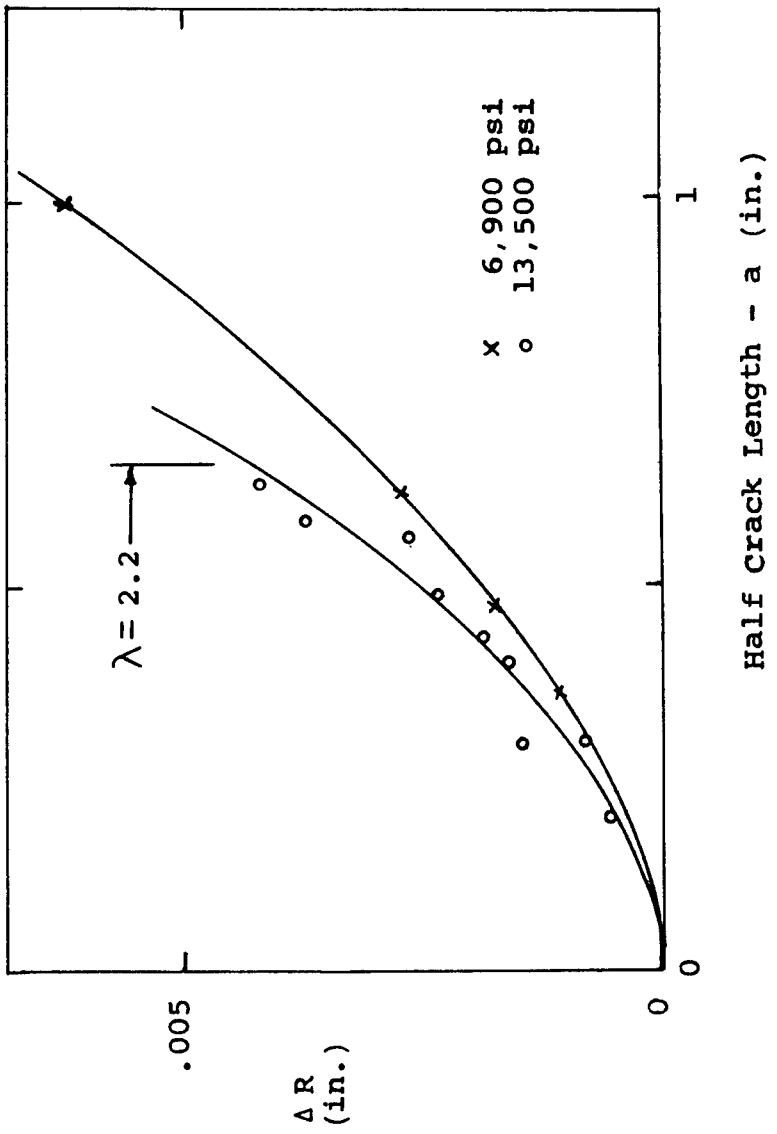

FIGURE 11

da/dn vs. K_r

Shell #9

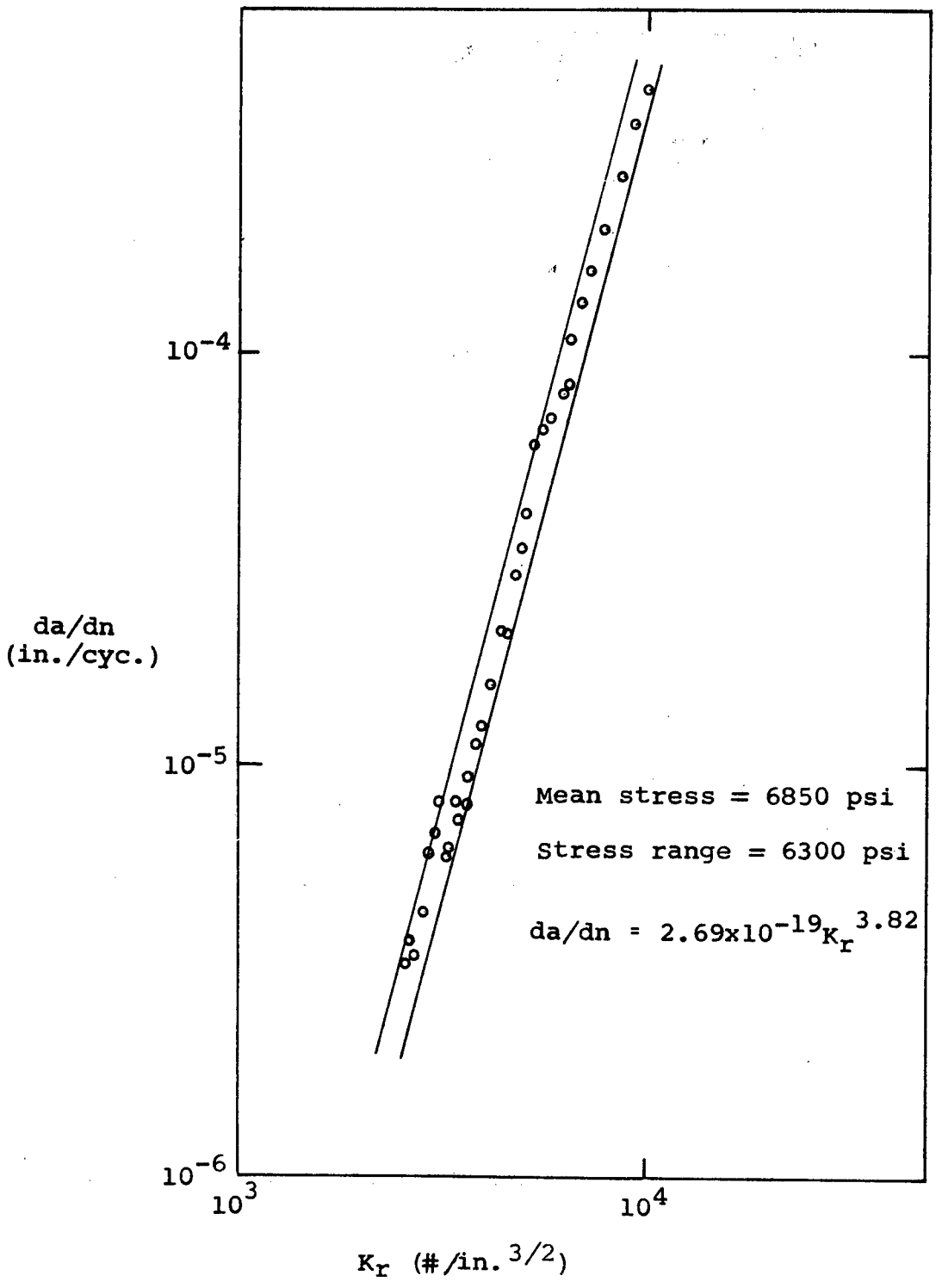

FIGURE 12

da/dn vs. K_r

Shell #10

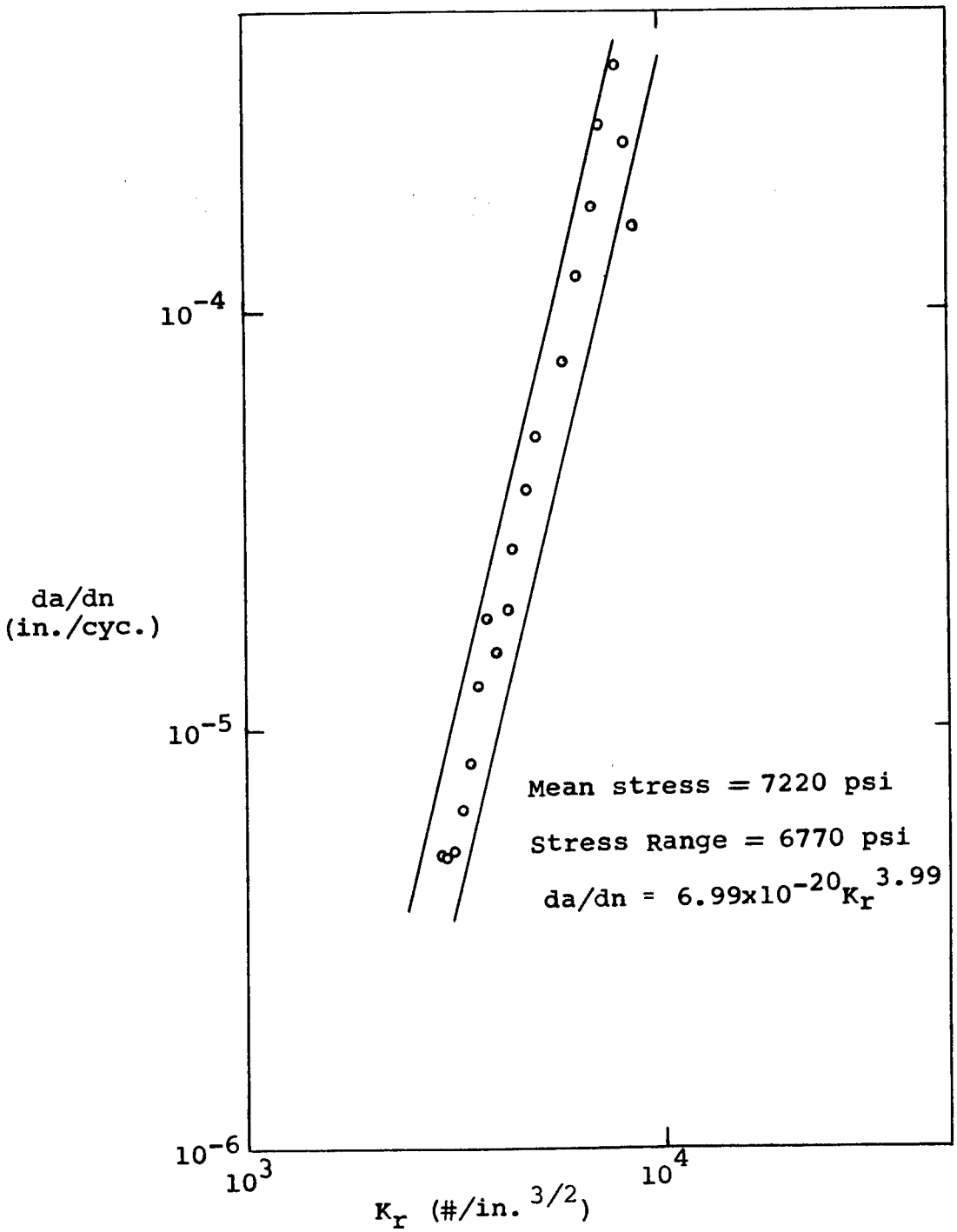

FIGURE 13

da/dn vs. K_r

Shell #11

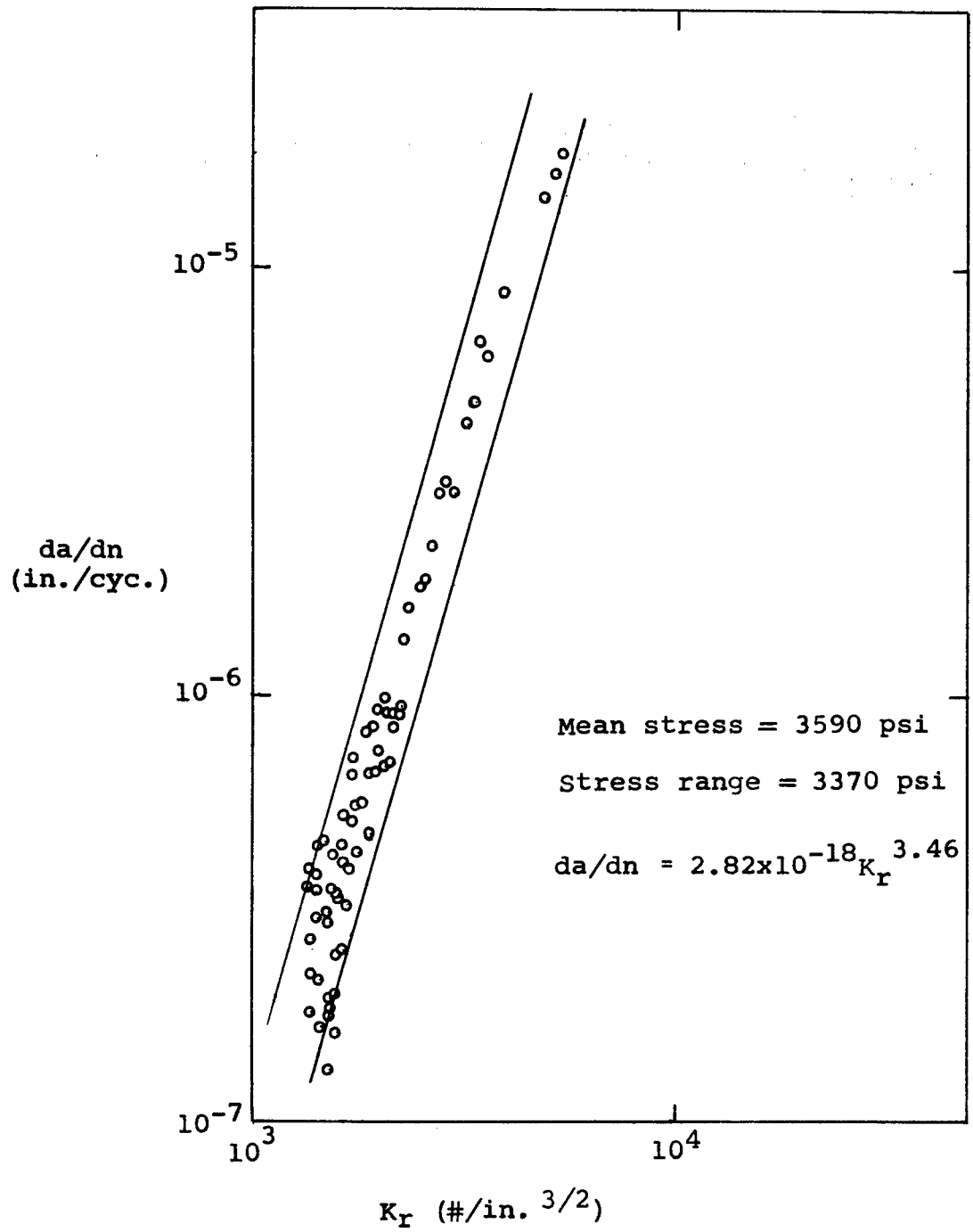

FIGURE 14

da/dn vs. K_r

Shell #12

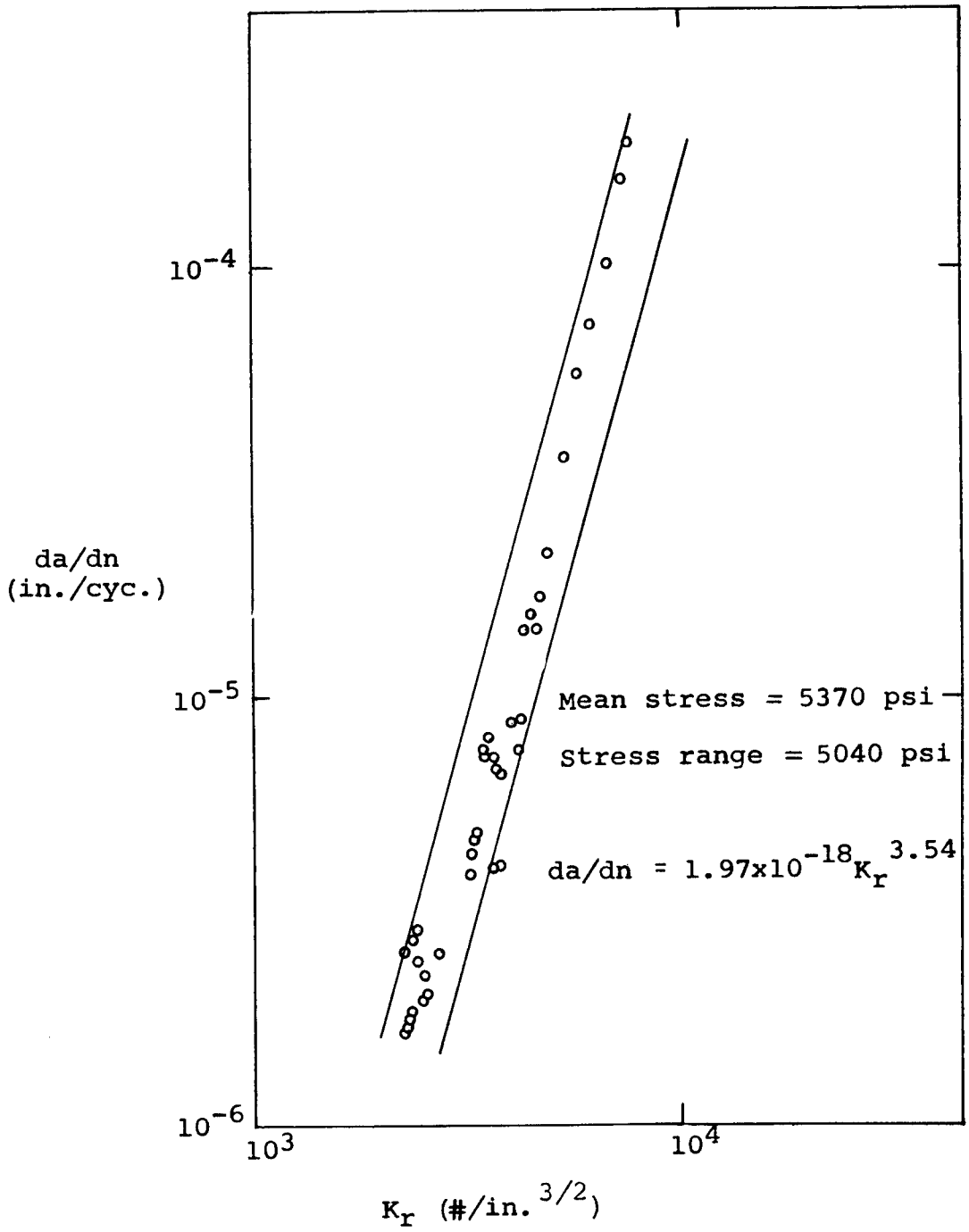

FIGURE 15

da/dn vs. K_r

Shell #13

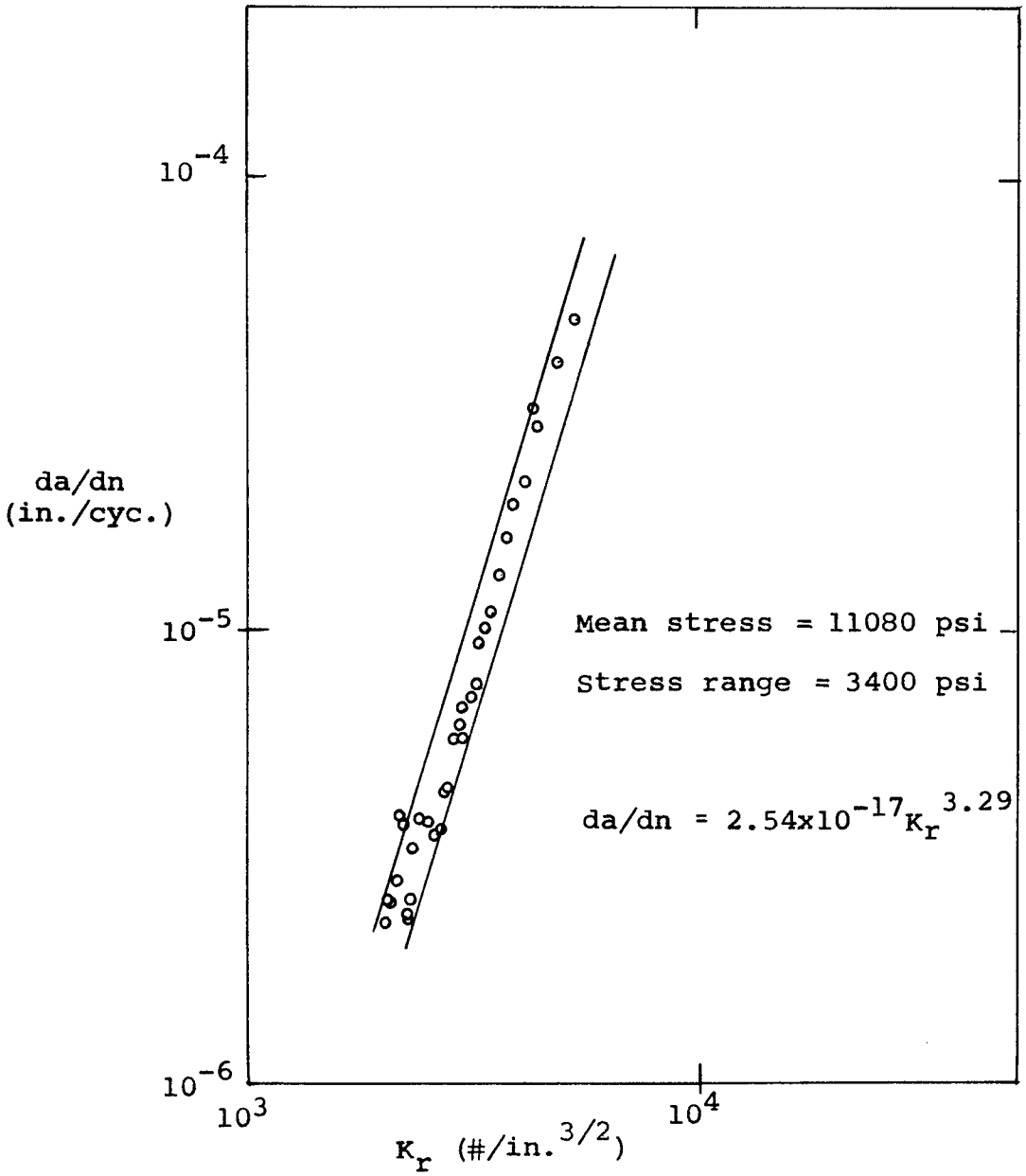

FIGURE 16

da/dn vs. K_r

Shell #14

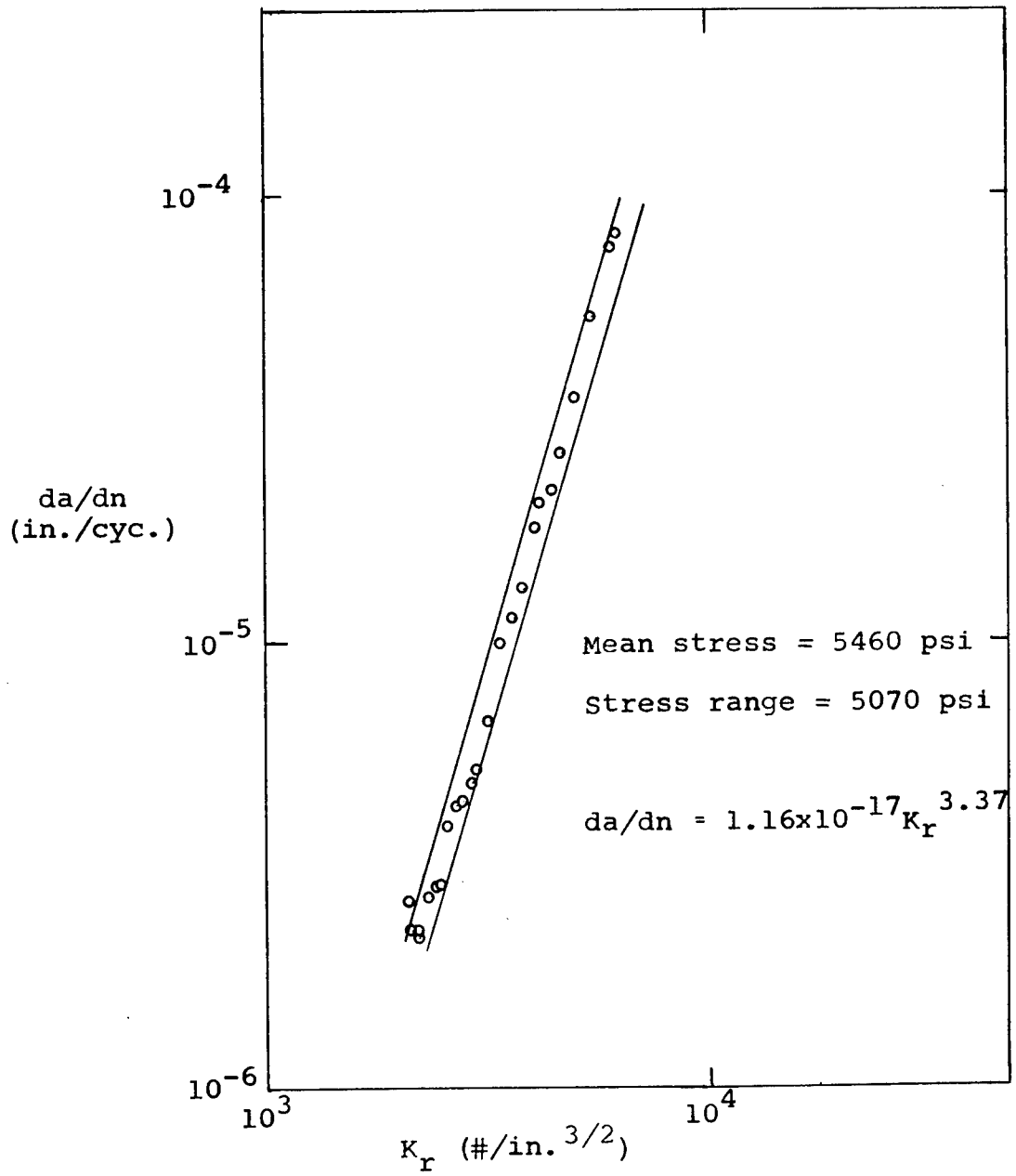

FIGURE 17

da/dn vs. K_r

Shell #15

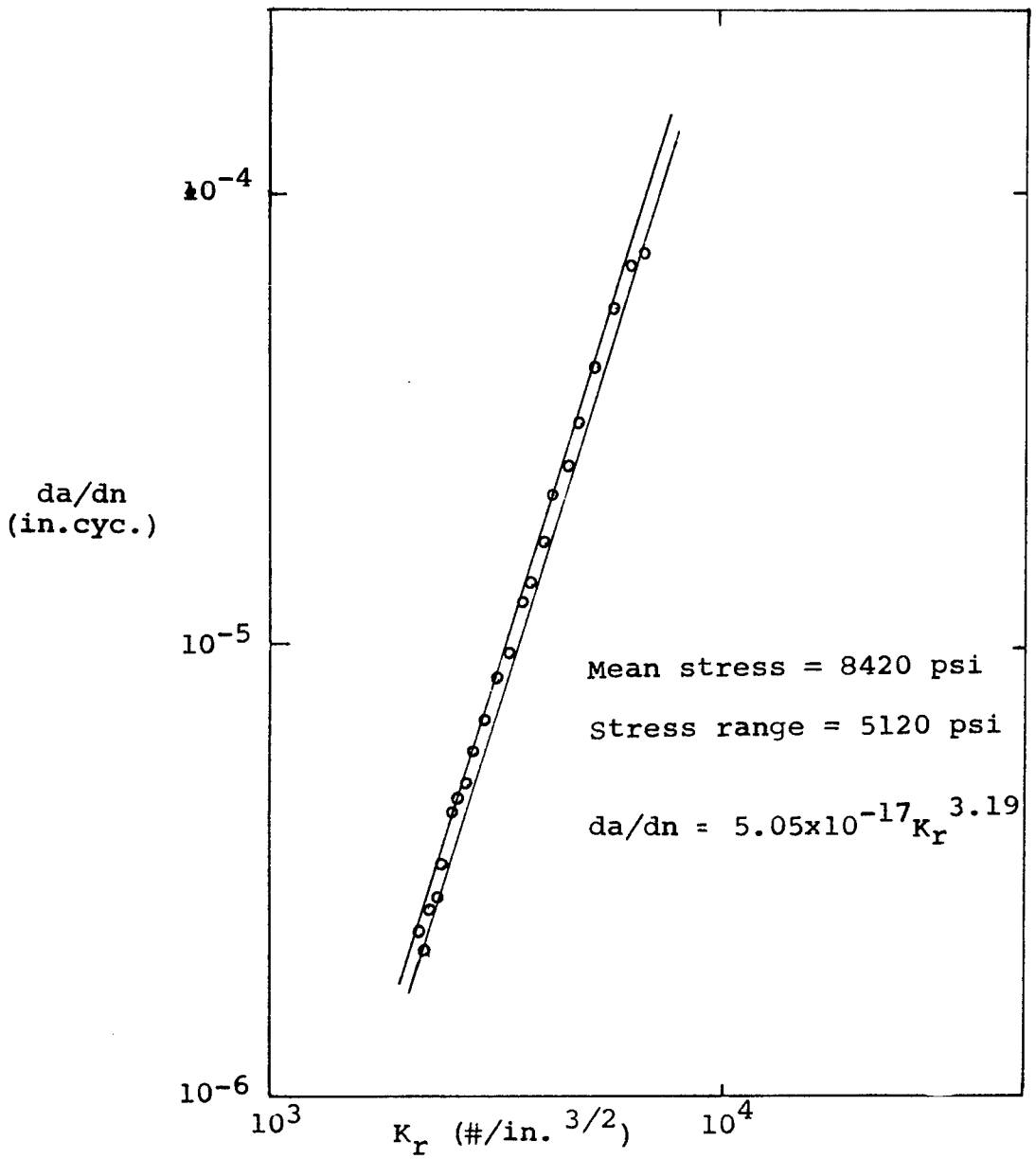

FIGURE 18

da/dn vs. K_r

Shell #18

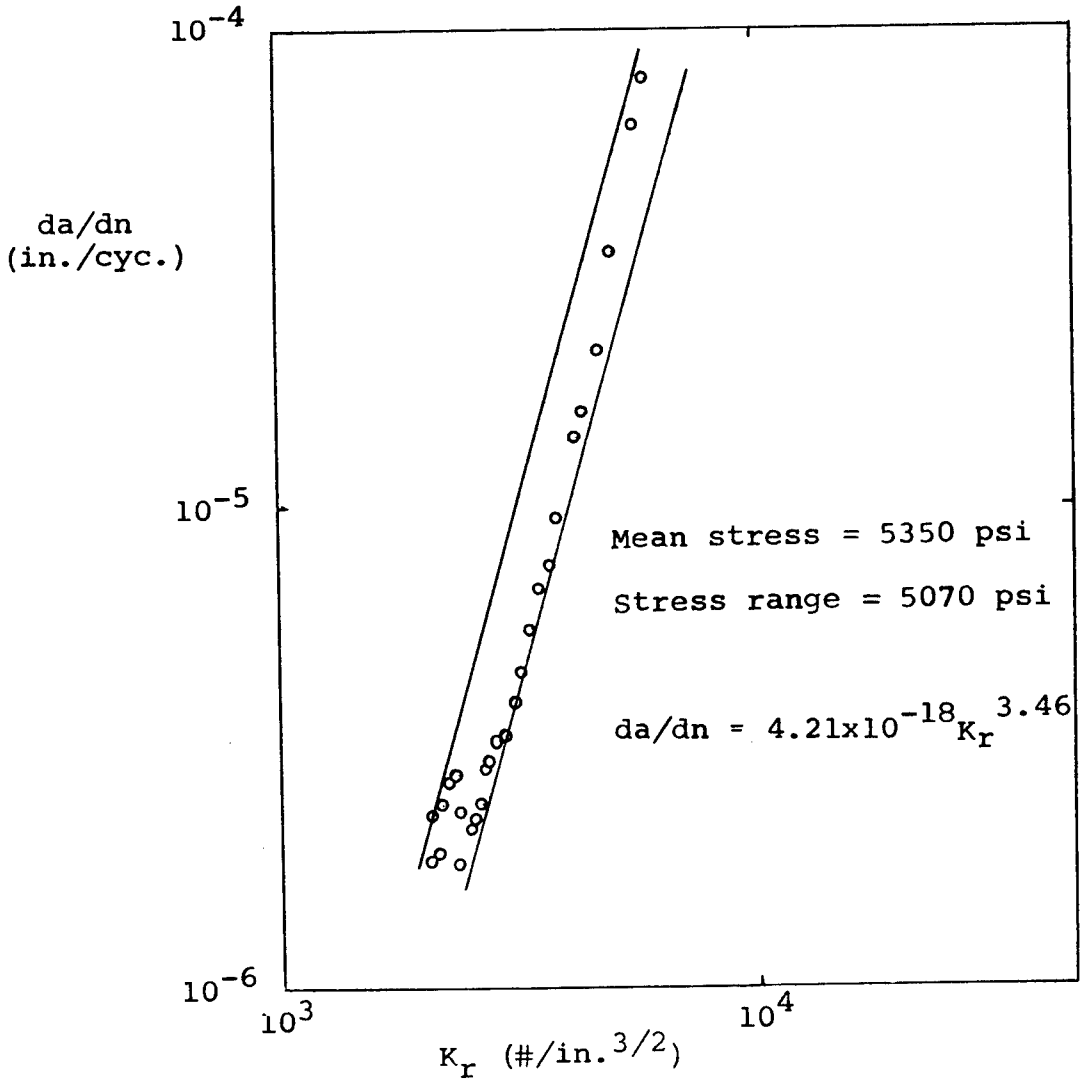

FIGURE 19

da/dn vs. K_r

Combined Data

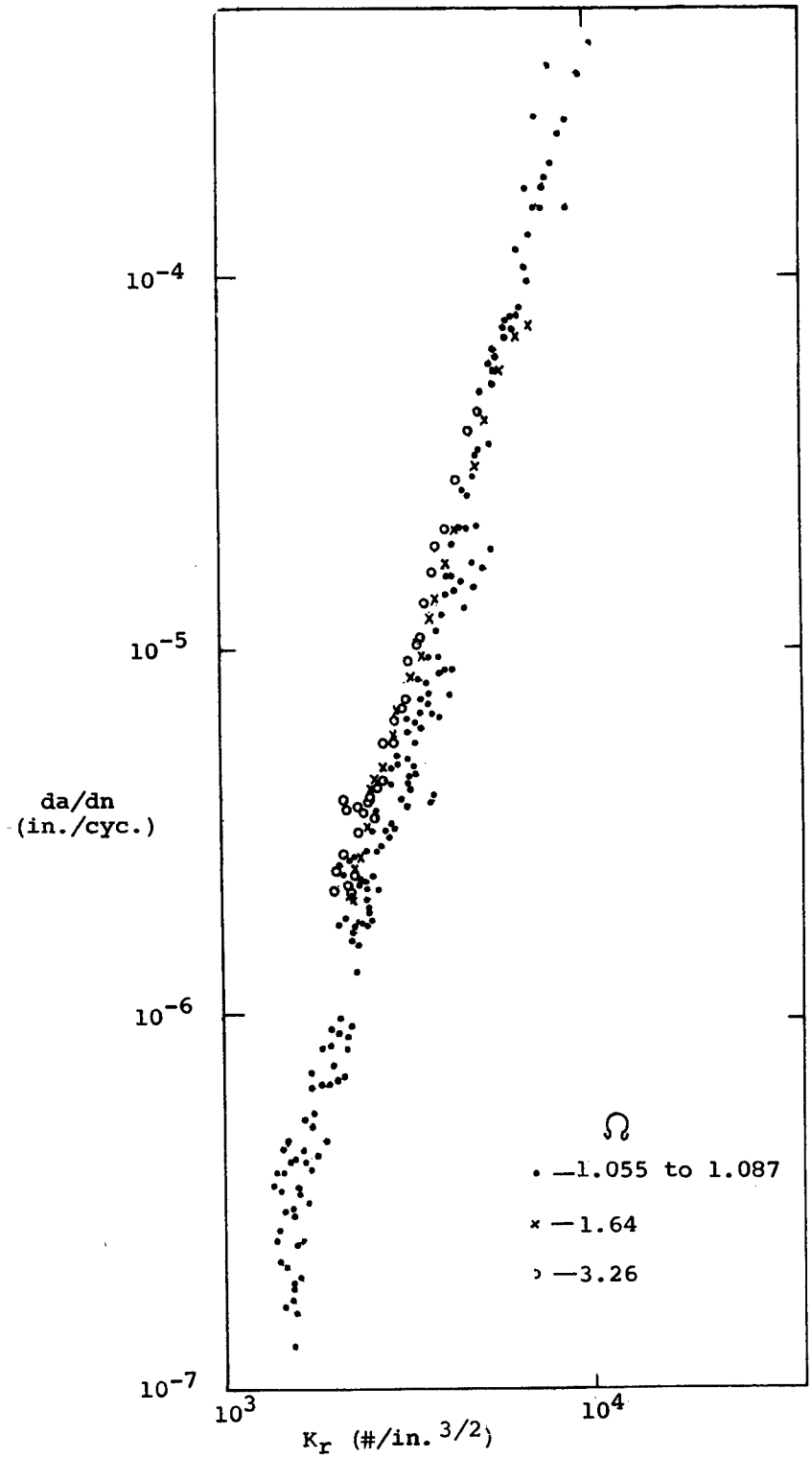

FIGURE 20

da/dn vs. K_r

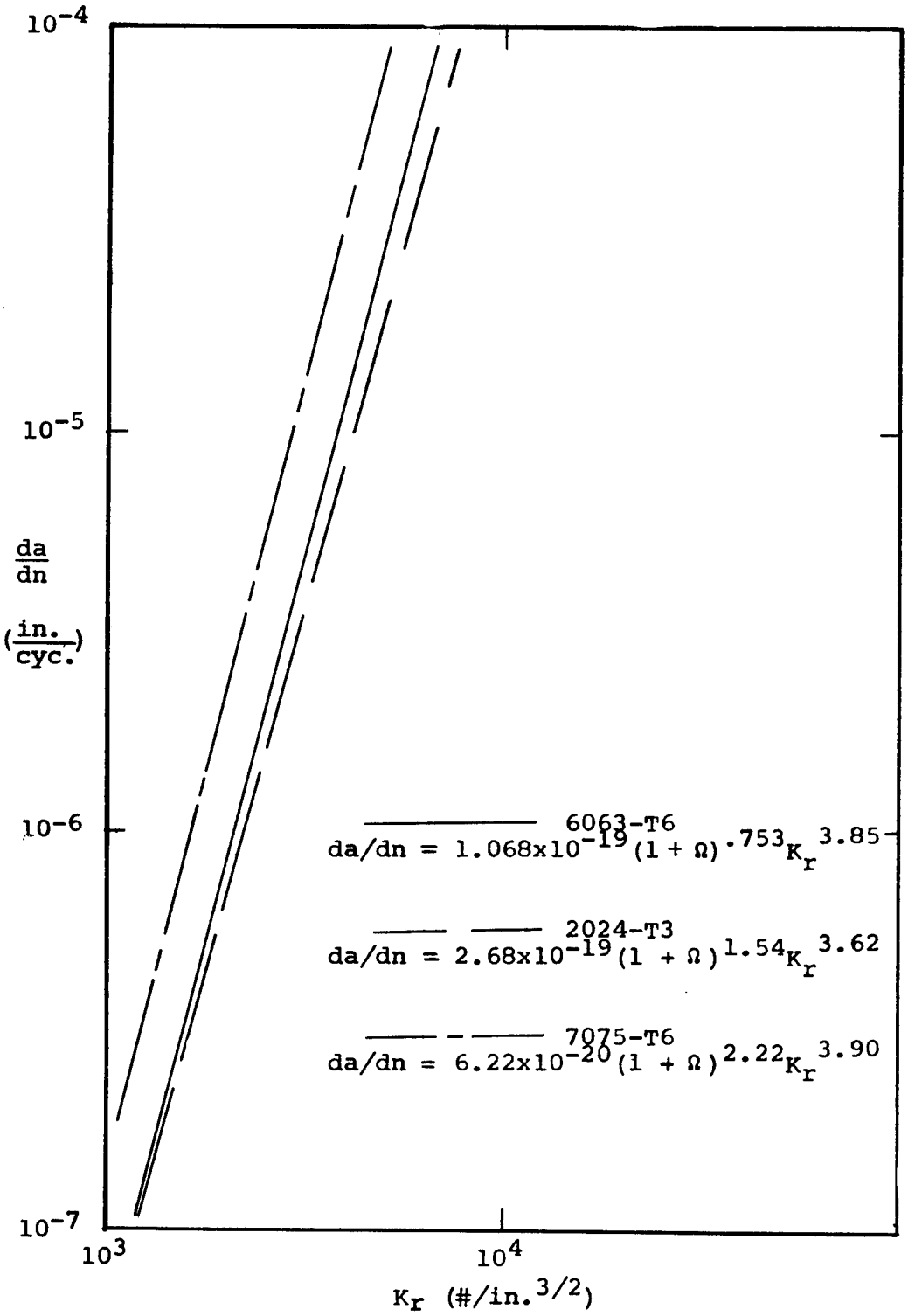

FIGURE 21

Measured and Theoretical Strain Ahead of Crack

Approximate Elastic Stress Distribution

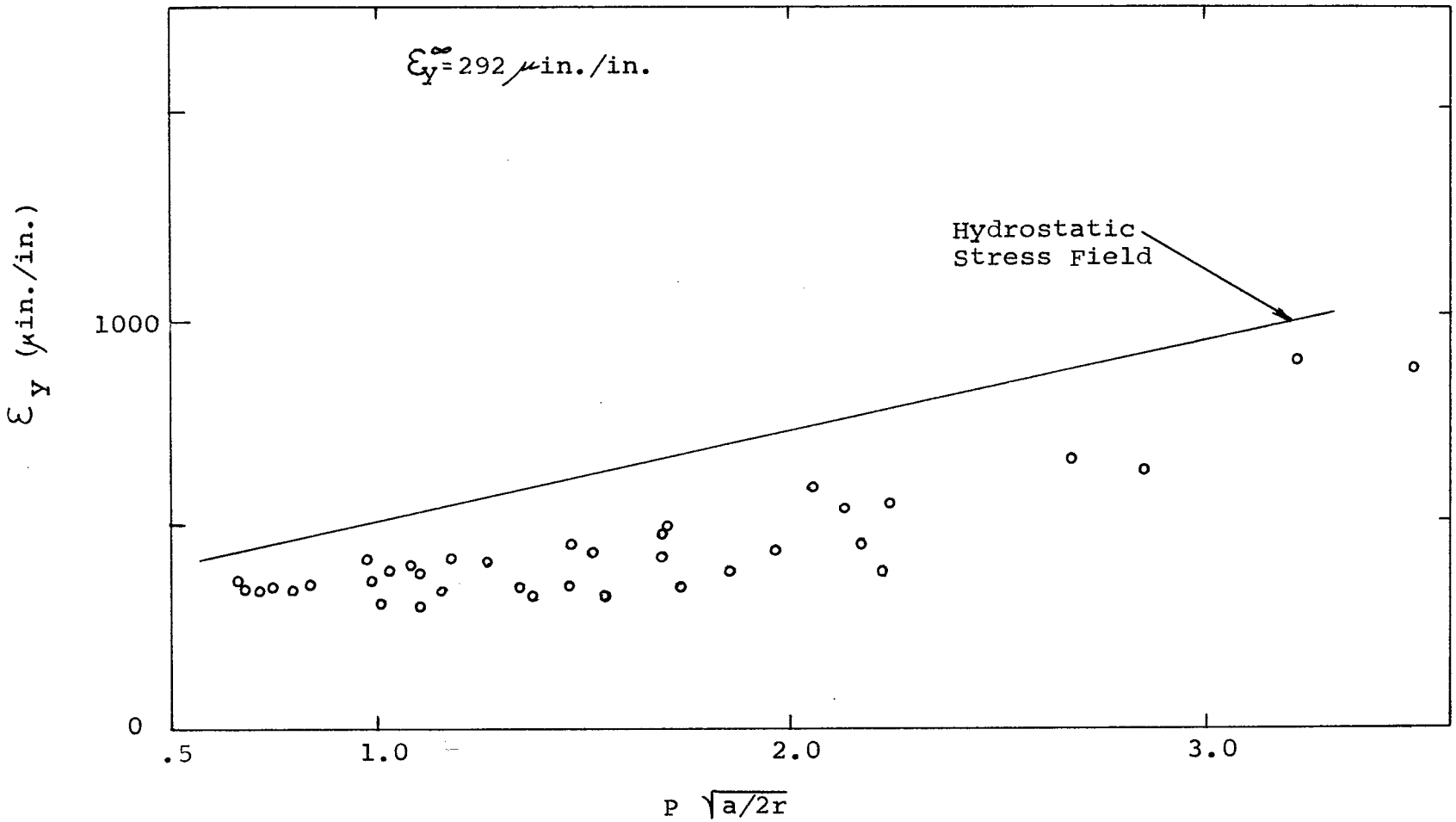

FIGURE 22

Measured and Theoretical Strain Ahead of Crack

Approximate Elastic Stress Distribution

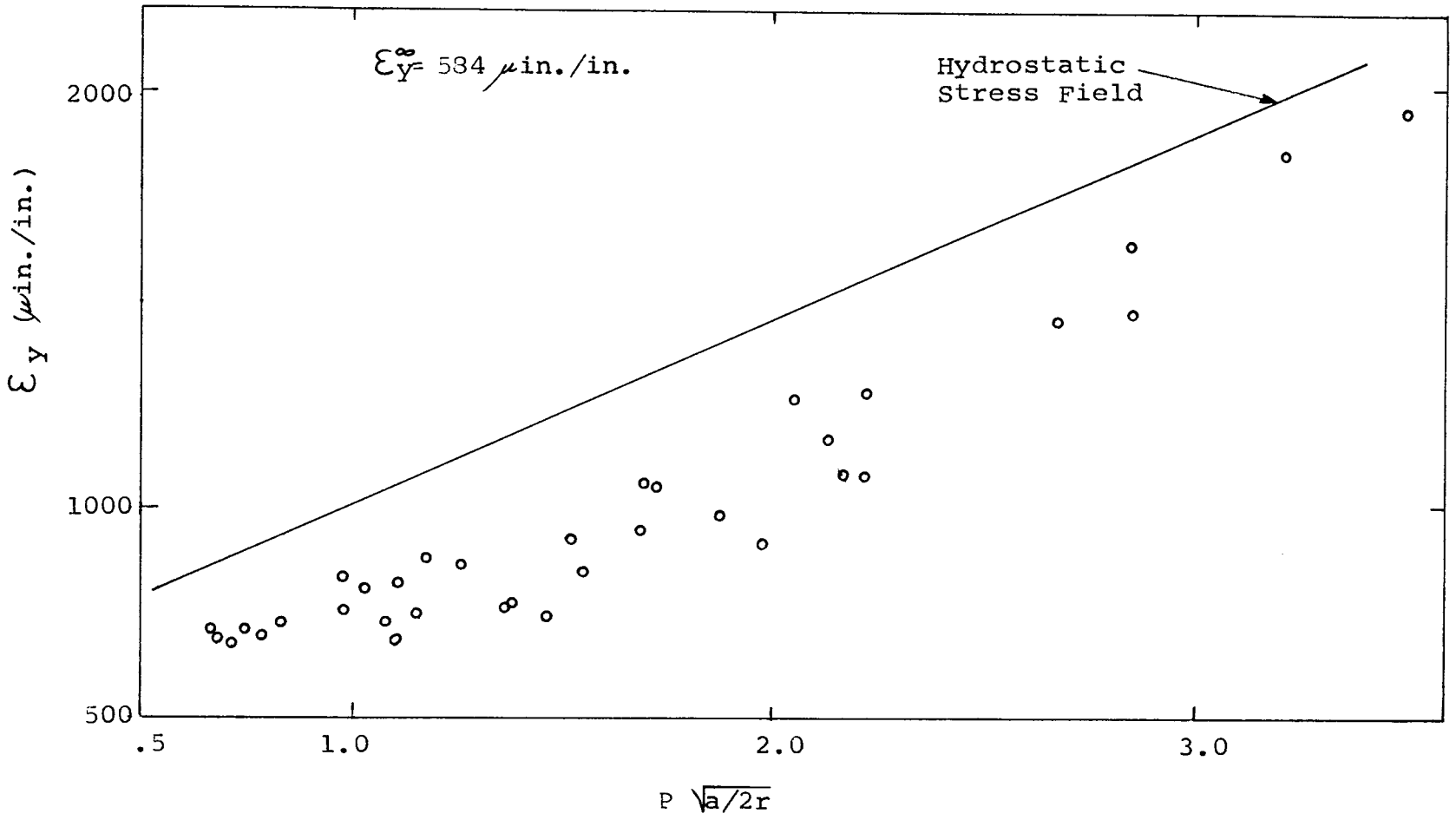

FIGURE 23

Measured and Theoretical Strain Ahead of Crack

Approximate Elastic Stress Distribution

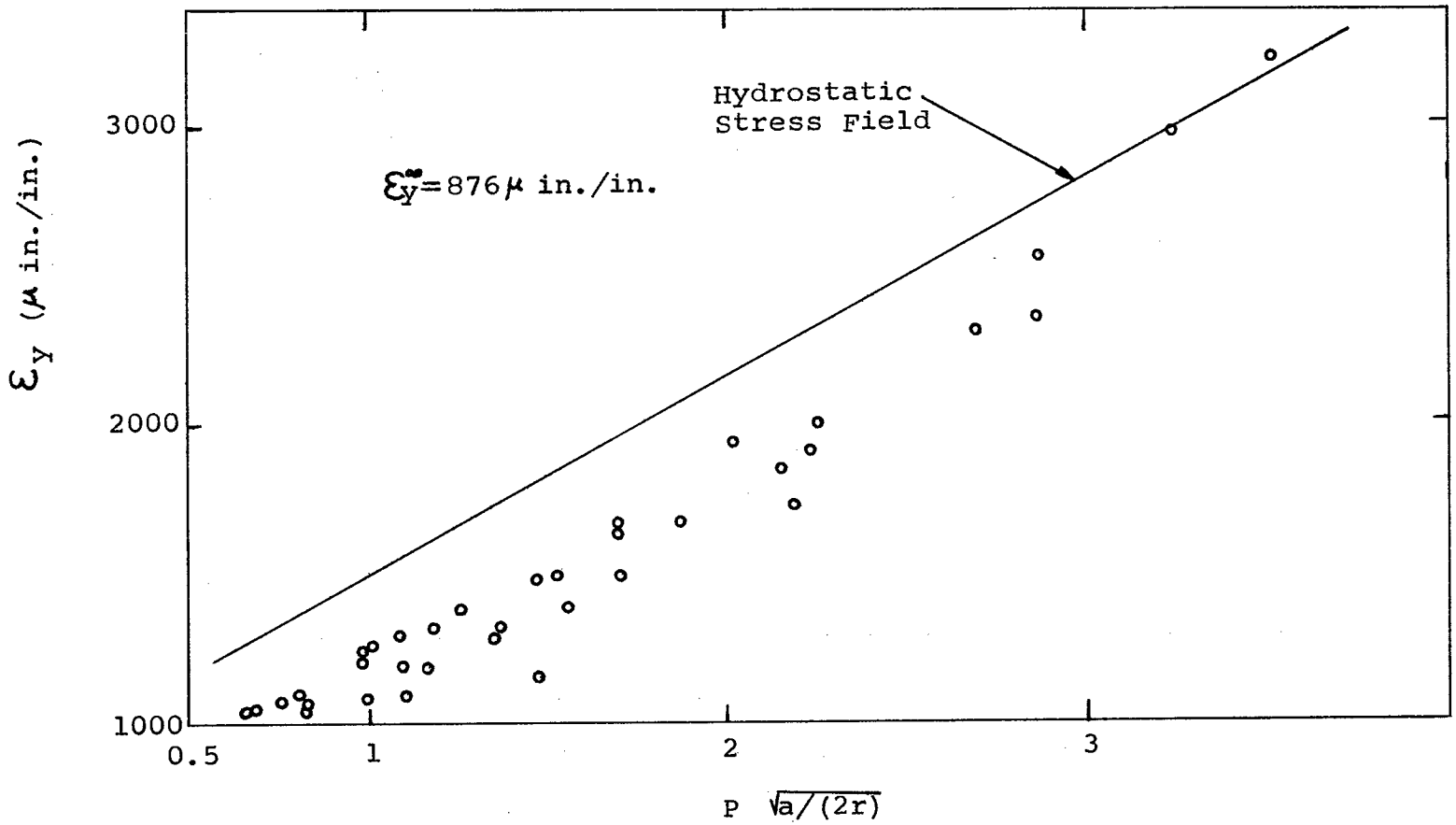

FIGURE 24

Measured and Theoretical Strain Ahead of Crack

Exact Elastic Stress Distribution

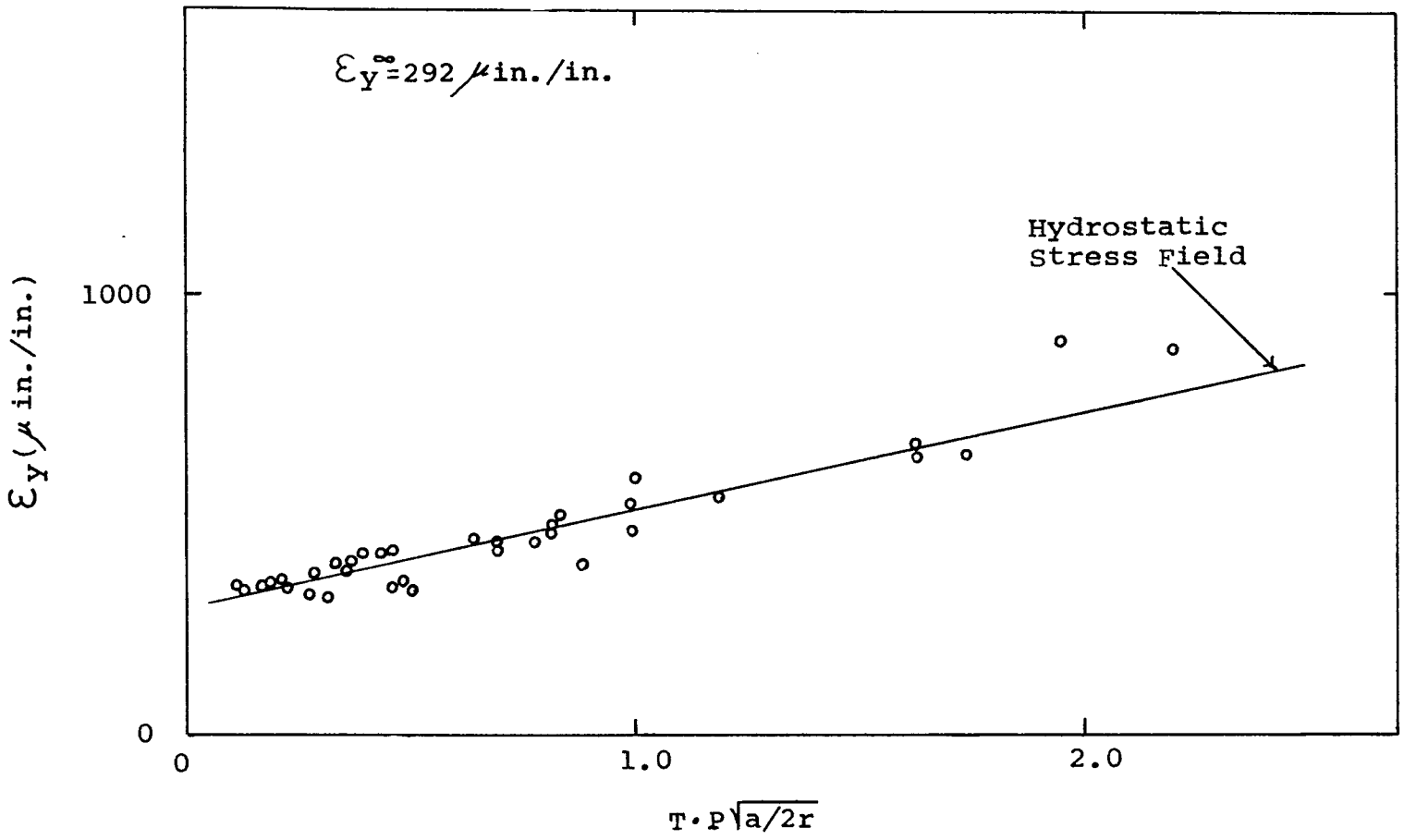

FIGURE 25

Measured and Theoretical Strain Ahead of Crack

Exact Elastic Stress Distribution

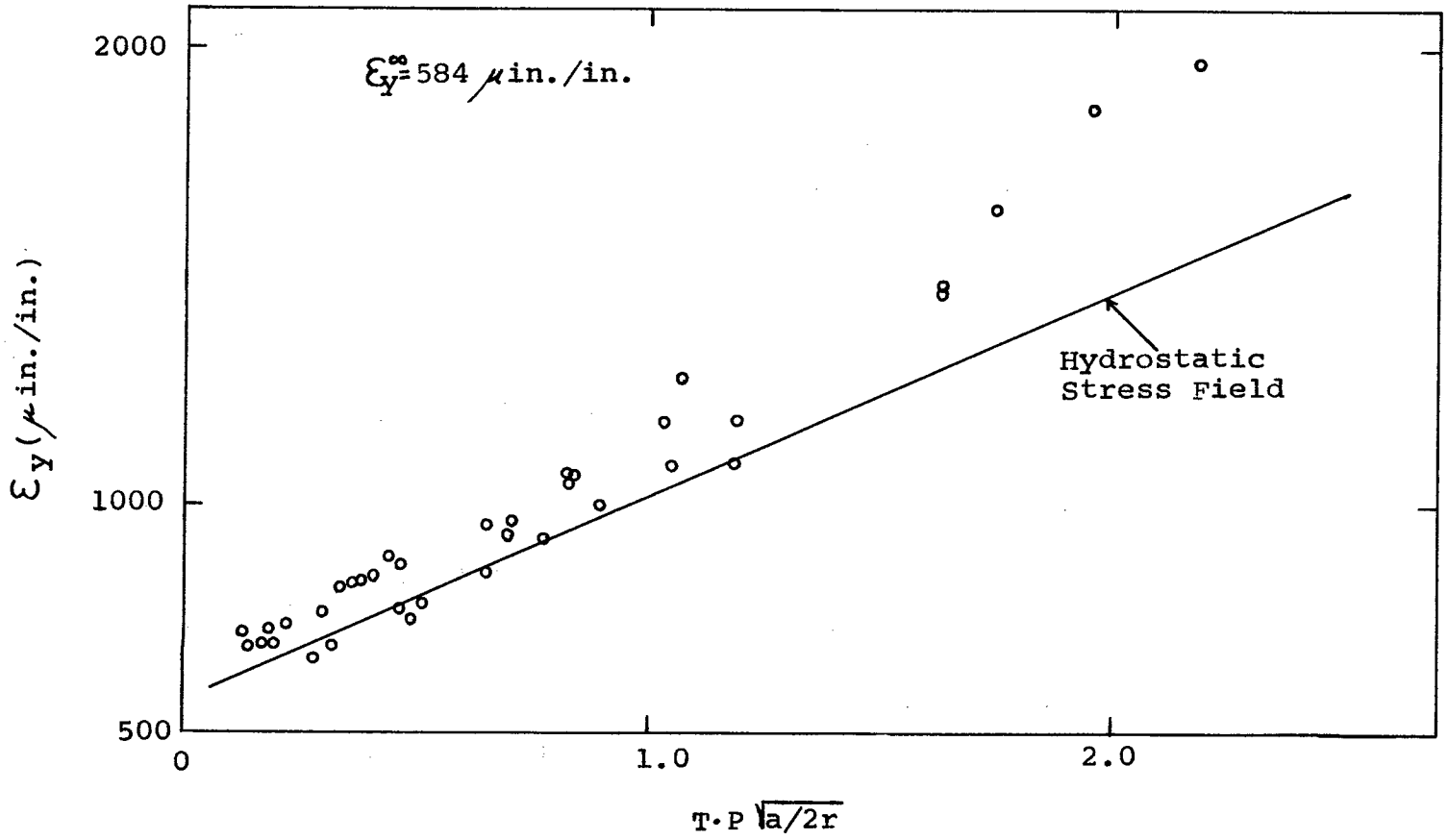

FIGURE 26

Measured and Theoretical Strain Ahead of Crack

Exact Elastic Stress Distribution

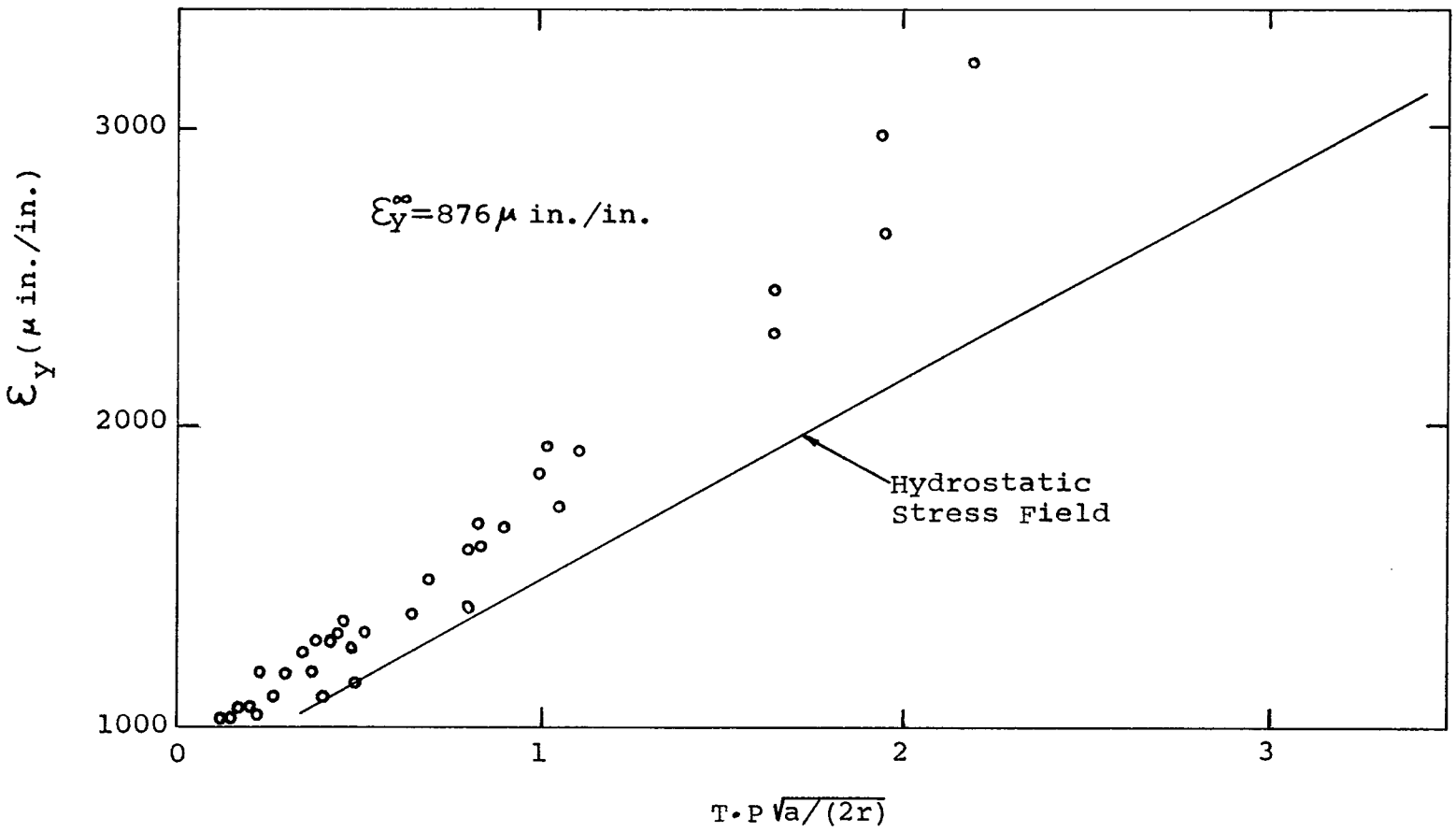

FIGURE 27

Comparison of Exact and Approximate Elastic Stress Distribution Ahead of Crack Tip of a Plate

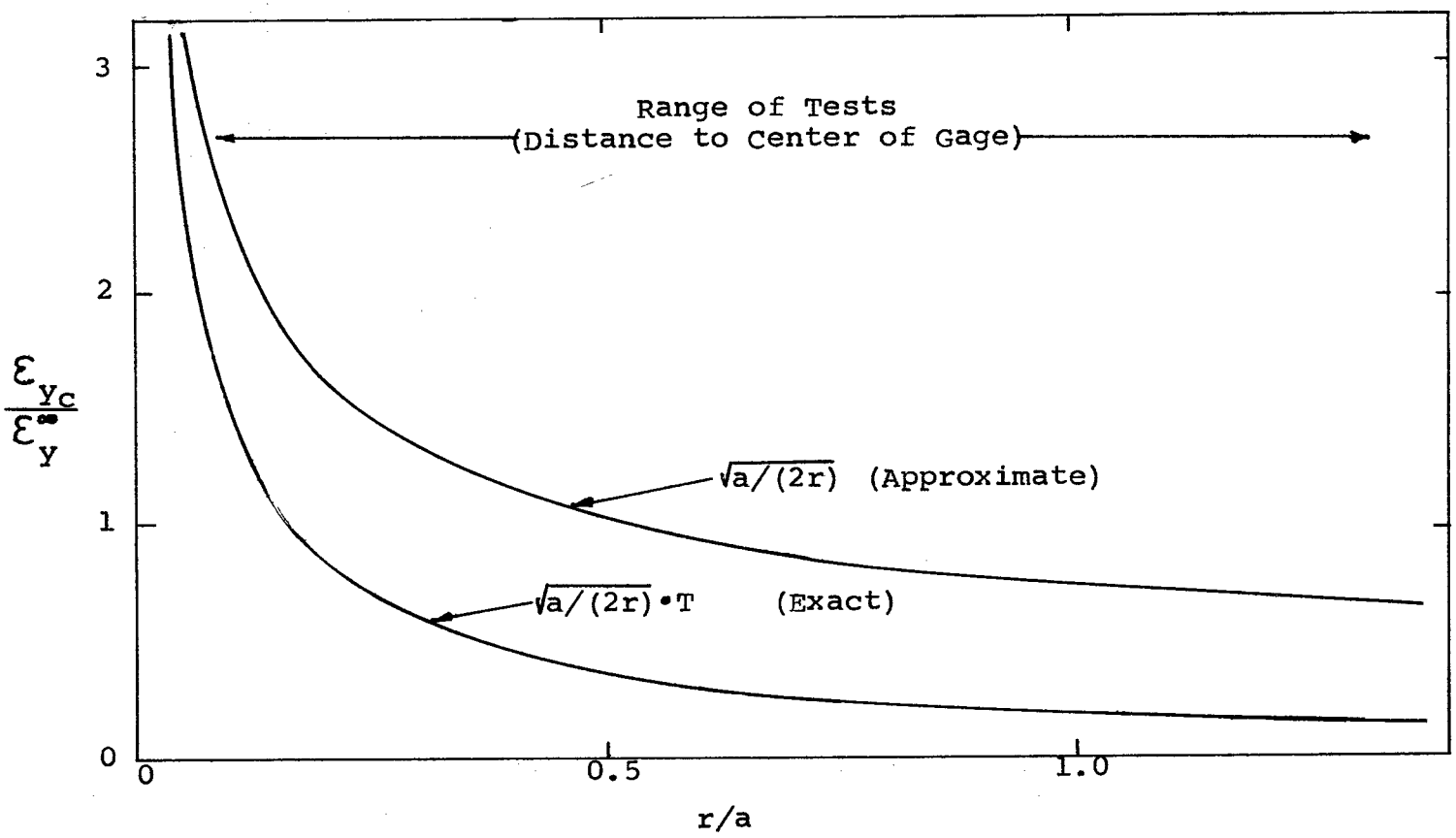

FIGURE 28

Strain Gage Measurement of Elastic

Strain Distribution Ahead of Crack Tip

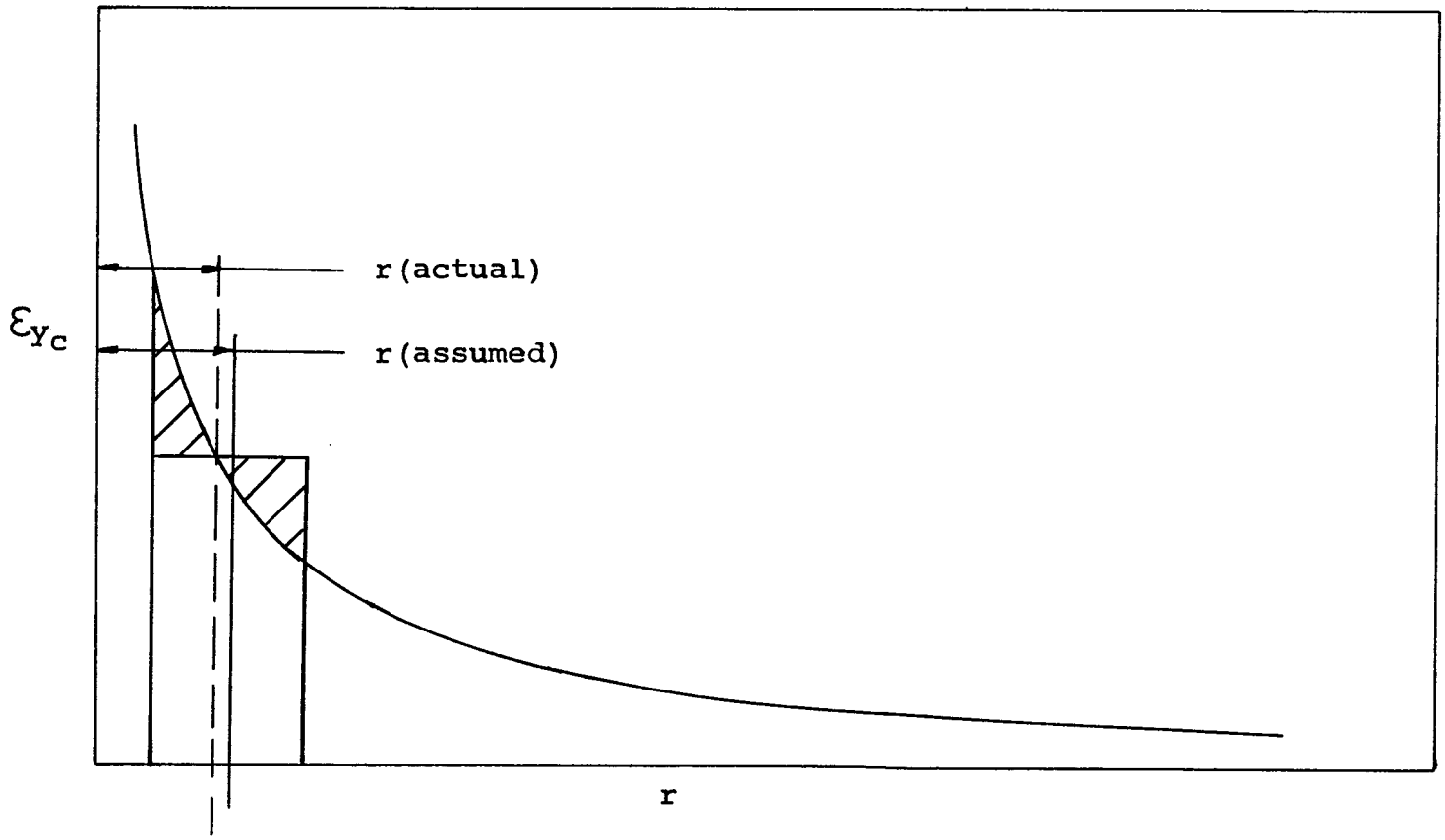

FIGURE 29

Ratio of Stress Intensity Factors

vs. Crack Length

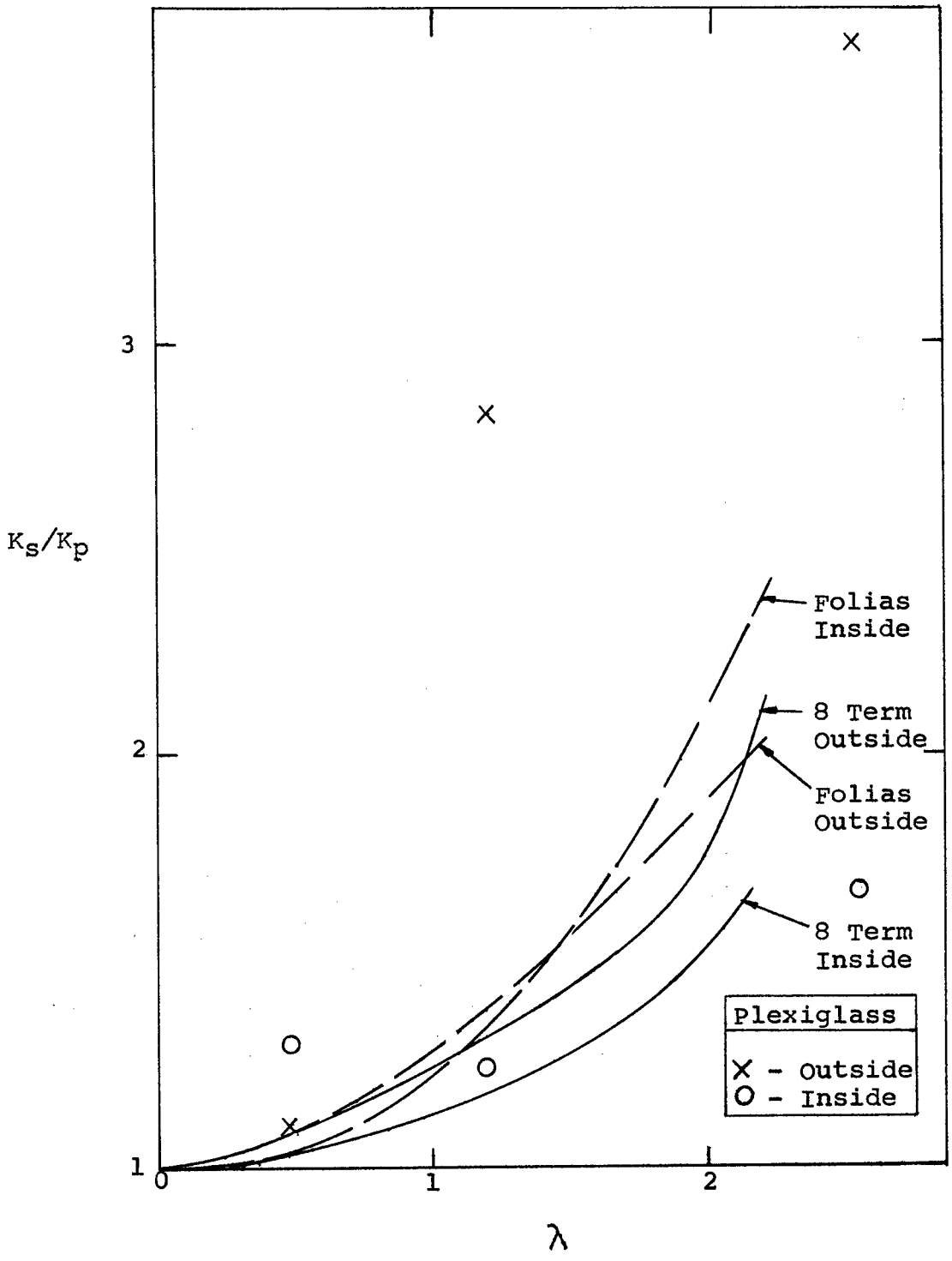

TABLE I

Ratio of Bending and Extension Stress Intensity Factors

Lambda	Number of Terms	P_b'	P_e
0.2	1	-.0051019192	1.0098910
	2	-.0041031887	1.0096026
	3	-.0041033655	1.0096165
	4	-.0041033621	1.0096165
	5	-.0041033620	1.0096165
0.4	1	-.015236659	1.0400153
	2	-.011216673	1.0365794
	3	-.011225325	1.0368121
	4	-.011225110	1.0368120
	5	-.011225111	1.0368120
0.6	1	-.028057980	1.0914843
	2	-.018787392	1.0770401
	3	-.018868454	1.0783070
	4	-.018866012	1.0783040
	5	-.018866060	1.0783044
0.8	1	-.042834541	1.1662898
	2	-.025568961	1.1262195
	3	-.025954295	1.1305623
	4	-.025940092	1.1305323
	5	-.025940806	1.1305365
1.0	1	-.059402877	1.2676320
	2	-.030603158	1.1788943
	3	-.031862534	1.1903994
	4	-.031803183	1.1902133
	5	-.031808820	1.1902435
1.2	1	-.077912602	1.4002587
	2	-.033109799	1.2299395
	3	-.036358222	1.2557787
	4	-.036151880	1.2549311
	5	-.036181704	1.2550822
1.4	1	-.098740334	1.5709013
	2	-.032583775	1.2749862
	3	-.039741104	1.3269937
	4	-.039103933	1.3238708
	5	-.039224727	1.3244645

Lambda	Number of Terms	P'_b	P_e
1.6	1	-.12246910	1.7888593
	2	-.028898230	1.3108542
	3	-.043134074	1.4087889
	4	-.041332584	1.3988892
	5	-.041742601	1.4008612
	6	-.041794437	1.4009645
	7	-.041820487	1.4010472
	8	-.041824244	1.4010507
1.8	1	-.14989761	2.0667491
	2	-.022320944	1.3355743
	3	-.049097614	1.5152988
	4	-.044323031	1.4869035
	5	-.045575215	1.4927968
	6	-.045875596	1.4936068
	7	-.046006773	1.4940039
	8	-.046040097	1.4940656
2.0	1	-.18205641	2.4213584
	2	-.013448964	1.3482143
	3	-.063462692	1.6848021
	4	-.051162538	1.6069464
	5	-.054819958	1.6237831
	6	-.056320724	1.6288229
	7	-.056919967	1.6305416
	8	-.057171478	1.6312284
2.2	1	-.22020109	2.8743619
	2	-.003138382	1.3491155
	3	-.10295845	2.0391259
	4	-.069631625	1.8161060
	5	-.080504750	1.8654519
	6	-.087935212	1.8963699
	7	-.090599756	1.9035743
	8	-.092476415	1.9106433

TABLE II

MECHANICAL PROPERTIES OF 6063-T6 ALUMINUM

Property	Typical Value	Average Value for Shell #10	
		Meridional	Circumferential
Strength (psi)			
Tensile	35,000	29,260	31,450
Yield	31,000	27,790	27,850
Elongation in 2" (%)	12 - 18	5.5	6.5
E (psi)	10^7	1.030×10^7	$.907 \times 10^7$
ν	1/3	—	—

TABLE III

DIMENSIONS OF 6063-T6 ALUMINUM SHELLS

	Nominal Size (in.)	Average Values (in.)				
		Shell 9	Shell 10	Shell 12	Shell 13	Shell 15
Diameter						
Outside	8.00					
Inside		3.7880	—	3.7881	3.7881	3.7879
Variation		+.0008 -.0006	—	+.0003 -.0005	+.0005 -.0008	+.0006 -.0011
Wall Thickness	.072	—	.0745	—	—	—
Variation	—	—	+.0006 -.0010	—	—	—

TABLE IV

Flat to Shear Fracture

Shell	Transition Zone					
	Initiation			Termination		
	a	K_r	da/dn	a	K_r	da/dn
9	--	--	---	.293	4140	1.75×10^{-5}
11	.360	2610	1.8×10^{-6}	.550	3910	8.00×10^{-6}
12	.285	3240	4.2×10^{-6}	.449	4760	1.75×10^{-5}
13	--	--	---	.465	3300	9.70×10^{-6}
18	.149	2100	1.6×10^{-6}	.422	4520	1.4×10^{-5}

TABLE V

Crack Growth Constants of

6063-T6 Aluminum

$K_{r_e} + 0.5K_{r_b}$

Shell	Ω	A'	$2(\alpha_1+\alpha_2)$	r_1	log S_{yx}
9	1.087	2.69×10^{-19}	3.82	0.994	0.153
10	1.066	6.99×10^{-20}	3.99	0.980	0.284
11	1.065	2.82×10^{-18}	3.46	0.970	0.303
12	1.065	1.97×10^{-18}	3.54	0.965	0.339
13	3.259	2.54×10^{-17}	3.29	0.979	0.171
14	1.077	1.16×10^{-17}	3.37	0.994	0.127
15	1.644	5.05×10^{-17}	3.19	0.998	0.069
18	1.055	4.21×10^{-18}	3.46	0.965	0.276

$$da/dn = 1.068\times10^{-19}(1+\Omega)^{.753}K_r^{3.85}$$

$$A' = B(1+\Omega)^{.753}$$

$K_{r_e} + K_{r_b}$

Shell	Ω	A'	$2(\alpha_1+\alpha_2)$	r_1	log S_{yx}
9	1.087	4.05×10^{-19}	3.76	0.994	0.156
10	1.066	1.00×10^{-19}	3.93	0.979	0.284
11	1.065	4.07×10^{-18}	3.40	0.970	0.304
12	1.065	2.87×10^{-18}	3.48	0.964	0.341
13	3.259	3.20×10^{-17}	3.25	0.978	0.171
14	1.077	1.61×10^{-17}	3.32	0.994	0.130
15	1.644	6.86×10^{-17}	3.15	0.998	0.069
18	1.055	6.09×10^{-18}	3.41	0.965	0.280

$$da/dn = 1.39\times10^{-19}(1+\Omega)^{.729}K_r^{3.80}$$

$$A' = B(1+\Omega)^{.729}$$

"The aeronautical and space activities of the United States shall be conducted so as to contribute . . . to the expansion of human knowledge of phenomena in the atmosphere and space. The Administration shall provide for the widest practicable and appropriate dissemination of information concerning its activities and the results thereof."

—NATIONAL AERONAUTICS AND SPACE ACT OF 1958

NASA SCIENTIFIC AND TECHNICAL PUBLICATIONS

TECHNICAL REPORTS: Scientific and technical information considered important, complete, and a lasting contribution to existing knowledge.

TECHNICAL NOTES: Information less broad in scope but nevertheless of importance as a contribution to existing knowledge.

TECHNICAL MEMORANDUMS: Information receiving limited distribution because of preliminary data, security classification, or other reasons.

CONTRACTOR REPORTS: Scientific and technical information generated under a NASA contract or grant and considered an important contribution to existing knowledge.

TECHNICAL TRANSLATIONS: Information published in a foreign language considered to merit NASA distribution in English.

SPECIAL PUBLICATIONS: Information derived from or of value to NASA activities. Publications include conference proceedings, monographs, data compilations, handbooks, sourcebooks, and special bibliographies.

TECHNOLOGY UTILIZATION PUBLICATIONS: Information on technology used by NASA that may be of particular interest in commercial and other non-aerospace applications. Publications include Tech Briefs, Technology Utilization Reports and Notes, and Technology Surveys.

Details on the availability of these publications may be obtained from:

SCIENTIFIC AND TECHNICAL INFORMATION DIVISION

NATIONAL AERONAUTICS AND SPACE ADMINISTRATION

Washington, D.C. 20546